Late breakdown behaviour of 72.5 kV vacuum interrupters during capacitive switching with a synthetic test method

vom Fachbereich Elektrotechnik und Informationstechnik
der Technischen Universität Darmstadt
zur Erlangung des akademischen Grades eines
Doktoringenieurs (Dr.-Ing.)
genehmigte Dissertation

von
Benjamin Surges, M.Sc.

1. Gutachten: Prof. Dr.-Ing. Volker Hinrichsen
2. Gutachten: Prof. Dr. René Smeets

Tag der Einreichung: 22.03.2022
Tag der mündlichen Prüfung: 16.09.2022

Darmstadt 2022

Surges, Benjamin: Late breakdown behaviour of 72.5 kV vacuum interrupters during capacitive switching with a synthetic test method

Darmstadt, Technische Universität Darmstadt
Jahr der Veröffentlichung der Dissertation auf TUprints: 2022
URN: urn:nbn:de:tuda-tuprints-229996
Tag der mündlichen Prüfung: 16.09.2022

Acknowledgement

This thesis is the result of my work as a scientific assistant at the *Fachgebiet Hochspannungstechnik* (Department of High Voltage Laboratories) of the *Technische Universität Darmstadt* (Technical University of Darmstadt). In this regard, I would like to thank the following people for their support in this research project.

First of all, I would like to thank my supervisor Prof. Dr.-Ing. Volker Hinrichsen, who gave me the opportunity to work on this research project. He granted me the freedom to implement my own ideas, but also the neccessary guidance to stay on the right track.

I am also grateful to Prof. Dr. René Smeets, formerly innovation engineer at KEMA Laboratories and still an ongoing expert in the field of high voltage switchgear. I am honoured that he agreed to be my co-examiner.

This research project would not have been possible without the financial contribution of Siemens AG and their provision of the test samples. Special thanks to Dr. Werner Hartmann†, Dr.-Ing. Thomas Heinz, Dr. Sylvio Kosse, Dr.-Ing. Thomas Rettenmaier, Dr. Erik D. Taylor and Dr. Norbert Wenzel, with whom I have had many helpful discussions.

Furthermore, I would like to express my deepest gratitude to Dr.-Ing. Benjamin Baum for the time he took to familiarise me with the complex test circuit in the laboratory. Even after his time at the department he was always helpful with advice when I encountered technical problems with the laboratory.

Maintenance work and technical modifications to the test circuit would often not have been possible without the assistance of the mechanical workshop at the department. Therefore, a special thank you also goes to the workshop staff for their support and their great wealth of ideas for the implementation.

The students who supported me in the laboratory also played their part in the success of the work and deserve a heartfelt thank you.

Besides the professional exchange, the great cohesion between colleagues in the department at colloquia, conferences, during daily work, but also privately, has constantly motivated me to continue. Many wonderful moments will remain in my memory. Thank you all from the bottom of my heart.

Last but not least, I would like to express my loving gratitude to my family who have supported me all these years and finally to my partner who has been with me through this challenging time.

Contents

Abbreviations, acronyms and symbols

List of abbreviations and acronyms

BD	Breakdown
DAQ	Data aqcuisition
DCP	Discharge current protection
DOE	Design of Experiments
DSO	Digital storage oscilloscope
FN	Fowler-Nordheim
LBD	Late breakdown
NSDD	Non-sustained disruptive discharge
OCP	Operating current protection
PTFE	Polytetrafluoroethylene
RMS	Root mean square
S_1	First circuit breaker
S_2	Second circuit breaker
S_{aux}	Auxiliary switch
S_{ion}	Current making switch
S_{sel}	Selection switch
S_{uon}	Voltage making switch
SF_6	Sulphur hexafluoride
TS1	First test sample
TS2	Second test sample
TS3	Third test sample
TS4	Fourth test sample
TS5	Fifth test sample
VCB	Vacuum circuit breaker
VI	Vacuum interrupter

List of symbols and units

Δd_{ovtr}	m	Max. distance from open position during overtravel
Δd_{rbd}	m	Max. distance from open position during rebound
β_{g}	1	Geometric (macroscopic) enhancement factor
β_{m}	1	Microscopic enhancement factor
δ	$\mathrm{rad\,s^{-1}}$	Damping factor
ε_{r}	1	Relative permittivity
φ_u	rad	Phase angle between two voltage phasors
Φ	J, eV	Work function of contact material surface
ω	$\mathrm{rad\,s^{-1}}$	Angular frequency
ω_0	$\mathrm{rad\,s^{-1}}$	Resonant angular frequency
ω_e	$\mathrm{rad\,s^{-1}}$	Natural angular frequency
a	$\mathrm{A\,eV\,V^{-2}}$	Variable from the Fowler-Nordheim equation
A_{fe}	$\mathrm{m^2}$	Effective field emission area
b	$\mathrm{eV^{-3/2}\,V\,m^{-1}}$	Variable from the Fowler-Nordheim equation
C	F	Capacitance, Capacitor
C_1, C_2	F	Capacitor banks
C_{b}	F	Capacitance of the breaking current source
C_{cc}	F	Coupling capacitor
C_{dc}	F	Capacitance of the direct voltage source
C_{equ}	F	Equivalent compensation capacitance
C_{m}	F	Capacitance of the making current source
C_{s}	F	Source side capacitance
d	m	Contact gap
d_{BD}	m	Contact gap during breakdown
d_{pre}	m	Contact gap during the first pre-strike
d_{tot}	m	Total stroke
e	C	Elementary charge
E	$\mathrm{V\,m^{-1}}$	Electrical field strength
E_{BD}	$\mathrm{V\,m^{-1}}$	Uniform electric field strength during breakdown
E_{pre}	$\mathrm{V\,m^{-1}}$	Uniform electric field strength during pre-strike
E_{rv}	$\mathrm{V\,m^{-1}}$	Uniform electric field strength during recovery voltage
f	Hz	Frequency
i	A	Current
i_{b}	A	Breaking current
$i_{C,\mathrm{equ}}$	A	Equivalent capacitive compensation current

i_{comp}	A	Computed current signal from sense resistor current
i_{fe}	A	Field emission current
i_{m}	A	Inrush current
i_{res}	A	Restrike current
i_{sense}	A	Sense resistor current
j_{fe}	$\mathrm{A\,m^{-2}}$	Field emission current density
k_{c}	1	Capacitive voltage factor
L	H	Inductance, Inductor
L_1, L_2	H	Stray inductances or damping reactors
L_{b}	H	Inductance of the breaking current source
L_{m}	H	Inductance of the making current source
L_{s}	H	Short circuit inductance of the power system
R	Ω	Resistance, Resistor
R_1, R_2	Ω	Resistances representing conductor losses
R_{d}	Ω	Damping resistor
R_{s}	Ω	Short circuit resistance of the power system
R_{sense}	Ω	Sense resistor
t	s	Time
T	s	Cycle duration
t_0	s	Moment of natural current zero crossing
t_{open}	s	Moment of contact separation
$t_{\mathrm{pre,S1}}$	s	Pre-strike moment of exemplary circuit breaker S1
$t_{\mathrm{pre,S2}}$	s	Pre-strike moment of exemplary circuit breaker S2
$t(y)$	1	Elliptical function from the Fowler-Nordheim equation
T	s	Cycle duration
u	V	Voltage
u_{ac}	V	Alternating voltage component of the recovery voltage
$U_{\mathrm{b,0}}$	V	Charging voltage of the breaking current source
u_{bb}	V	Busbar voltage
u_{bd}	V	Breakdown voltage
U_{dc}	V	Direct voltage component of the recovery voltage
u_C	V	Capacitive voltage drop
u_{l}	V	Load voltage
u_L	V	Inductive voltage drop
$U_{\mathrm{m,0}}$	V	Charging voltage of the making current source
u_{pre}	V	Pre-strike voltage
u_R	V	Resistive voltage drop

U_{r}	V	Rated voltage
u_{rv}	V	Recovery voltage
u_{s}	V	Supply voltage of the power system
$v(y)$	1	Elliptical function from the Fowler-Nordheim equation
v_{close}	$\mathrm{m\,s^{-1}}$	Closing speed
v_{open}	$\mathrm{m\,s^{-1}}$	Opening speed
W	J, eV	Energy
W_{f}	J, eV	Fermi level
W_{vac}	J, eV	Vacuum level
x	m	Distance from the emitter's electrical surface
y	1	Variable from the Fowler-Nordheim equation
Z	Ω	Impedance

Standard notation of time dependent quantities

x is a representation of any time dependent symbol.

$x(t)$ or x	Instanteneous value
$\hat{x}$	Peak value
X	Root mean square value
$\underline{X}$	Complex phasor

Kurzfassung

Das Trennen kapazitiver Lasten stellt eine kritische dielektrische Beanspruchung für Vakuumschaltröhren der Hochspannungsebene dar. Dabei sind späte Spannungsdurchschläge noch bis zu mehreren Hundert Millisekunden nach Stromunterbrechung möglich. Durch die anschließenden Umladungsvorgänge können noch höhere Schaltüberspannungen hervorgerufen werden, die wiederholte Durchschläge und ein gefährliches Aufschaukeln der Überspannung begünstigen. Darüber hinaus können insbesondere beim Zuschalten von Kondensatorbänken hohe transiente Ströme fließen, die die Kontakte der Vakuumschaltröhre zusätzlich vorbelasten.

Zur Untersuchung des Durchschlagsverhaltens von Vakuumschaltröhren für die Bemessungsspannung von 72.5 kV wird eine synthetische Prüfmethode angewendet, die den kapazitiven Schaltfall nachbildet. Im ersten Teil der Arbeit wird untersucht, wie verschiedene Prüfkreisparameter die Durchschlagswahrscheinlichkeit beeinflussen. Dazu werden faktorielle Versuchspläne eingesetzt, die eine effiziente Durchführung und Analyse der Experimente ermöglichen. Die Ergebnisse bestätigen den deutlichen Einfluss des hochfrequenten Einschaltstroms auf die Durchschlagshäufigkeit. Allerdings lässt sich kein nennenswerter Einfluss bei den weiteren Parametern, wie beispielsweise dem Ausschaltstrom oder der Lichtbogenzeit, innerhalb der gewählten Parameterbereiche feststellen.

Im zweiten Teil der Arbeit werden Untersuchungsergebnisse zu Vordurchschlagsphänomenen präsentiert, die üblicherweise mit der dielektrischen Durchschlagsentwicklung in Vakuum assoziiert werden. Die Messung von Feldemissionsströmen erfolgt mithilfe eines bereits bewährten Strommesswiderstands, während die Detektion von Mikropartikeln auf einem Messverfahren aus dem Bereich der Teilentladungsmessung basiert. Bei einem eingestellten Kontakthub von 38 mm sind Feldemissionsströme nur selten und dann ausschließlich zu Beginn der Wiederkehrspannung bei gleichzeitig später Kontakttrennung präsent. Demgegenüber erscheinen diese Ströme bei einem reduzierten Kontakthub von 20 mm häufig auch über längere Zeiträume mit Amplituden bis in den zweistelligen Milliampere-Bereich. Das Phänomen selbstbegrenzender Strompulse, oft auch als Mikroentladungen bezeichnet, tritt ebenfalls mehrfach auf. Es zeigt sich, dass das Auftreten sowohl von Feldemissionsströmen als auch von Mikroentladungen bei vorhergehender Belastung durch einen hohen

Einschaltstrom wahrscheinlicher wird. Dennoch gehen der Mehrzahl später Durchschläge weder signifikante Feldemissionsströme noch Mikroentladungen voraus. Darüber hinaus führen selbst die höchsten Feldemissionsströme nicht zwangsläufig zu einem dielektrischen Versagen. Dieses Ergebnis bekräftigt die Hypothese, dass die Feldemission bei größeren Kontaktabständen einen geringen Einfluss auf das Durchschlagverhalten ausübt. Im Fall der Mikropatikelmessung konnte ein wiederkehrendes Strompulsmuster identifiziert werden, das auf mögliche Mikropartikelbewegungen in der Vakuumschaltröhre schließen lässt. Allerdings lässt sich im Rahmen dieser Arbeit keine Korrelation zwischen dem vermehrten Auftreten dieser Strompulse und dem Auftreten von späten Durchschlägen feststellen. Es wird daher geschlussfolgert, dass der Durchschlagsprozess nicht durch wiederholte Mikropartikelkollisionen, sondern hauptsächlich durch ein singuläres Ereignis eingeleitet wird, bei dem genügend Energie für die Freisetzung von Elektronen und gasförmiger Materie für die rapide Entwicklung des dielektrischen Durchschlags in der Vakuumschaltröhre bereitgestellt wird.

Abstract

The interruption of capacitive currents involves a demanding dielectric stress for high voltage vacuum interrupters. Dielectric breakdowns up to several hundreds of milliseconds after current interruption are possible, which may result in harmful voltage escalations. Additionally, high inrush currents prestress the vacuum interrupter especially during the energisation of capacitor banks.

A synthetic test method is applied to study the late breakdown behaviour of vacuum interrupters of 72.5 kV rated voltage during capacitive switching. The first part of this work focuses on factorial experiments that are applied to determine the influence of different test circuit parameters on the breakdown behaviour in an efficient way. The results confirm the significant impact of inrush currents on the breakdown rate. However, a relevant effect of the other tested parameters, e.g. breaking current and arcing time, cannot be ascertained for the investigated range.

In the second part of this work measured pre-breakdown phenomena are presented and discussed. While field emission currents are measured with a commonly applied sense resistor, the detection of charged microparticles is conducted by utilising a partial discharge measurement technique. With a contact stroke set to 38 mm field emission currents occur only rarely and only during the beginning of the recovery voltage with preceding late contact separation, when the full contact gap has not yet been established. For a reduced contact stroke of 20 mm high field emission currents can be present for long periods of time with magnitudes up to several tens of milliamperes. The phenomenon of self-limiting current pulses, often referred to as microdischarges, has also been observed repeatedly. Field emission currents and microdischarges are more likely to appear after the vacuum interrupter is stressed by an inrush current. However, the majority of breaking tests with late breakdowns include neither significant preceding field emission current nor microdischarges. Moreover, the mere presence of the highest field emission currents does not necessarily result in a disruptive discharge. This result supports the hypothesis that field emission at larger contact gaps has a negligible influence on the late breakdown behaviour. In the case of the microparticle detection measurement, a recurring current pulse pattern was detected that is likely to be linked to microparticles impacting with the contact surface. However, no correlation can be drawn between the frequency of occurrence of this pulse pattern and the occurrence of late breakdowns. Therefore, it is concluded that the breakdown process is not triggered by multiple microparticle collisions but rather by a singular event supplying sufficient energy for the release of electrons and gaseous matter for the fast development of dielectric breakdown inside the vacuum interrupter.

1 Introduction

The circuit breaker is one of the key elements to control the safe transmission and distribution of energy in the power system. It has to be able to switch on, carry and switch off high currents and to withstand overvoltages reliably even in the case of faults. Besides fault switching, circuit breakers are also utilised for special load switching tasks such as switching of inductive or capacitive loads [Ito18].

Over the last decades, gas circuit breakers with sulphur hexafluoride (SF_6) have been applied almost exclusively in the transmission voltage levels above 52 kV. This synthetic gas is characterised, among other advantages, by its high dielectric strength while simultaneously providing excellent arc quenching capabilities. Its outstanding properties allow for the application as switching medium up to the highest voltage levels. However, SF_6 also contributes to global warming. Its global warming potential based on a 100-year period is approximately 23,500 times larger than the global warming potential of carbon dioxide and has an expected atmospheric lifetime of around 3,200 years [IPCC13]. With the signing of the Kyoto Protocol in 1997, the member states have agreed to limit and reduce the usage of greenhouse gases like SF_6. In consequence, intensive efforts are also aimed at replacing SF_6 circuit breakers. A potential substitute is given by the application of vacuum circuit breakers [RKT+10, Cig14].

Since the late 1960s the vacuum switching technology has increasingly been established in the medium voltage levels below 52 kV as the leading technology due to its various advantages. Vacuum circuit breakers are characterised by their compact design, nearly maintenance-free operation and fast dielectric recovery even at high current rise times. Despite these advantages, no economic reasons arose to progress this technology to the higher voltage levels with only minor exceptions worldwide. However, the necessity to find substitutes for SF_6 led to an intensive research and development in recent years to advance vacuum circuit breakers into the higher voltage levels. One major challenge manufacturers are faced with is the required dielectric strength at higher voltages. The dielectric strength of vacuum only scales less than proportionally with larger contact gaps unlike for SF_6 and other gases. This necessitates changes and further development in the common design of a vacuum interrupter, which is the core component of any vacuum circuit breaker. At present, vacuum interrupters are commercially available for the sub-transmission levels up to 145 kV [Mei16, Sie18, Cig14].[1]

The increasing demand for reactive power control in a network to fulfil the requirements of power quality can be met by mechanically switched capacitor banks. This switching task is especially challenging for vacuum interrupters. On the one hand, a severe inrush current up to several kiloamperes may arise during the energisation of the capacitors, which results in accelerated contact wear. On the other hand, after capacitive load current interruption the vacuum interrupter is stressed by an overvoltage over long durations of time. Although rare, this may result in a dielectric breakdown up to hundreds of milliseconds after the switching operation. Harmful voltage escalations that may damage surrounding equipment are a potential consequence of these late breakdowns. Since capacitor bank switching can be necessary on a daily basis, a high number of switching operations during the lifetime of a vacuum interrupter is achieved. This in turn increases the probability of late breakdowns. Up to date, the physical origins of this phenomenon are still not fully understood and are a debated issue in the scientific community. Two different pre-breakdown phenomena are typically associated with the development of dielectric breakdowns in vacuum: field emission and microparticles [Cig20, SvK^{+}15].

Even though several obstacles in the development of the vacuum switchgear technology towards the higher voltage levels have been overcome, further research is still required. This applies in particular to the late breakdown phenomenon during the switching of capacitive loads. Within this work, laboratory experiments were carried out to study the late breakdown behaviour of 72.5 kV vacuum interrupters during capacitive switching tests by utilising a synthetic test method.

[1] By connecting multiple interrupter units in series or by integrating two contact systems into a single interrupter unit an even higher voltage withstand may be achieved. However, this requires a more complex design of the switch mechanism. Additionally, grading capacitors to equalise the voltage distribution across the individual interrupters become necessary [KKG^{+}18, FK03, GKK01].

2 Background and theory

Following a short introductory section on the categorisation of vacuum circuit breakers, their basic design is presented. Since the phenomenon of arcing is present in any switching operation under load, the basics of vacuum arcs are explained. This leads to different contact designs that can deal with the various requirements. Thereafter, an overview of the physical processes associated with dielectric breakdown in vacuum is given. In the last section the characteristics of capacitive load switching and its challenges are described.

2.1 Vacuum circuit breaker technology

To this day, circuit breakers for high-voltage grid applications are implemented exclusively as electromechanical switches. They have in common at least one pair of contacts that touches during conduction and that is separated during insulation. The transition from one state to the other is provided by an operating mechanism that exerts a stroke movement on one of the opposing contacts [Flu82].

Circuit breakers can be categorized by the medium that surrounds its contacts. The medium can be a fluid or a gas. Besides a high dielectric strength, good arc extinguishing properties are necessary. Since the beginning of the twentieth century mineral oil or compressed air and since the 1950s the gas mixture SF_6 have been widely applied for circuit breakers. Vacuum is an alternative to the application of substances. It describes the theoretical concept of complete absence of matter in a closed system. However, for technical applications it is rather defined as a state that exhibits an absolute pressure in a vessel less than the ambient environment or a pressure level below 300 mbar (equivalent to $3 \cdot 10^4$ Pa)[2] [DIN90]. A vacuum circuit breaker (VCB) operates at pressure levels even lower than 10^{-2} Pa [Cig14, SvK+15, Sla08].

Circuit breakers are realised as single-pole or three-pole switching devices. The basic components consist of the interrupting unit(s), an operating mechanism, the base frame

[2] This value corresponds to the lowest atmospheric pressure on earth's surface.

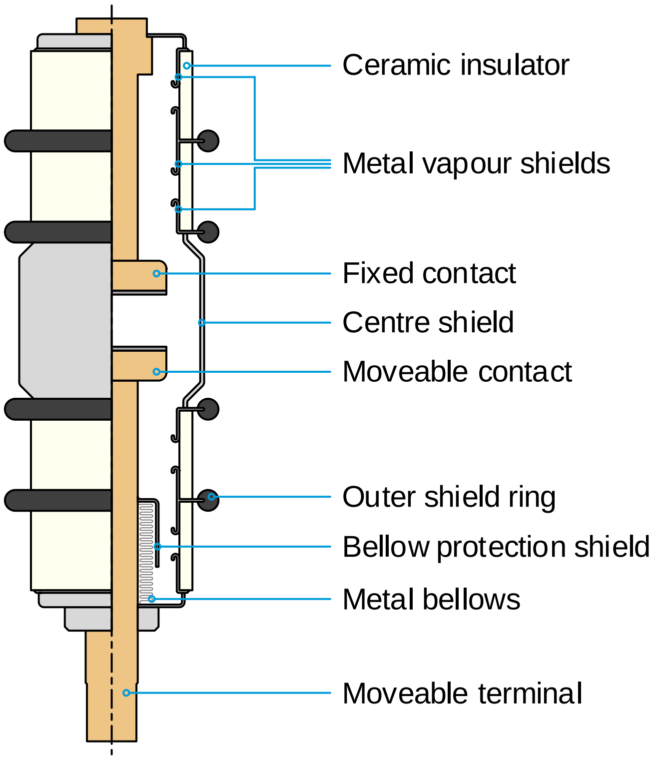

Figure 2.1: Schematic sectional drawing of a 72.5 kV VI - left side: exterior view, right side: interior view

and secondary electronics for control and monitoring. In the case of a VCB the interrupting unit is referred to as vacuum interrupter (VI). The VI is directly applicable in ambient air if used indoors for medium voltage applications. For higher voltages and for outdoor applications an external enclosure filled with a pressurised insulation gas becomes necessary to guarantee a sufficient outer dielectric strength and protection against the environmental impact. If the interrupting unit is located inside an earthed metallic enclosure, the circuit breaker is referred to as a dead-tank circuit breaker. By contrast, in live-tank circuit breakers the interrupter is located within an insulating housing made of polymeric or ceramic materials with the setup being insulated from the earth potential. The VI can be aligned either horizontally, which is more common for the dead-tank configuration, or vertically, which is more common for the live-tank configuration [Ito18].

Even though VIs vary in their shape and size depending on the manufacturer and the different voltage and current ratings, they all exhibit many similarities in their design. In Figure 2.1 a schematic cross section of a 72.5 kV VI is illustrated. Its insulating enclosure is made of ceramic hollow cylinders and metallic parts, which are soldered together to accomplish a vacuum-tight body. The contact pair is the centrepiece of the interrupter. In its open position the gap spacing is typically in the order of around 10 mm for medium voltage applications, whereas for a rated voltage of 72.5 kV contact gaps are reported for a range of 30 mm to 40 mm [GRR+12, GSE+08]. To allow for the transition of movement to the outside of the vacuum-tight body, the moveable contact is connected to the enclosure via the metal bellows. The bellow protection shield protects against punctures due to molten particles that originate from the contacts during arcing. The metal vapour shields protect the insulating ceramic cylinders from condensing metal vapour, which would otherwise create a conductive coating across the insulation. Furthermore, the vapour shields relieve the stress at dielectric weak points, so-called triple points or triple junctions, that exist at the transition between insulator, conductor and vacuum. In most applications the vapour shields and the metallic centre shield are electrically floating. Therefore, their electric potential is only defined by the internal and external stray capacitances of the VI. To reduce the external electric field strength at the edges of the protruding parts of the vapour shields, conductive outer shield rings can be applied [SvK+15, Sla08].

2.2 Vacuum arc and contact design

The contact design and the selection of suitable contact materials are highly dependent on the arcing phenomena in vacuum. Arcing commonly occurs during switching operations under load. When disconnecting a load from the power grid the current flow is not interrupted immediately after contact separation. The conducting state is rather maintained by a switching arc at least until the next natural zero crossing. In vacuum the necessary charge carriers and matter to sustain the arc can only be supplied by the metallic contact surfaces due to the absence of any matter in between. Depending on the instantaneous value of the current, the contact spacing, the contact geometry and the contact material two different vacuum arc modes can be distinguished [Lip03, Sla08, BMS96]:

- For currents up to a few kiloamperes the arc is in its *diffuse* mode. In this mode the space between the contacts is filled by an evenly distributed arc plasma with only minor electrical erosion of the contact surfaces. The plasma is sustained by metal vapour and electron supply from 40 µm to 100 µm wide spots, which randomly move on the cathode[3] surface. The lifespan of these cathode spots is up to 100 µs. Once one spot ceases to exist, a new one is created on the crater rim left behind

[3] The cathode is defined as the electrode from which electrons enter from an external circuit. Its counterpart is the anode.

by its predecessor. This recurring process creates fine traces of overlapping craters along their path. Cathode spots may also move down the contact sides, where they eventually fade out. The number of spots grows with increasing current, since each spot can only carry a current of about 100 A depending on the contact material. Additional spots can arise either by splitting of already existing ones or by the formation on new sites. A minimum current is required to maintain a cathode spot. Approaching the current zero crossing, the number of spots declines until only a single spot remains. At values of a few amperes, the arc current is suddenly interrupted when the last spot vanishes almost instantaneously. This phenomenon is termed current chopping. In contrast to the cathode, the anode only acts as a passive electron collector.

- The *constricted* mode typically develops at currents above a few kiloamperes, when the arc transitions into a single high-pressure column. At the arc roots, the high temperature results in a strong local erosion of contact material both on the cathode and the anode. This leads to an accelerated wear and consequently to a reduced switching capability if no countermeasures are taken. With decreasing current the arc transitions to the diffuse mode.

Two key design concepts have been developed for VI contacts to reduce wear during arcing. In both cases, the current flow is deliberately guided by the contact system to create an additional magnetic field that influences the arc behaviour. A radial magnetic field (RMF), which is orthogonal to the direction of the arc, can be accomplished by RMF-contacts[4]. This direction of magnetic field forces constricted arcs to a rotational movement on the edges of the contacts. Consequently, by the distribution of thermal stress over a larger area the effect of erosion is reduced. An axial magnetic field (AMF) that is in the direction of the arc can be achieved by more complex AMF-contacts. In this case, the arc is forced to stay in the diffuse mode even at higher currents, thereby decreasing the overall contact wear [SvK+15].

Both concepts are faced with the challenge of lower current interruption capability at larger contact strokes in the range of a few centimetres. For RMF-contacts the arc motion becomes less controllable, whereas for AMF-contacts the reduction of magnetic field strength in the larger gap impedes the arc to stay in the diffused mode [HGW+18, GCG+14]. However, in [Ren00] it was demonstrated that for high-voltage applications better results can be accomplished by optimised AMF-contact designs.

[4] Manufacturer dependent, this type of contacts is also termed as transversal magnetic field (TMF) contacts.

Suitable contact materials must meet several requirements. On the one hand, they have to be highly conductive to reduce ohmic losses in the closed state. On the other hand, a minimal welding tendency and a low erosion rate should be provided during arcing. Since pure metals do not fulfil all these requirements, various composite materials have been extensively investigated. To this day, the most suited contact material is based on a combination of copper and chromium. This composite is also characterised by a low metal vapour density after arc interruption, which results in a fast dielectric recovery. Furthermore, the diminished release of particles into the vacuum gap and a smoother contact surface that remains after arcing ensure better dielectric properties over longer time periods compared to other contact materials [Sla94, Lip03].

2.3 Dielectric breakdown in vacuum

In gaseous environments the dielectric breakdown is initiated by start electrons randomly available in the gas. These free electrons are accelerated by the electric field between the electrodes and thus gain sufficient energy to ionise gas molecules. A self-sustained discharge occurs when enough additional free charge carriers are generated during this process as well as secondary processes arising from it. In vacuum, however, the nearly total absence of gas molecules between the contacts prevents this kind of discharge development. The required free charge carriers and ionisable matter has to be supplied instead by contact material that can be evaporated in various ways. Hence, a breakdown in vacuum is considered more a surface than a volume effect. The theories of the breakdown processes are manifold. However, two phenomena are typically considered a root cause for the initiation: *field emission* and *microparticles* [Küc18, Sla08]. Such pre-breakdown phenomena and potential explanations for the development of a disruptive discharge will be presented in the next subsections. At the end certain dielectric charateristics that apply specifically to vacuum are described.

2.3.1 Field emission

Under the impact of a sufficiently high electric field strength, an emission of electrons from the surface of the cathode into the vacuum can be observed even at low temperatures. Hence, this effect is termed *cold field electron emission* or just *field emission*. Usually, the potential barrier between metal and vacuum prevents free electrons to be released into the vacuum. The minimum amount of energy required to overcome this barrier is

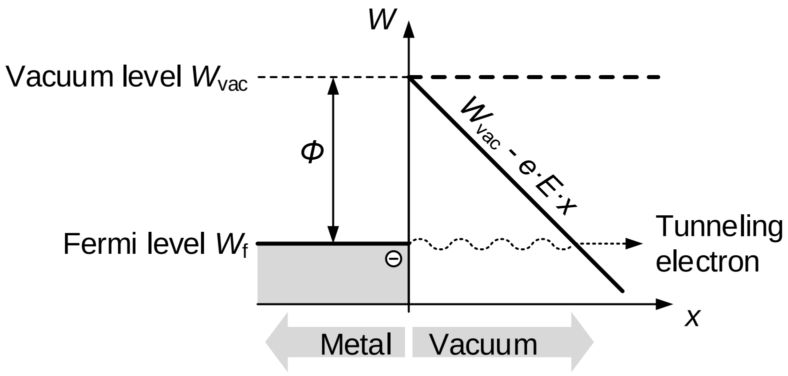

Figure 2.2: Simplified representation of the potential barrier decrease due to the field emission effect

defined by the work function Φ.[5] If, however, a strong electric field is applied, the potential barrier narrows to a roughly triangular shape, see Figure 2.2.[6] Thereby, electrons close to the Fermi level W_f obtain a certain probability to penetrate through this reduced barrier width due to their wave-like nature. This effect is also termed quantum tunnelling [And08, For08].

The non-linear relationship between local field strength E and resulting field emission current density j_{fe} can be described by an approximate equation first formulated by R. H. Fowler and L. Nordheim in 1928. Based upon the original equation, various modifications, also known as Fowler-Nordheim (FN) equations, have been proposed.[7] One commonly used form is expressed in Equation 2.1 with j_{fe} in $\mathrm{A\,m^{-2}}$, E in $\mathrm{V\,m^{-1}}$ and Φ in eV:

$$j_{fe} = a \cdot \Phi^{-1} \cdot E^2 \cdot \exp\left(-b \cdot \Phi^{3/2} \cdot E^{-1}\right) \tag{2.1}$$

with

$$a = \frac{1.541 \cdot 10^6}{t^2(y)} \cdot 1\,\mathrm{A\,eV\,V^{-2}} \tag{2.2}$$

and

$$b = 6.831 \cdot 10^9 \cdot v(y) \cdot 1\,\mathrm{eV^{-3/2}\,V\,m^{-1}} \tag{2.3}$$

The correction factors $t(y)$ and $v(y)$ denote dimensionless, mathematical elliptic functions

[5] Electrons may overcome the potential barrier for example by thermal energy input larger than the work function, which is referred to as thermionic emission.

[6] The additional distortion at the top of the potential barrier due to Schottky's image force is neglected in this depiction.

[7] For the rather complex derivation of the FN equations, refer to the relevant literature, e.g. [FN28, Flü56, Jen18].

that are dependent on the dimensionless variable $y = 3.795 \cdot 10^{-5} \cdot \sqrt{E}/\Phi$ using E in $\mathrm{V\,m^{-1}}$ and Φ in eV. Their respective values can be obtained either by tabulated functions or approximation equations [And08, For08, Sla08].

Field emission becomes relevant at electrical field strengths above $10^9\,\mathrm{V\,m^{-1}}$. Such high values can appear locally on the surface of electrodes on a microscopic scale. This field strength can be expressed as the uniform field determined by the ratio of applied voltage u and contact spacing d multiplied by an enhancement factor β.

$$E = \beta \cdot \frac{u}{d} = \beta_\mathrm{g} \cdot \beta_\mathrm{m} \cdot \frac{u}{d} \tag{2.4}$$

This enhancement factor β can be split further into two separate components. The *geometric* enhancement factor β_g takes the increase of field strength due to the design of the electrode arrangement into account. Within a VI the shape of the electrodes, the adjusted contact gap and the design of the vapour shields affect its value. The value of the *microscopic* enhancement factor β_m is strongly influenced by ever-present microscopic imperfections on the electrode surface. These are formed by protrusions, cracks, adsorbed gas layers and grain boundaries. During the operation of a VI the numbers and the degree of these imperfections can change over the lifetime, due to the applied electrical, thermal and mechanical stresses [Sla08].

Assuming a single emitting site with an area A_fe and an equally distributed current density j_fe the resulting current is defined by

$$i_\mathrm{fe} = j_\mathrm{fe} \cdot A_\mathrm{fe}. \tag{2.5}$$

Applying Equation 2.4 and Equation 2.5 in Equation 2.1 yields

$$i_\mathrm{fe} = A_\mathrm{fe} \cdot a \cdot \Phi^{-1} \cdot \left(\frac{\beta u}{d}\right)^2 \cdot \exp\left(-b \cdot \Phi^{3/2} \cdot \frac{d}{\beta u}\right). \tag{2.6}$$

If this equation is expressed in logarithmic form, a linear dependency between $\left(\frac{1}{u}\right)$ and $\ln\left(\frac{i_\mathrm{fe}}{u^2}\right)$ is achieved.

$$\ln\left(\frac{i_\mathrm{fe}}{u^2}\right) = \ln\left(A_\mathrm{fe} \cdot a \cdot \Phi^{-1} \cdot \frac{\beta^2}{d^2}\right) - b \cdot \Phi^{3/2} \cdot \frac{d}{\beta} \cdot \left(\frac{1}{u}\right) \tag{2.7}$$

Hereby, $t(y)$ and $v(y)$ are treated as constants due to their only slightly varying behaviour for the relevant ranges of E. Hence, plotting experimentally obtained data of field emission current and applied voltage in such a diagram, also known as FN plot, should result in an approximately straight line [Lat95].

In some instances, the slope and the ordinate intercept determined by the FN plot are used to calculate the enhancement factor and the emission area, respectively, e.g. as proposed by [Lat95]. However, several assumptions and simplifications have to be made. On the one hand, it has to be assumed that only one emitting site with equally distributed current density is present. Yet, experiments have shown that many emission sites will exist simultaneously on broad area electrodes like those applied in VIs. Therefore, only an effective value for A_e and β can be determined. On the other hand, the emission site does not necessarily have to be present in the area of the cathode with maximum geometric field strength. Therefore, a distinction between β_g and β_m is hardly possible. Furthermore, the work function is often assumed to be $\Phi = 4.5\,\mathrm{eV}$, which is valid for a wide range of electrode materials. However, thin layers of oxide, other residual gases or impurity contaminations on the electrode surface can result in alterations of the work function. Therefore, A_e and β values attained from FN plots have to be interpreted with caution and are better suited for specific experimental setups with carefully prepared electrodes [Jüt69, Lat95, Sla08].

2.3.2 Microparticles

Metallic particles up to the order of micrometres are typically referred to as microparticles[8]. They can appear as leftovers from contact polishing or may originate from solidified droplets after arcing. Moreover, field emission or a particle impact with the contact surface may also create new microparticles. Therefore, the occasional presence of these particles is an inevitable feature of any VI [Lat95, And08].

Typically, microparticles stick loosely to contact or vapour shield surfaces. Thus, they obtain electrostatic charge by the galvanic contact. Such a particle can eventually be released by electrical, mechanical or thermal impact. For example, throughout a switching operation mechanical shocks occur at various points of time, which strongly depend on the kinematic behaviour of the mechanical drive system. One excessive shock may occur during impact with the mechanical stop. From that moment on, a shock wave propagates to the moving contact and other mechanical structures of the VI. This triggers high frequent vibrations, which may release microparticles [Sla08, Far93, GH93].

[8] They are also called *macroparticles* due to their enormous size difference compared to ions and electrons, see e.g. in [And08].

2.3.3 Microdischarges

Another pre-breakdown phenomenon is the microdischarge. It describes a temporary flow of current that typically does not evolve into a full breakdown, but rather deceases after some time. Its duration can vary in a range of 0.1 ms to 100 ms, and its peak value can reach up to several milliamperes. Different explanatory approaches for the cause of this phenomenon exist. One theory is based on the exchange of positive and negative ions that are created from adsorbed gas layers on the metallic surfaces. In that case, negative ions may be released due to positive ions impacting on the cathode. These, in turn, will traverse towards the anode and might release further positive ions during impact. This process may repeat itself until it is limited due to the alteration of the impurity layers by the sputtering effect. Another cause might be an explosive evaporation of a protrusion or the release of gas atoms previously bound to the contact's subsurface [ZM93, SC76, Sla08].

2.3.4 Transition to breakdown

Pure field emission only constitutes a source for electrons. However, without gaseous matter to ionise within the vacuum gap, a disruptive discharge cannot evolve from field emission alone. The required matter may be supplied from either the cathode or the anode. When the current density increases at the cathode emitter, this may result in excessive local heating, inter alia due to ohmic losses. This may ultimately lead to an explosive vaporisation of the emitter, which in turn releases metal vapour into the vacuum gap. Alternatively, the created electron beam might affect the anode. The accelerated electrons can pass through the surface layer, once they attain energies above several tens of kilo-electron-volts. Their local energy deposit beneath the surface results in a rapid expansion of pressure with an eruption of dense metal vapour into the vacuum gap. Another possible consequence is the release of a microparticle at the anode due to weakening of the surface structure. This particle is further heated up by the electron beam and evaporates during its travel towards the cathode [Lat95, Sla08].

Once a microparticle is released in the presence of an electric field, it starts traversing the vacuum gap by electromechanical force. It will attain kinetic energy during its travel, which will be dissipated in the event of a collision. The velocity prior to impact depends on the microparticle's size, its density, its acquired charge and the voltage applied across the gap. Different follow-up mechanisms may evolve, which depend on the impact velocity [Lat95]:

- **Low impact velocity**: On the one hand, an elastic impact can occur with the microparticle bouncing off the surface without permanent deformation. If the particle's charge is reversed during contact, it may be accelerated again into the opposite direction accumulating further kinetic energy during the progressing transit. On the other hand, the microparticle might enhance the field distortion in close vicinity to the contact surface, which in turn leads to an increase of field emission. Consequently, the particle is heated up by the resulting electron beam and may stick to the surface creating a new field emission site.

- **Intermediate impact velocity**: The impact results in an irreversible deformation. This in turn leads to the formation of either a protrusion with the particle welded to the surface or a crater. From the thornlike edge of this crater further microparticles may be released.

- **High impact velocity**: Hereby, the microparticle or material from the electrode can be vaporised, creating a cloud of metal vapour that allows for ionisation.

In accordance with these explanations it can be seen that the mere presence of field emission or released microparticles does not have to result in a dielectric breakdown, but may cause a chain of events leading up to it. Moreover, both phenomena can exert a mutual influence on each other. Therefore, it is possible that not just a single process is present prior to a disruptive discharge. When a discharge occurs, the voltage across the vacuum gap breaks down rapidly. However, if the plasma cannot be sustained by a rapid and constant electron supply from the cathode and further ions by metal vapour, the formation of a fully developed vacuum arc cannot be established, and the discharge decays again [Sla08].

2.3.5 Characteristics of dielectric breakdown

It is commonly observed that voltage breakdowns can improve the voltage withstand level of a vacuum gap, which is referred to as *conditioning*. This effect is typically utilised for VIs during a pre-conditioning process after they have been manufactured. Hereby, the VI is stressed by a high pulsating or alternating voltage with limited power supply until a spark discharge occurs. By repetition of this process, the withstand voltage can be shifted towards higher values through smoothing of microprojections, gentle removal of microparticles and desorption of embedded residual gases on the contact surface. However, during service life the contact system of a VI will be constantly affected by electrical, thermal and mechanical stresses. These stresses can result in uncontrollable conditioning or, on the contrary, deconditioning. Thus, the history of a VI has to be considered with regard to its dielectric withstand behaviour as well [Sla08, Lat95, SvK+15].

Similar to other insulating media the voltage withstand capability can be increased with a larger contact spacing. However, in vacuum the breakdown voltage u_{bd} rather exhibits a disproportionately lower increase, which follows the relation

$$u_{\mathrm{bd}} \propto d^{\alpha} \tag{2.8}$$

with an exponent $\alpha < 1$. Since the breakdown voltage is not solely determined by the contact gap, but is also influenced by several surface properties of the electrodes, this relationship cannot be quantified in absolute terms even for uniform field electrode arrangements. Furthermore, the surface properties may significantly change over time, which also results in a larger scatter compared to commonly applied gaesous or liquid switching media especially at larger contact spacings in the centimetre range. This allows for occasional voltage breakdowns even at comparatively low voltages [Lat95, SvK+15].

2.4 Switching of capacitive loads

The interruption of faults poses one of the most severe switching tasks for circuit breakers. However, faults are rare incidents in the power grid. In contrast, load switching is carried out on a more regular basis with far more switching operations in the lifetime of a circuit breaker. Loads can be categorized into three groups: dominantly resistive loads with a power factor close to one, inductive loads and capacitive loads. In this work, the focus is on capacitive loads. The most common ones are described below [SvK+15]:

- **Overhead lines and power cables** form capacitive loads, when one end is disconnected from the grid. The capacitance is determined by the stray capacitance, depending on the geometric properties, the surrounding insulating medium and the length of the conductor. For overhead lines the capacitance per unit length is in the range of $9\,\mathrm{pF\,m^{-1}}$ to $14\,\mathrm{pF\,m^{-1}}$, and load currents are in the range from only a few amperes up to few hundred amperes. The compact design of power cables and the higher relative permittivity[9] of solid dielectrics result in a much higher capacitance per unit length. Typically, the capacitance per unit length ranges from $160\,\mathrm{pF\,m^{-1}}$ to $445\,\mathrm{pF\,m^{-1}}$ [BN16]. Because cable links are usually shorter compared to overhead lines, the reactive current is up to few hundred amperes as well.

[9] Relative permittivity of gases: $\varepsilon_{\mathrm{r}} \approx 1$; relative permittivity of typically applied cable dieletrics: $\varepsilon_{\mathrm{r}} = 2...5$

- **Capacitor banks** consist of multiple capacitors in parallel or series connection. They are applied for the compensation of reactive power or as filters for the damping of undesirable harmonics. If they are equipped with circuit breakers, they can be used for a flexible adjustment of reactive power. On account of the changing reactive power demands, these loads have to be adapted usually on a daily basis. This results in a high number of switching operations, significantly higher than for unloaded overhead lines or power cables. Load currents are typically in the range of several hundred amperes.

In the following subsections the switching behaviour during connecting and disconnecting capacitive loads is characterised.

2.4.1 Energisation

During the connection of a capacitive load to the grid a transient balancing process takes place while the capacitance is charged to the instantaneous system voltage. The resulting high-frequency current is referred to as inrush current. Its emergence can be explained appropriately by application of a series RLC resonant circuit mesh equation:

$$u(t) = R \cdot i(t) + L \cdot \frac{\mathrm{d}i(t)}{\mathrm{d}t} + \frac{1}{C} \cdot \int i(t)\,\mathrm{d}t \tag{2.9}$$

For an instantaneous value of the system voltage unequal to the capacitor voltage during switch on, an initial voltage jump is induced. Therefore $u(t)$ can be treated as a step function with peak value U_0. Three solutions to the differential Equation 2.9 do exist: An overdamped, a critically damped and an underdamped case. Hereinafter, only the underdamped case is considered. For that case, the condition $R < 2\sqrt{\frac{L}{C}}$ has to be fulfilled, which is commonly given in power grids with inherent low ohmic losses. The resulting current is

$$i(t) = \frac{U_0}{\omega_\mathrm{e} L} \cdot \mathrm{e}^{-\delta t} \cdot \sin(\omega_\mathrm{e} t) \tag{2.10}$$

with a natural angular frequency $\omega_\mathrm{e} = \sqrt{\omega_0^2 - \delta^2}$, a resonant angular frequency $\omega_0 = \frac{1}{\sqrt{LC}}$ and a damping factor $\delta = \frac{R}{2L}$. This equation describes an exponentially decreasing oscillation. The highest instantaneous value of the oscillation is reached after one quarter of the first cycle and is calculated by

$$\hat{\imath} = i\left(\frac{T}{4}\right) = \frac{U_0}{\omega_\mathrm{e} L} \cdot \mathrm{e}^{-\frac{\delta\pi}{2\omega_\mathrm{e}}} \tag{2.11}$$

with $T = \frac{2\pi}{\omega_\mathrm{e}}$. For negligible ohmic losses this peak value can be approximated by

$$\hat{\imath} \approx U_0 \cdot \sqrt{\frac{C}{L}}. \tag{2.12}$$

In this case the natural angular frequency of the oscillation can also be approximated by the resonant angular frequency calculation:

$$\omega_\mathrm{e} \approx \omega_0 = \frac{1}{\sqrt{LC}} \tag{2.13}$$

As a result, with a given capacitive load the effective inductance determines the frequency of the oscillation. In addition to the inductance the initial voltage drop determines the peak value of the current.

Figure 2.3 shows an equivalent circuit for a grid configuration with two mechanically switched capacitor banks. The two capacitor banks C_1 and C_2 are connected to a busbar via the circuit breakers S_1 and S_2. The source side is represented by a voltage source supplying the system voltage u_s and a source side short-circuit impedance formed by the inductance L_s and resistance R_s. The inductances L_1 and L_2 include the stray inductances of the supply lines and the busbar, but may also represent additional damping reactors. These inductances are typically much smaller than the short-circuit inductance:

$$L_{1,2} \ll L_\mathrm{s} \tag{2.14}$$

Ohmic conductor losses are considered by the resistances R_1 and R_2. Hereinafter, two different switching operations are presented with this topology.

At the beginning, both capacitor banks are discharged, while both circuit breakers are in their open position. The voltage across the circuit breakers is equal to the busbar voltage u_bb. Initially, only capacitor bank C_1 shall be connected to the grid. During closing of S_1 its dielectric strength is reduced continuously with the decreasing contact gap until a pre-strike occurs, and the insulating property of the circuit breaker is lost.

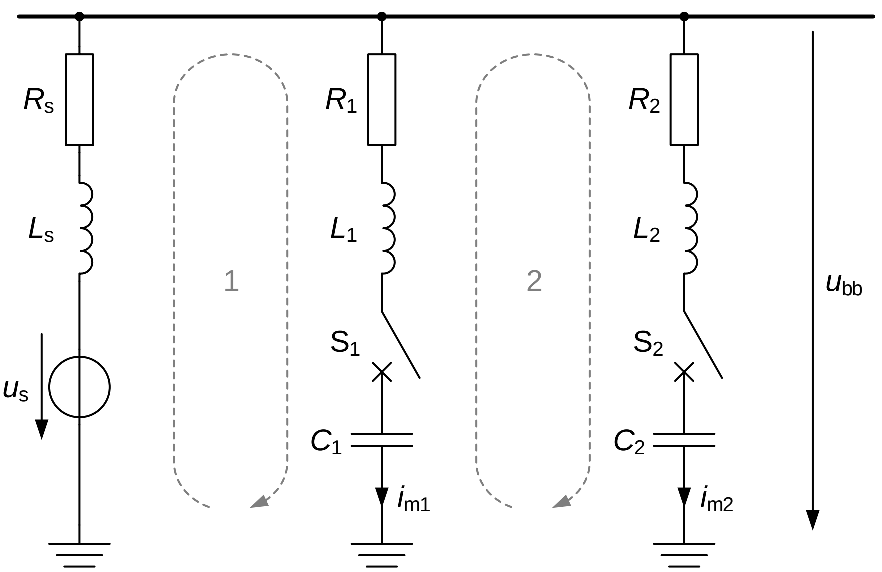

Figure 2.3: Equivalent circuit for single capacitor bank switching and back-to-back capacitor bank switching

From then on the current flow is established even before the contacts touch each other galvanically. Between the soure side and the load side a resonant circuit with elements $C = C_1$, $L = L_s + L_1$ and $R = R_s + R_1$ is formed. This is represented by *loop 1* in Figure 2.3. The highest current flows, when the pre-strike occurs during the voltage peak. In Figure 2.4 the resulting time sequence for current and voltage can be seen at time instant $t_{pre,S1}$. The inrush current peak and frequency are limited predominantly by the high short-circuit inductance. Thereby, current peaks usually reach only a few single-digit kiloamperes at frequencies of around a few hundred hertz.[10] Although this imposes no significant stress on the circuit breaker, the initial busbar voltage drop can result in power quality issues. This process, with current supplied mainly by the grid, is termed single capacitor bank switching [Cig15].

Connecting the second capacitor bank to the busbar while the first is already connected, can be more harmful to the switching device. This process is referred to as back-to-back capacitor bank switching. In this case, the balancing current is primarily supplied by the already connected capacitor bank. This is emphasised by *loop 2* in Figure 2.3. The contribution of inrush current from the grid does no longer play a major role, because of the larger inductance L_s, see Equation 2.14. The resulting inductance $L = L_1 + L_2$ drives a signifanctly larger inrush current with a higher frequency. This is shown in

[10]The power-frequency load current superimposed by the inrush current can be neglected due to its comparatively small magnitude.

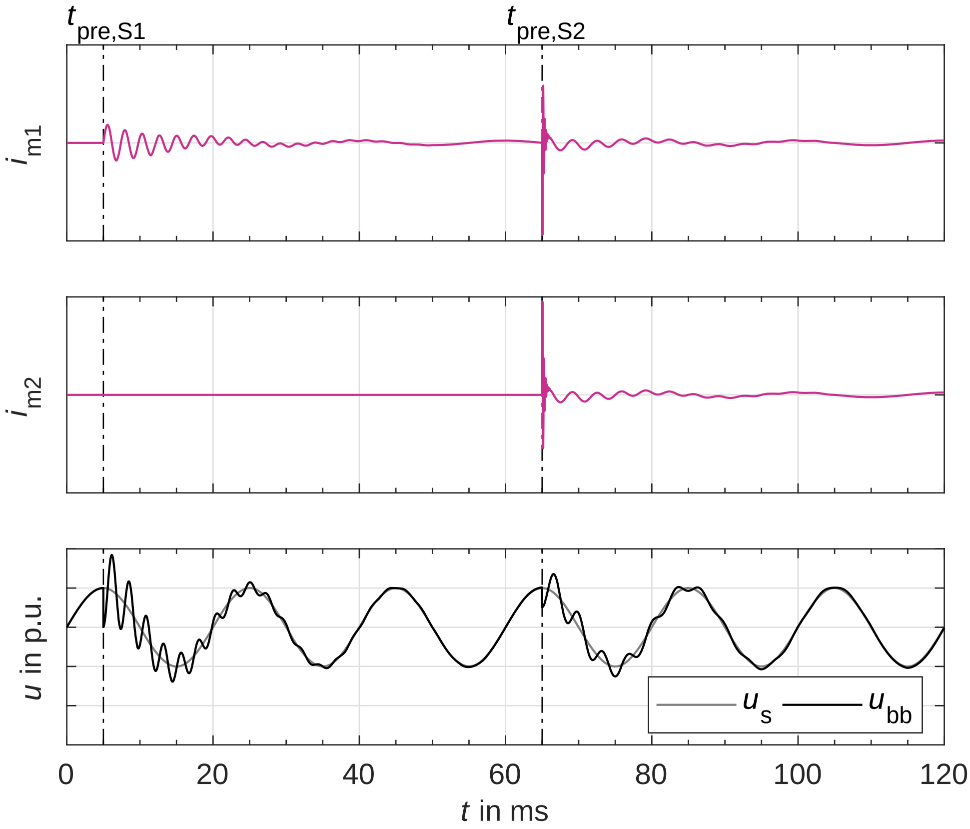

Figure 2.4: Simulated currents and voltages during capacitive energisation

Figure 2.4 beginning at time instant $t_{\mathrm{pre,S2}}$. In this case, the busbar voltage has a far lower voltage drop than before, whereas the inrush current can reach values up to a few tens of kiloamperes. Common frequency values are in the range of kilohertz. These high currents can be harmful to any circuit breaker. In the case of VCBs local melting of the contact surface occurs during arcing. Once the contacts touch, a microscopic weld is formed. With subsequent opening this weld is broken, thereby increasing the roughness of the contact surface. This high degree of newly formed microprotusions may reduce the subsequent dielectric withstand capabilities [Cig15].

In order to counteract the arise of high inrush currents, especially during back-to-back capacitor bank switching, additional current limiting devices like pre-insertion resistors or damping reactors are typically installed. Alternatively, synchronous switching at zero crossing of the applied voltage can be used to prevent inrush currents. In comparison to capacitor banks, unloaded overhead lines and power cables cause less severe inrush current stress because of their comparatively higher surge impedance [Ito18, SvK+15].

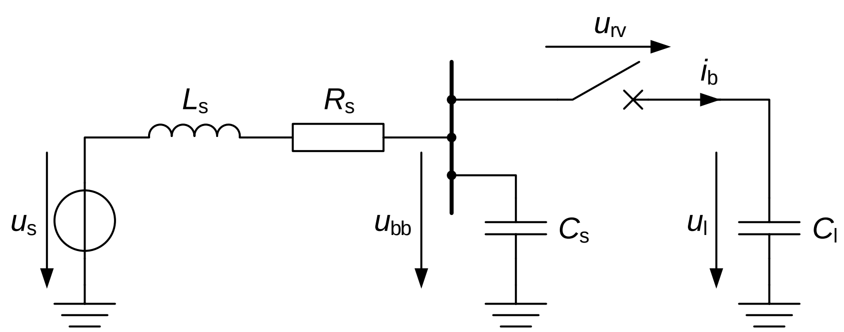

Figure 2.5: Single-phase equivalent circuit for capacitive current interruption

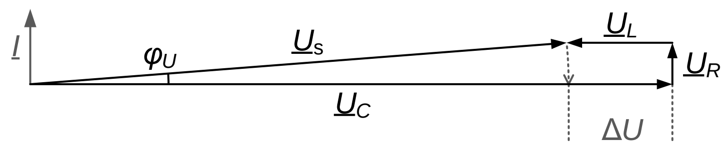

Figure 2.6: Schematic phasor diagram for capacitive loads in steady state condition

2.4.2 Current interruption

The process of capacitive load current interruption is described by the single-phase equivalent circuit depicted in Figure 2.5. The capacitive load C_l is connected to a busbar via the circuit breaker. Stray capacitances to the surroundings are summarised by capacitance C_s. As before, the grid is represented by a voltage source u_s and the short-circuit impedance formed by inductance L_s and resistance R_s.

At first, the circuit breaker is in its closed position, and a capacitive current i_b is present. This current is usually small and in the range of up to only a few hundred amperes. The load voltage u_l is equal to the busbar voltage u_bb. Under steady state condition the system behaviour can be described by the schematic phasor diagram given in Figure 2.6. The voltage drops across $L = L_\mathrm{s}$, $R = R_\mathrm{s}$ and $C = C_\mathrm{s} + C_\mathrm{l}$ are represented by the complex phasors $\underline{U}_L$, $\underline{U}_R$ and $\underline{U}_C$ respectively. Depending on the value of the capacitive load and the short circuit impedance, the busbar voltage increases in magnitude by a component ΔU compared to the system voltage U_s.[11] The small phase angle φ_u between the system voltage and the load voltage is determined by the amount of ohmic losses.

The current and voltage wave shapes during the interruption process are depicted in Figure 2.7. At arbitrary time instant t_open the circuit breaker starts to open. During

[11] With increasing capacitance the resonance frequency of the system is shifted towards the grid frequency, which results in a higher load side voltage.

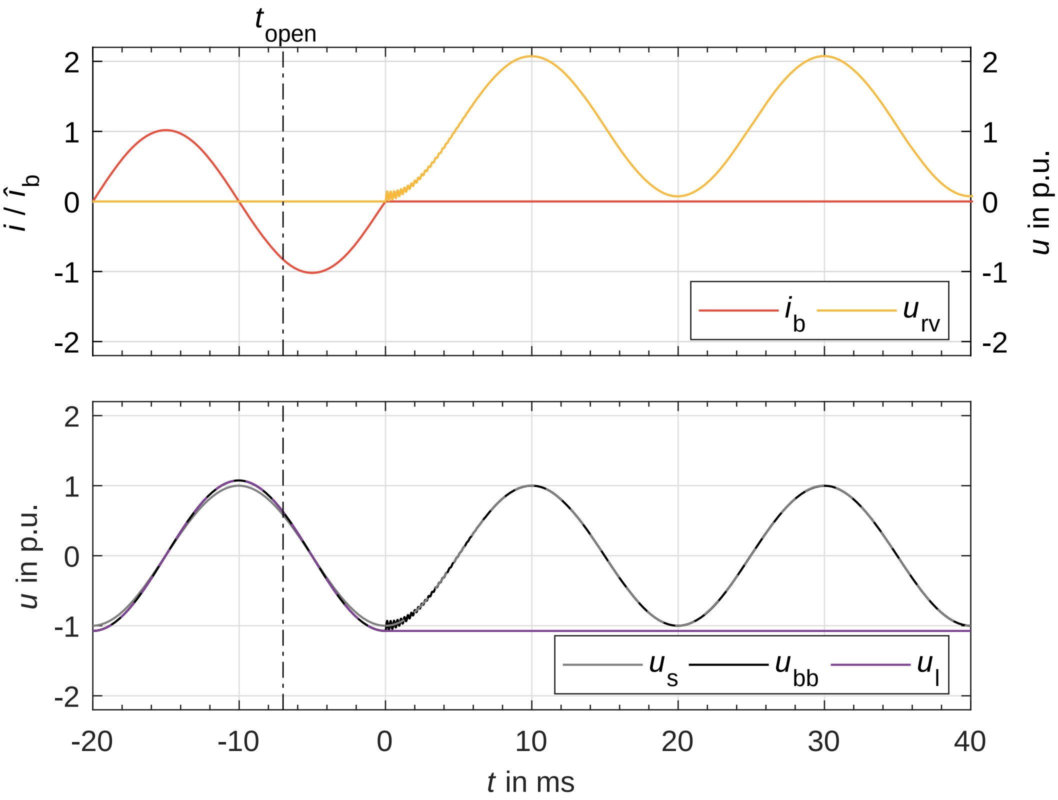

Figure 2.7: Simulated current and voltages during capacitive current interruption

contact separation a switching arc is formed between the contacts. This arc is usually interrupted at the next zero crossing of current. At that moment the busbar voltage and thus the load voltage are at their peak, due to the leading capacitive current. From then on, the charge on the capacitive load stays trapped. Consequently, u_l will remain almost constant over long durations of time.[12] On the source side the instantaneous reduction of capacitive load results in a decaying balancing process for the busbar voltage. Apart from that, it follows the system voltage course.[13] The resulting voltage across the circuit breaker, determined by the difference between source side and load side voltage, is referred to as recovery voltage u_rv. Except for the small increase in amplitude ΔU on capacitor C_l and the short balancing process at the beginning, the recovery voltage exhibits the characteristic of a $[1 - \cos(\omega t)]$ function at power frequency. Because of this characteristic behaviour, the recovery voltage has the slowest rise to peak compared to other load switching tasks. For a power frequency of 50 Hz it takes 10 ms to reach its first peak. In comparison, inductive loads cause a steep rise to peak in the range of tens to hundreds of microseconds. However, in the case of capacitive switching the peak value is comparably higher and can be present repeatedly over a long period of time [Cig15, IEEE14].

2.4.3 Re-ignitions, restrikes and non-sustained disruptive discharges

The high and long lasting recovery voltage allows for the emergence of dielectric breakdowns. These breakdowns have to be distinguished by their time of occurence and their evoked successive current flow because of their differing impact on the grid. When a breakdown occurs during the first rise of recovery voltage up to one quarter cycle of power frequency after current interruption, this is termed re-ignition. A re-ignition can occur if the increasing contact gap distance is insufficient during the rise of voltage, especially when the contacts separate just before current zero crossing. It is further supported to occur by the initial transient balancing process. Since re-ignitions do not result in dangerous overvoltages, the standard IEC 62271-100 permits their appearance during capacitive current switching [IEC08, IEEE14, SvK$^+$15].

A voltage breakdown later than one quarter cycle of power-frequency can evolve into either a restrike or a non-sustained disruptive discharge (NSDD). These breakdowns may occur even after the first peak value of the recovery voltage within periods of up to several hundred milliseconds after current interruption. Such events are also referred to as *late*

[12] The self-discharge of the capacitive load may be accelerated by the application of additional discharge resistors.

[13] Since the stray capacitance C_s is only in the range of a few nanofarads, the remaining voltage rise and phase angle with respect to the system voltage is negligible.

breakdowns. In the case of an NSDD only parasitic capacitances in the direct vicinity of the VCB contribute current to the initial breakdown process. Due to the capability of a VI to interrupt high-frequent currents, the discharge is self-extinguished before the current flow supplied by the highly charged load capacitance will commence. Since this does not affect the performance of the circuit breaker, an NSDD is usually considered harmless. If, however, the conduction of current continues with the main load circuit getting involved, the breakdown is categorised as a restrike [SvK$^+$15].

In Figure 2.8 a possible scenario with multiple restrikes during capacitive load interruption is shown. During the peak of the recovery voltage u_{rv} the interrupter fails to withstand the dielectric stress, and the current i_{res} starts to flow. If the interrupter is able to interrupt this current at the first zero crossing, the insulation in the gap will be restored again. However, during the time of current flow a balancing process between load side and source side takes place, when the capacitive load voltage u_{l} tries to adapt to the system voltage u_{s}. Because of the early interruption of the process, the capacitance is reversely charged from -1 p.u. to approximately 3 p.u.[14] The recovery voltage is substantially increased from then on. Consequently, the interrupter is more vulnerable to a second breakdown, which may occur during the following peak at -4 p.u. with yet another voltage rise after the next current interruption. This recurring process is thus termed voltage escalation and may damage connected electric equipment [SvK$^+$15].

[14]Only minimal damping is effective.

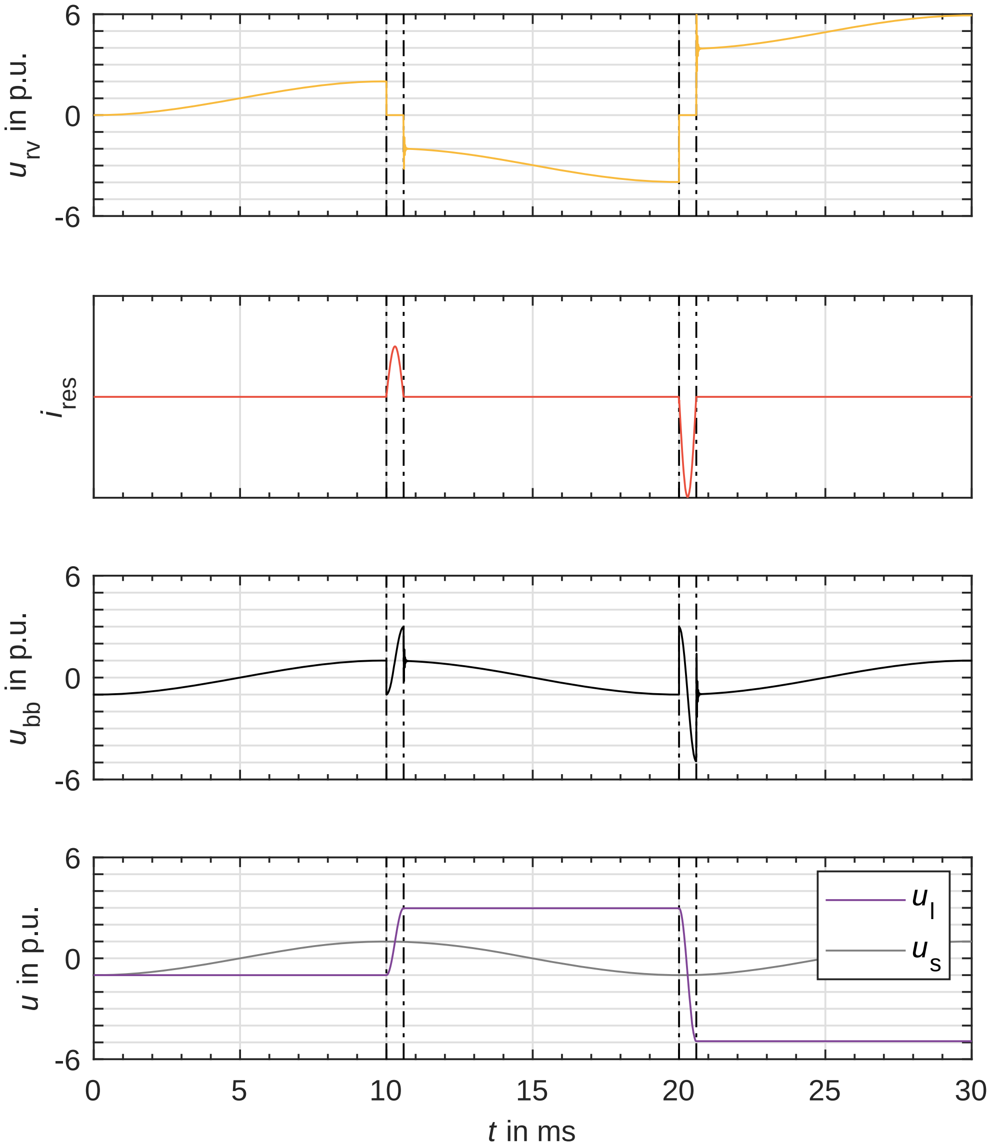

Figure 2.8: Simulated voltage escalation due to multiple restrikes

3 Research objectives

For the lower transmission voltage levels up to 245 kV a replacement of SF_6 circuit breakers by VCBs, which are successfully used in distribution systems, is being pursued. However, the advancement of the vacuum switching technology towards higher voltage levels requires further development in the design of a VI, among other things owing to the non-linear dependency of breakdown voltage with regard to contact gap spacing. This is further complicated by the fact that the physical processes leading to a dielectric voltage breakdown in vacuum are not yet completely understood. Moreover, most research work to date has been conducted primarily for the medium voltage range. However, the larger contacts gaps required for high-voltage VIs and the adapted vapour shield arrangements due to the larger volume can affect the processes that precede a dielectric breakdown. Lastly, the operational experience of VIs in the sub-transmission voltage ranges is still limited.

Especially the switching of capacitive loads becomes more challenging at the higher voltage levels. After current interruption, high recovery voltages stress the vacuum gap over long periods of time. This duration of dielectric stress increases the probability of breakdowns even after the recovery voltage has reached its first peak. These so-called late breakdowns, which are reported for VIs to occur up to several hundreds of milliseconds after current interruption, can evolve into restrikes. The appearance of restrikes has to be avoided because of the risk of voltage escalation. In the case of capacitor banks, switching operations can occur on a daily basis. This results in a high number of switching operations during the lifetime of a circuit breaker. Even though circuit breakers have to provide low restrike probabilities, frequent switching operations necessitate the consideration on a statistical basis.

The aim of this work is to achieve a deeper understanding of the late breakdown phenomenon and its causes during capacitive switching with VIs. The particular focus is on two possible causes: field emission and microparticles. To investigate both pre-breakdown phenomena simultaneously, a synthetic test circuit for capacitive switching was designed and built in a preceding research project. Two different measurement methods are used to measure each of the two phenomena. On the one hand, the currents caused by field emission are conventionally measured with the help of a current sense resistor. On the other hand, the application of the modern partial discharge measurement method aims to detect microparticle impacts. This represents a novel approach, as this phenomenon has been investigated with the aid of optical observation methods so far. Even though an optical measurement system allows for a detailled analysis of microparticle movements, a transparent viewing port into the vacuum chamber and thus a modification of the vapour shield design is required. In contrast, the new measurement approach is a non-invasive method that can also be applied to commercially available VIs.

For the investigation on late breakdowns, two different practical approaches can be considered as test objects: a model vacuum chamber or commercially available VIs. For the model vacuum chamber the assembly of a switchable contact pair and a vapour shield configuration would be required in order to simulate the dielectric properties of VIs as close as possible. This approach offers a comparatively quick and flexible adaptation of its internal design. For example, it would be feasible to insert different contact systems or apply different vapour shield geometries and arrangements in order to systematically analyse their influence on the late breakdown behaviour. Commercially available VIs do not provide this level of flexibility, as changes in the manufacturing process go with high costs on the part of the manufacturer. Furthermore, commercially available VIs do not allow for an easy and non-destructive opening of the enclosure to analyse the current condition of the interior parts. Therefore, the current state of the VI in between switching tests is always unknown. Since the application of higher voltages requires larger distances between the components, the volume of the entire housing also increases. This makes it more difficult to handle the required vacuum quality and tightness in model vacuum chambers, which are already guaranteed in commercial VIs. In addition, foreign particles can enter the model vacuum chamber during a modification that is not carried out under cleanroom conditions. The unknown degree of contamination by these particles may significantly affect the appearance of the different pre-breakdown mechanisms and thus enable false conclusions to be drawn about real VI applications. While the manual assembly of a model vacuum chamber is highly dependent on the skill of the user, the machined production of commercial VIs guarantees a higher degree of precision in the installation of the individual components. Even though a model vacuum chamber offers some crucial advantages, it is unclear wether the knowledge gained from it about late breakdowns are directly applicable to commercially available VIs. Ultimately, it was therefore decided to use commercially available VIs as test objects for the investigation.

Since late breakdowns are typically rare events, a large number of tests is required to attain sufficient information regarding this phenomenon. Frequent test runs in conjunction with the duration needed to conduct a test[15] therefore result in a considerable amount of time, which must be factored in when planning the experiments. A high number of tests also increases wear and the risk of failure of sensitive test circuit components in the demanding electromagnetic environment, which leads to an increased expenditure on maintenance. In order to keep the number of switching tests as low as possible, it would therefore be advantageous to find a set of influencing factors that maximise the propability of late breakdowns within the most realistic possible conditions of the capacitive switching case.

The previously identified issues result in the following research objectives of this work:

- In a first step, potential influencing factors are defined that can be reliably and reproducibly adjusted with the given test circuit. Their influence on the breakdown rate is efficiently assessed in experiments. This is accomplished with statistical tools provided by the Design of Experiments. Ideally, suitable factor settings shall be defined that yield the highest possible breakdown rate. Thereby, optimisation of late breakdown analysis by the reduction of necessary test runs for future investigations can be achieved.

- The second objective is the analysis of the measurement results obtained by the field emission current measurement and the new microparticle detection during the conducted switching tests. Their occurence, their behaviour and how they affect late breakdowns is characterised and correlated.

Based on the specified research objectives, the following content of the thesis is structured as follows. Chapter 4 introduces the basic operating principle of the synthetic test circuit and the different measurement systems for conducting the experiments. Both measuring methods used for the measurement and detection of pre-breakdown phenomena are dealt with in detail. Thereafter, Chapter 5 outlines the experimental methodology that is used to conduct the experiments and analyse their results in an efficient way. In this work, factorial designs provided by the Design of Experiments are used. Chapter 6 and Chapter 7 present and discuss the respective results that have emerged from the research objectives. The former chapter deals with the influence of various test circuit parameters on the late breakdown rate, while the latter deals with the data obtained by the measurement of pre-breakdown phenomena. At the end, Chapter 8 reflects on the main findings and elaborates recommendations for future work.

[15] Even though the actual switching tests last less than a second, the charging process of the sources, in particular the direct voltage source and the inrush current source, takes a few minutes in the preparation phase.

4 Test circuit and measurement procedures

There are two types of laboratory test circuits for testing high-voltage circuit breakers under capacitive switching condition: direct test circuits and synthetic test circuits. In the case of direct test circuits, the required power is provided by a single source, similar to the power grid. This necessitates a high power demand that can only be supplied by high-power test facilities. In contrast, synthetic test circuits use separate power sources with a much lower power demand to generate both the required load current and the recovery voltage. This takes advantage of the fact that once the circuit breaker opens only a low voltage is required to maintain the arc until the load current is interrupted and then during the subsequent recovery voltage period little to no current flows through the circuit breaker. Therefore, only a comparatively small amount of power is required in each case, which can be drawn directly from the low-voltage power grid or can be stored temporarily in capacitors. However, this principle requires additional auxiliary switches that have to connect or disconnect the current source or the voltage source from the different subcircuits to the test object. But despite the resulting higher complexity of synthetic test circuits, they can be constructed in a comparatively compact and cost-effective manner [SvK+15].

This chapter introduces the basic operating principle of the synthetic test circuit and the implemented measurement systems for the data acquisition used in this research project. The test circuit was developed and set up in a preceding research project. A more detailed description can be found in [Bau17].

Different standards, e.g. *IEEE C37.09* and *IEC 62271*, provide guidelines and specify requirements for capacitive load switching tests of high-voltage switchgear. The dimensioning of the test circuit is oriented at the latter. The specifications applied from this standard are listed in the relevant sections.

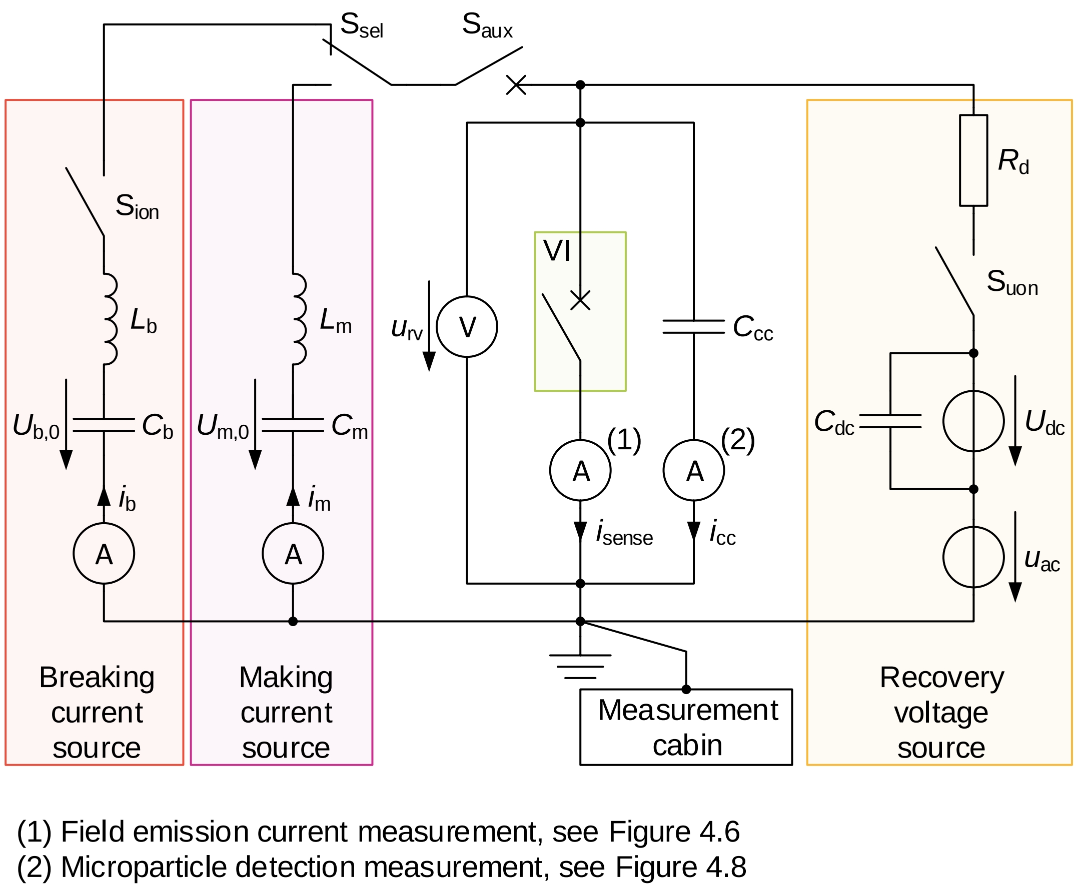

Figure 4.1: Equivalent circuit of the test circuit

4.1 Basic design

In Figure 4.1 a simplified equivalent circuit of the test circuit is illustrated.[16] The VI under test is located at the centre of the graphic. Two capacitive current switching tests can be performed with this setup: a *capacitve inrush current making test* and a *capacitive current breaking test*[17]. The making current source is utilised for the former, whereas the breaking current source and the recovery voltage source are uitilised for the latter. The four additional auxiliary switches, i.e., selection switch S_{sel}, auxiliary switch S_{aux}, current making switch S_{ion} and voltage making switch S_{uon}, allow for the connection and disconnection of the different sources during testing. The reference points for the measurement of electrical quantities are shown as well. A customised control system, which is located inside the measurement cabin, realises the preparation and the timing sequence for testing. The communication is carried out via fibre optic cables to protect against electromagnetic interferences [Bau17].

4.2 Supporting framework and operating mechanism

The supporting framework and the operating mechanism for the VI under test, both shown in Figure 4.2, were customised specially for the test setup. The VI is mounted horizontally inside an acrylic glass housing filled with the insulating liquid FC-40. This fluid with a resistivity of $4 \cdot 10^{13}\,\Omega\mathrm{m}$ and a relative permittivity of 1.9 guarantees an outer dielectric strength of $18.1\,\mathrm{kV\,mm^{-1}}$ [3M10]. External electric field control is realised by grading rings on both sides of the VI. For the entire investigation the moveable contact of the VI is connected to the low potential close to common ground, whereas the fixed contact is connected to the high potential of the test circuit. A hydraulic drive system is used for the mechanical operation of the VI.[18] The linear motion of the hydraulic cylinder is transferred via a mechanical spring and a connector rod to the moveable contact of the VI. This contact-pressure spring allows for the configuration of contact force in the closed position and additionally dampens mechanical shocks during contact opening. Within this work the contact force is adjusted to 2.7 kN. A 5 mm wide disk made of polytetrafluoroethylene (PTFE) is attached as mechanical stop. The total stroke of the contact system is adjustable in a range of 4 mm to 40 mm. For the measurement of the contact gap, a linear transducer

[16] Photos of the test setup can be found in Appendix C.

[17] The terms *making* and *breaking* are referred to switching on and off, respectively.

[18] Even though the hydraulic drive system provides different stroke speeds, it was found that adjustments lead to varying switching delay times with differing temporal scatter. Since this behaviour is unfavourable for the synchronisation of the test sequence during breaking tests, the opening speed was kept fixed within this work.

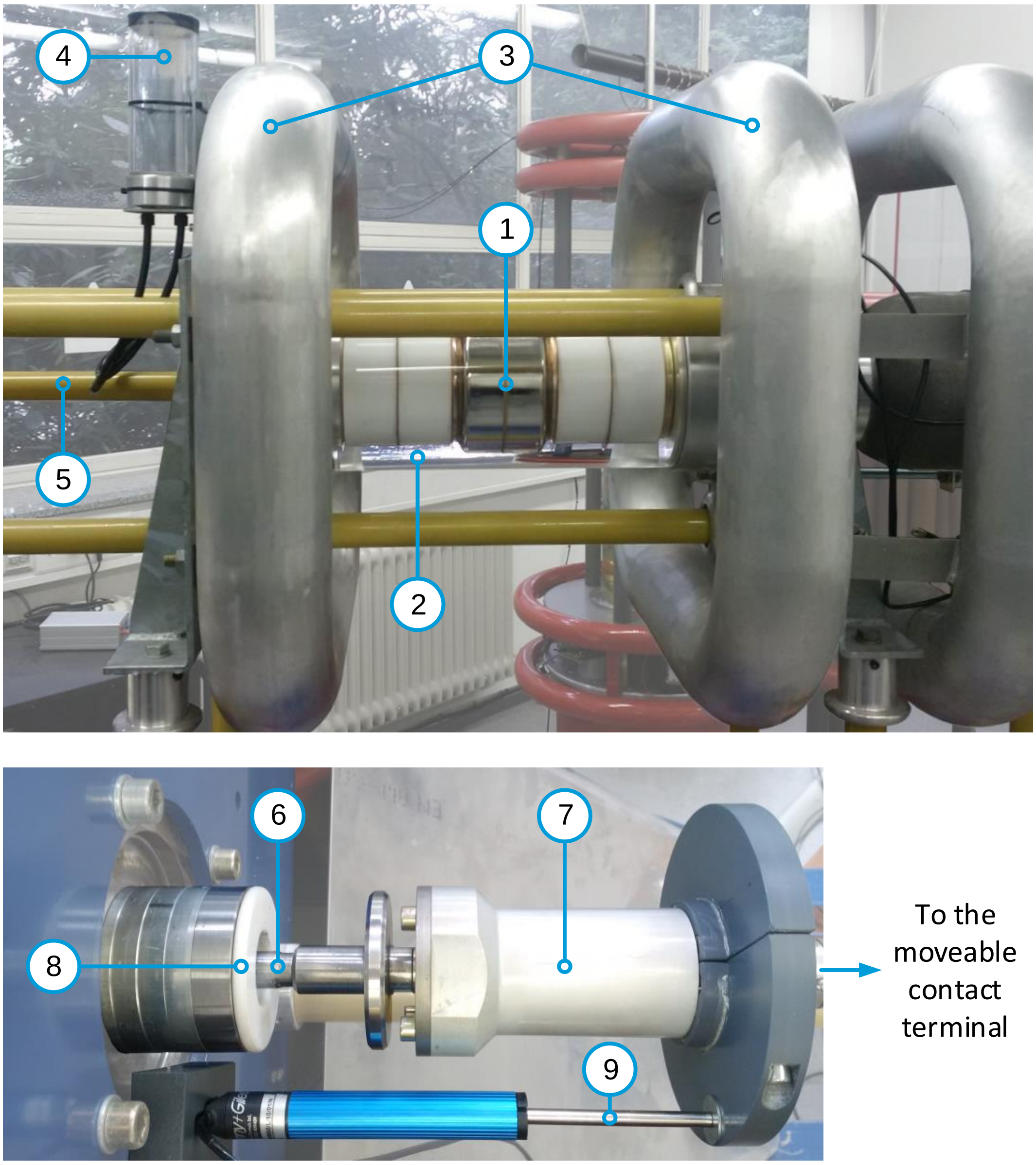

Figure 4.2: Supporting framework and operating mechanism: 1 - VI, 2 - Acrylic glass housing filled with insulating liquid FC-40, 3 - Grading rings, 4 - Equalising tank for insulating liquid, 5 - Connector rod to moveable contact terminal, 6 - Piston rod of hydraulic cylinder, 7 - Contact-pressure spring, 8 - Mechanical stop made of PTFE, 9 - Linear transducer

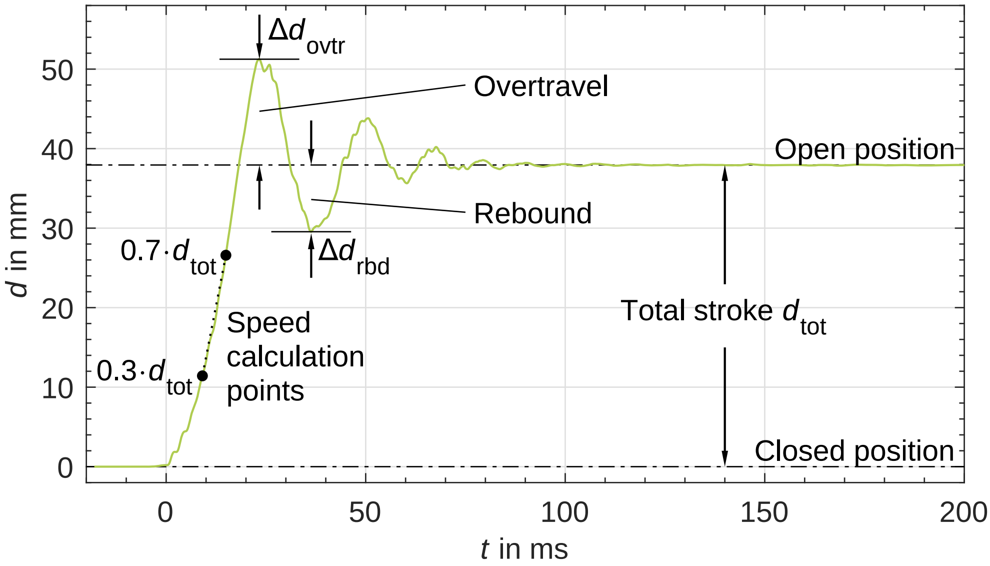

Figure 4.3: Characteristic travel curve during opening

is placed adjacent to the contact-pressure spring between the housing of the supporting framework and the connector rod [Bau17].

A characteristic travel curve for the opening of the VI is illustrated in Figure 4.3. At the beginning, the contact separation is initiated by a short acceleration phase before the moveable contact reaches an almost constant speed. The average speed is determined based on two points on the curve at 30 % and 70 % of the total stroke d_{tot}. Once the mechanical stop is reached, the moving mass of the moveable contact and the connector rod starts to compress the contact-pressure spring. As a result, the contact gap increases beyond the adjusted stroke, which is referred to as overtravel. The maximum displacement between the open position and overtravel is denoted by Δd_{ovtr}. Afterwards, the mechanical excursion of the spring also causes the contact to rebound, thereby decreasing the contact gap beneath the adjusted stroke. The maximum displacement between the open position and rebound is labeled as Δd_{rbd}. In total, the oscillation lasts about 100 ms with a deviation of more than 1 % from the total stroke.

4.3 Capacitve inrush current making test

In [IEC08] an inrush current peak of 20 kA with a frequency of 4250 Hz for back-to-back capacitor bank switching is defined. It is further stated that the ratio between the second

Table 4.1: Measured making test values for two different coils

Category	Coil 1	Coil 2
1st current peak $\hat{\imath}_{\mathrm{m}(1)}$	(16.5 ± 0.5) kA	(19.8 ± 0.2) kA
Oscillating frequency f	≈ 4.1 kHz	≈ 4.9 kHz

and the first peak of the same polarity shall not be lower than 85 %.

The generation of the inrush current is realised by a series RLC resonant circuit. The frequency of the resulting oscillation depends on the capacitance and the inductance, whereas the current peak value is determined by the capacitance, the inductance and additionally by the initial charging voltage, see Equation 2.12 and Equation 2.13, respectively.[19] The capacitor bank C_{m} with a capacitance of 11.25 µF is pre-charged to an initial voltage of approximately 59.2 kV, which corresponds to the phase-to-ground peak value in a 72.5 kV system. This charging voltage has a direct influence on the moment of pre-strike and is kept constant between tests. With these values fixed, the inductance determines both the peak value and the frequency of inrush current. During the investigation two different air-core coils with 115 µH and 79 µH are used.[20] The former coil design is in favour of a frequency closer to the value given by the standard, whereas the revised version allows for a higher current peak value. The resulting values for inrush current depending on the different inductors are listed in Table 4.1. No additional resistors are included to minimise damping. A ratio above the required 85 % between the second and first peak of current is obtained during testing [Bau17].

Prior to the test procedure, the selection switch $\mathrm{S}_{\mathrm{sel}}$ is connected to the making current source. The auxiliary breaker $\mathrm{S}_{\mathrm{aux}}$ is set to its closed position, while the VI is in its open state. When the capacitor bank is fully charged to the voltage $U_{\mathrm{m},0}$, the inrush current making test is initialised by closing the vacuum interrupter. The making current, contact spacing and pre-strike voltage are recorded.

In Figure 4.4 the relevant time segment of an exemplary inrush current making test is depicted. In the presented case, the first pre-strike occurs at a contact gap of $d_{\mathrm{pre}} = 3.0$ mm followed by a first current peak of $\hat{\imath}_{\mathrm{m}(1)} = 19.9$ kA and a second current peak of $\hat{\imath}_{\mathrm{m}(2)} = 17.7$ kA. The current flow is maintained for 32 half cycles, when it is suddenly interrupted. Just prior to contact touch a new arc ignites, and the remaining current flow occurs with another interruption during contact bouncing. The transient spikes at

[19] In a first approximation ohmic losses can be neglected.

[20] Stray inductances of the conductor loop (approximately 13 µH) and ohmic losses need to be taken into account for the final design.

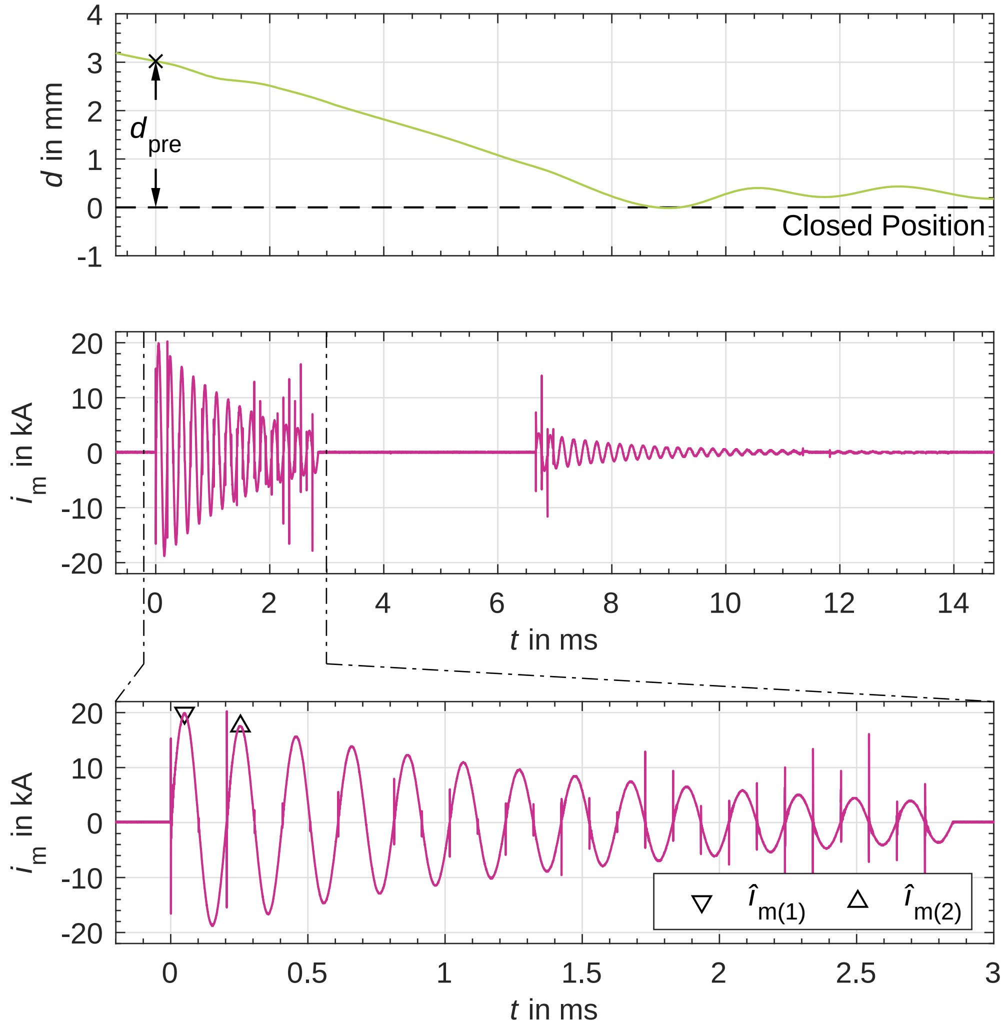

Figure 4.4: Oscillograms of an exemplary making test: $d_{\mathrm{pre}} = 3.0\,\mathrm{mm}$, $\hat{\imath}_{\mathrm{m(1)}} = 19.9\,\mathrm{kA}$, $\hat{\imath}_{\mathrm{m(2)}} = 17.7\,\mathrm{kA}$

the beginning of almost every half cycle of current, especially visible in the zoomed-in representation of inrush current, are caused by repeated pre-striking. This highlights that the arc extinguishes frequently at current zero crossings and either re-ignites immediately or is interrupted, partially with time intervals up to a few milliseconds.

4.4 Capacitive current breaking test

The breaking test can be separated into two successive parts: the breaking current period during which the VI is opened with subsequent arcing and the following recovery voltage period. Current and voltage are supplied by the breaking current source and the recovery voltage source, respectively. Both sources have to be switched precisely with the help of auxiliary switches.

Similar to the making current source, the breaking current source is realised by a series RLC resonant circuit. Hereby, the inductance and the capacitance are matched to generate a current with a frequency of 50 Hz. In order to test different breaking current values, the initial charging voltage of the capacitor bank $U_{\mathrm{b},0}$ is varied due to its proportional relationship with the current. In [IEC08] the rated breaking currents are specified for a rated voltage of 72.5 kV as 10 A for overhead lines, 125 A for cables and 400 A for capacitor banks.

For single-phase capacitive current switching tests the peak value of the recovery voltage is determined as follows [ABB14, GKS02]:

$$\hat{u}_{\mathrm{rv}} = k_{\mathrm{c}} \cdot 2 \cdot \frac{\sqrt{2}}{\sqrt{3}} \cdot U_{\mathrm{r}}. \tag{4.1}$$

It corresponds to the phase-to-ground peak value of the rated network voltage, i.e., to 1 p.u., and is doubled by the equal level of direct voltage trapped on the capacitive load. For single-phase testing a capacitive voltage factor k_{c} is added. It takes into account the additional voltage increase in three-phase systems, which depends on the type of grounding in the network. For example, a factor of 1.4 is defined for capacitor bank applications with isolated neutral. The highest value is given by 1.7, which also takes into consideration the presence of a nearby earth fault. Even though this special case is rarely applied for standardised capacitive current switching tests, it was taken as a reference for the design of the test circuit used within this work. As a result, for the rated voltage of 72.5 kV a maximum value of $\hat{u}_{\mathrm{rv}} \approx 201$ kV is given. Furthermore, as required by the standard the decay of the direct voltage component is less than 10 % for a time period of at least 300 ms after arc extinction [SvK+15, Bau17, IEC08].

To generate the characteristic $[1 - \cos(\omega t)]$ wave shape of the recovery voltage, a direct voltage source is connected in series to an alternating voltage source.[21] Thereby, each voltage source has to supply a potential difference of approximately 100 kV. The alternating voltage is generated by a high-voltage test transformer that obtains its reference signal via a sine wave signal generator.[22] The generation of the direct voltage is accomplished by a voltage multiplier that is supplied by batteries via an inverter.[23] An additional capacitor with a capacitance of $C_{\mathrm{dc}} = 626\,\mathrm{nF}$ is connected in parallel to the direct voltage source to decrease the decay of direct voltage over time. Beyond that, it reduces the alternating voltage drop across the direct voltage source.[24] A damping resistor $R_{\mathrm{d}} = 50\,\mathrm{k\Omega}$ is used as a protection measure during a dielectric breakdown [Bau17].

Prior to the test procedure the selection switch $\mathrm{S_{sel}}$ is connected to the breaking current source. The auxiliary breaker $\mathrm{S_{aux}}$ and the VI are in their closed positions. Once the breaking current capacitor bank C_{b} and the direct voltage capacitor C_{dc} are fully charged and the hydraulic drive system reaches its target pressure, the control system initiates the switching sequence for the test.[25] At $t = 0\,\mathrm{s}$ the trigger signal for the data aqcuisition (DAQ) is given. At $t = 5\,\mathrm{ms}$ the current making switch $\mathrm{S_{ion}}$ connects the current source to the VI, and the breaking current i_{b} is realised for one full current cycle as is shown in Figure 4.5. The magnitude of the current is slightly higher during the positive half cycle compared to the negative half cycle. This reduction is caused by ohmic losses in the current path. Since the second half cycle contains the moment of the VIs contact separation, the characteristic value for breaking current is derived only for this half cycle. A sufficiently accurate determination of the root mean square value is given by

$$I_{\mathrm{b}} = \frac{\hat{\imath}_{\mathrm{b}}}{\sqrt{2}}. \tag{4.2}$$

The period of time between the adjustable moment of contact separation t_{open} and the next current zero crossing at time instant t_0 determines the arcing time of the VI. In order to isolate the current source from the high recovery voltage, $\mathrm{S_{aux}}$ is opened shortly before

[21] The initial balancing process at the beginning is of no concern, since it only increases the probability of re-ignitions [SvK+15].

[22] The waveform generator is connected via a pre-amplifier, a power amplifier stack and an insulation transformer to the high-voltage test transformer.

[23] The power supply has to be realised on the high potential side of the alternating voltage source.

[24] A capacitive divider is formed between the inherent capacitance of the direct voltage source and primarily the coupling capacitor C_{cc}.

[25] The switching sequence is synced to the primary voltage of the high-voltage test transformer.

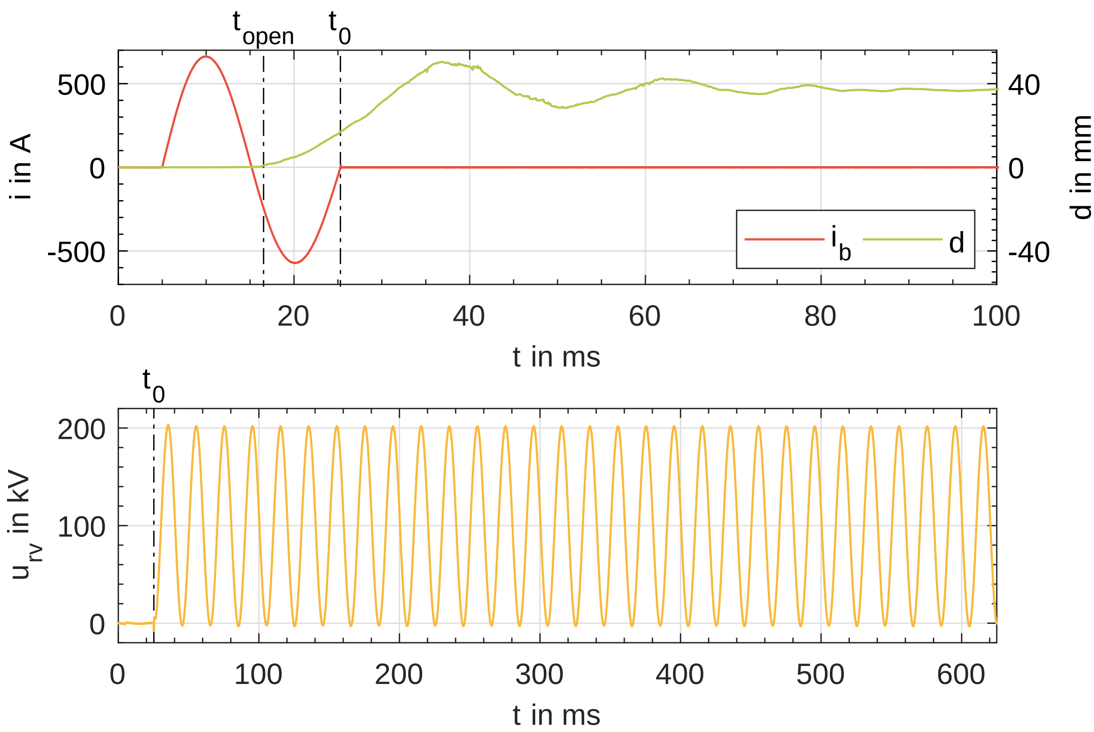

Figure 4.5: Oscillograms of an exemplary breaking test

the current zero crossing.[26] The voltage making switch S_{uon} is timed to reach its closed position at the moment of natural zero crossing.[27] From then on, the recovery voltage is applied for at least 600 ms.[28] Typically, the voltage peaks remain above 201 kV over the entire duration of the breaking test. However, in case of currents arising in the range of several milliamperes, e.g. caused by field emission, the voltage peaks can drop by a few kilovolts because of the higher load on the low power alternating voltage source and the increased discharge of the direct voltage source capacitance C_{dc} [Bau17].

4.5 Measurement systems and data acquisition

The DAQ is accomplished by two different devices: the *PXI–6123 (National Instruments)* and the digital storage oscilloscope (DSO) *WaveSurfer 3024 (Teledyne LeCroy)*. Their

[26] Thereby, the influence due to arcing in S_{aux} is kept at a minimum while ensuring a sufficient gap spacing during the first rise of recovery voltage.
[27] Premature current zero crossing because of current chopping is disregarded.
[28] The transient balancing process at the beginning of the recovery voltage is not included, since this phenomenon is mainly related to re-ignitions and thus is of no interest for this investigation.

Table 4.2: Main specifications of DAQ devices [Nat05, Tel15]

	PXI–6123	Wavesurfer 3024
Manufacturer	National Instruments	Teledyne LeCroy
Vertical resolution	16 bit	8 bit
Sampling rate	500 kS/s	up to 4 GS/s
Memory	32 MS	10 MS
Phys. bandwidth	511 kHz	200 MHz
Input impedance	100 MΩ || 10 pF	50 Ω or 1 MΩ || 16 pF
Input range	±10 V	±5 V (50 Ω) or 400 V (1 MΩ)

Table 4.3: Main specifications of measurement sensors

Signal name	Measurement principle	Model name	Uncertainty
i_{m}	Rogowski current transducer	PEM CWT 150	±1 %
i_{b}	Hall effect current transducer	LEM HTA 1000–S	±1 %
u_{rv}	Resistive-capacitive voltage divider	North Star VD–150	±1 % (10 Hz – 1 MHz)
d	Linear transducer	Penny & Giles SLS190–50, Ixthus Instrumentation KTC–75–P	±1 mm ±1 mm
i_{sense}	Sense resistor	–	±1 %
u_{cc}	PD measurement impedance	Omicron CPL 542A	–

specifications are listed in Table 4.2. Both are placed inside the measurement cabin. The measurement signals are transmitted via coaxial cables to the DAQ devices except for the coupling capacitor signal u_{cc}, which is transferred via a fibre optic cable. The digitisation of u_{cc} is conducted by the DSO, as this measurement demands a high sampling rate, whereas all other signals are recorded by the *NI–6123*. Subsequent to testing, the recorded signals are processed and analysed with the software *MATLAB*® [Bau17].

All measurement signals with their associated measurement principles are listed in Table 4.3. The making current i_{m} and the breaking current i_{b} are measured in the return wire of their respective current source. For the measurement of the recovery voltage u_{rv} a resistive-capacitive voltage divider with a ratio of 10000:1 is used. Since the DAQ device has an input voltage range limited to ±10 V and an input impedance of 100 MΩ, an additional

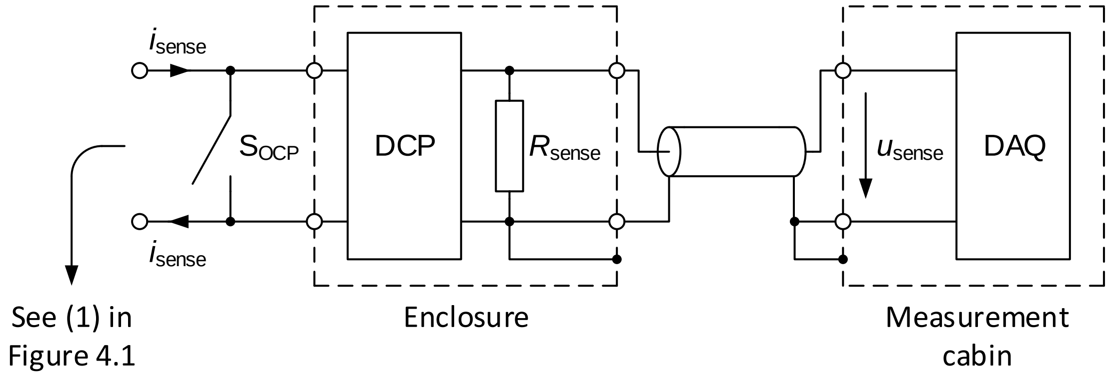

Figure 4.6: Measurement setup for the measurement of field emission currents

feed-through terminal is used to divide the voltage by a further ratio of 3:1 and to adapt to the required input impedance of 1 MΩ [Nor13]. For the measurement of contact gap the linear transducer *SLS190–50* was exchanged early during the course of the investigation by the *KTC–75–P* because of its insufficient stroke length. The measurement systems for capturing pre-breakdown phenomena are described in more detail in the following sections.

4.5.1 Field emission current measurement

Emerging field emission currents are captured by the current sense resistor R_{sense} in the low potential return wire of the VI. Typical field emission currents are in the range of up to several milliamperes and thus much smaller than the applied breaking and inrush currents. To protect the measurement system against the latter two currents, two separate bypassing switches are connected in parallel, which function as an overcurrent protection (OCP). This protection measure is represented by S_{OCP} in Figure 4.6. The discharge current protection (DCP) protects the measurement system in the case of a dielectric breakdown.[29]

For the relevant frequency range up to a few kilohertz the resulting voltage drop across the sense resistance can be satisfactorily transferred to the appropriate current by applying Ohm's law:

$$i_{\text{sense}} = \frac{u_{\text{sense}}}{R_{\text{sense}}}. \tag{4.3}$$

Throughout this work different resistance values (466.8 Ω, 249.4 Ω and 166.8 Ω) have been

[29] Further information regarding the operating principle of these protection measures can be found in [Bau17].

applied to adjust the measurement range accordingly.[30]

The measured field emission current i_{fe} is superimposed by a capacitive current i_C because of the capacitive behaviour of the VI. Additionally, a small leakage current across the low conductive ceramic body of the VI is present [Sla08]. Since this resistive current is smaller by several orders of magnitude compared to the other currents, it is negligible. The field emission current is therefore given by

$$i_{\mathrm{fe}} \approx i_{\mathrm{sense}} - i_C = i_{\mathrm{sense}} - C \cdot \frac{\mathrm{d}u_{\mathrm{rv}}}{\mathrm{d}t}. \tag{4.4}$$

Similar to the approach suggested in [Koo11] and [Bau17], a self-created software solution is used to attain i_{fe} from i_{sense}. For this, a compensation current signal $i_{C,\mathrm{equ}}$ is computed that should ideally be identical to i_C. The waveform of $i_{C,\mathrm{equ}}$ is obtained by numerical derivation of the measured recovery voltage signal u_{rv}.[31] Afterwards, a potential set of compensation currents with varying amplitude within the expected range for the capacitance C is generated. The equivalent compensation capacitance C_{equ} stems from the computed current signal

$$i_{\mathrm{comp}} = i_{\mathrm{sense}} - i_{C,\mathrm{equ}} = i_{\mathrm{sense}} - C_{\mathrm{equ}} \cdot \frac{u(t+\Delta t) - u(t-\Delta t)}{2 \cdot \Delta t} \approx i_{\mathrm{fe}} \tag{4.5}$$

that contains the lowest remaining signal energy in this set.

Two examplary capacitive current compensation results are shown in part (a) of Figure 4.7. At the beginning of the recovery voltage the displacement of the separating contacts and the following balancing process result in a fluctuating change of the VIs inherent capacitance. This dynamic change affects the quality of the compensation up to approximately 100 ms, until the contact system reaches its static state. Therefore, for the the detection of field emission current a threshold level of 100 µA is defined for the automated data analysis. The resulting zero line of i_{fe} in the upper diagram reveals the absence of field emission current, whereas in the lower diagram a current with peak values of approximately 800 µA is present. Its peaks are in phase with the peaks of the recovery voltage during steady state. By fitting the highlighted area of data into a FN-plot, see part (b) in Figure 4.7, a linear dependency is obtained. This demonstrates that this current characteristic can be assigned to the field emission effect.

[30] The total sense resistance consists of three resistors in parallel. A sense resistance of 466.8 Ω corresponds to a measurement range of ±21 mA, 249.4 Ω to a range of ±40 mA and 166.8 Ω to a range of ±60 mA.

[31] The derivative is calculated by the central difference approximation of the smoothed recovery voltage signal.

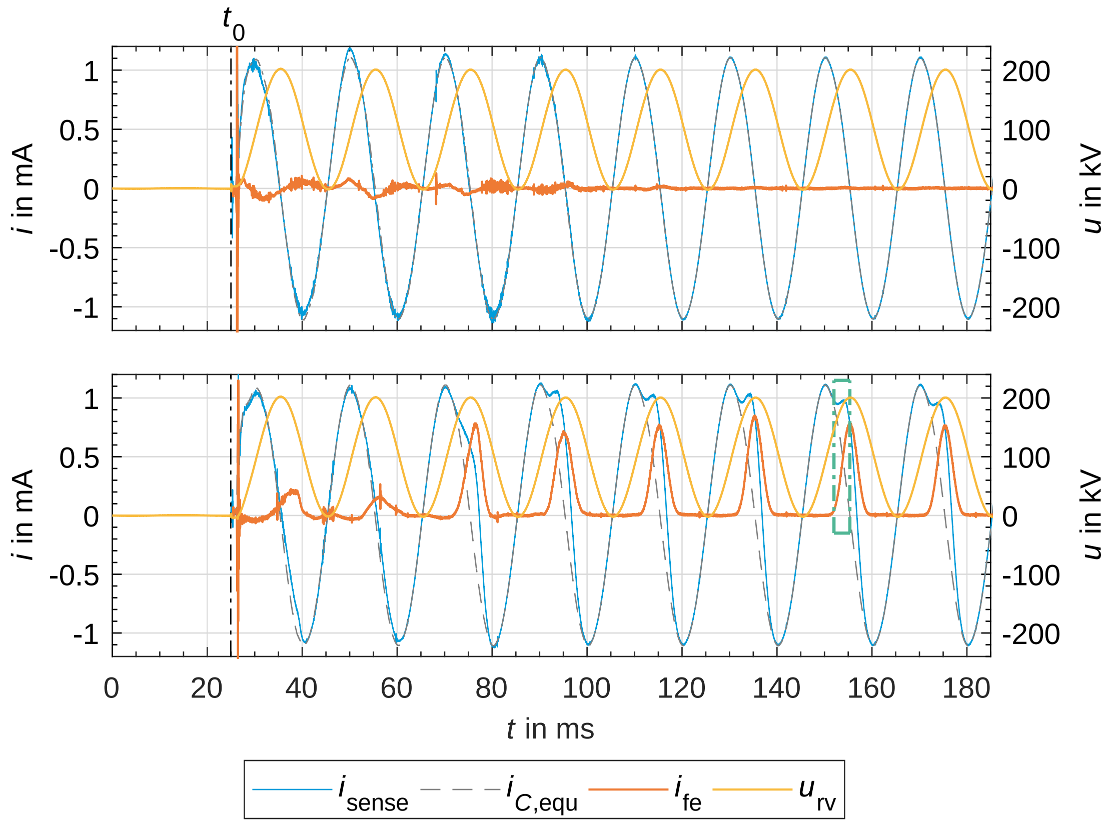

(a) Two exemplary breaking tests with different software compensation results

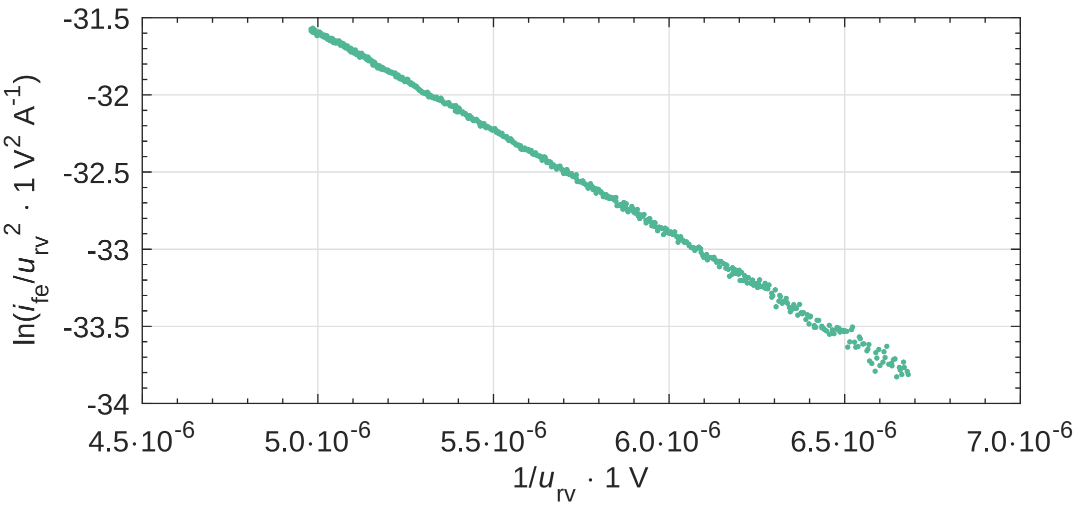

(b) FN-Plot for the data selected by the area in (a)

Figure 4.7: Software compensation result for field emission current

4.5.2 Microparticle detection measurement

Optical measuring methods are commonly applied to study microparticle movement in vacuum gaps, see e.g. in [YWC+20], [EKH+19] and [SKF00]. However, this approach is unfeasible with commercially applied VIs because of their non-transparent ceramic housing and completely closed metal vapour shields. Therefore, a different method for the detection of traversing microparticles is proposed in [BSH15], which is further discussed in [SHT16] and [Bau17]. In these contributions, a measurement setup commonly applied for partial discharge measurements is suggested. For this approach to work, it must be ensured that the test environment guarantees both a sufficiently low partial discharge level and a sufficiently low electromagnetic interference level, which was demonstrated in [Bau17] for the given test circuit.

Once a charge, in this case a charged microparticle, starts moving in the space of an electric field, a high frequent current is induced through the external circuit over the course of its transit and impact [Sho38]. Because of the comparatively high impedance of the recovery voltage source, the effective current source for this current consists primarily of the stray capacitance in the VIs surrounding. By connection of the low impedance coupling capacitor C_{cc} in parallel to the VI, part of this current is expected to be supplied by this capacitor as well. This current component i_{cc} is then converted to a voltage signal u_{cc} by the measuring impedance connected in series to the capacitor, see Figure 4.8 for reference. Within this work, the quadripole measurement impedance *Omicron CPL 542* with a frequency range of 0.02 MHz to 5 MHz is used [Bau17, Omi17]. In addition, the fibre optic transmission system *HBM ISOBE5600* is integrated into the transmission path to reduce signal losses and to avoid electromagnetic interferences by ground loops [SK11]. Because the measuring impedance needs to be terminated with 50 Ω, a feed-through termination is connected in between. The surge impedance of the intermediate coaxial cable is also 50 Ω. A high sampling rate is required to capture the measurement signal in the time domain with a sufficiently high temporal resolution. Futhermore, the signal has to be recorded over several hundreds of milliseconds. Since the memory space of the DSO is limited to 10 MS a trade-off between sampling rate and recording length becomes necessary. For the measurement of the microparticle detection the recording length is adjusted to 500 ms with a sample rate of 20 $\mathrm{MS\,s^{-1}}$.

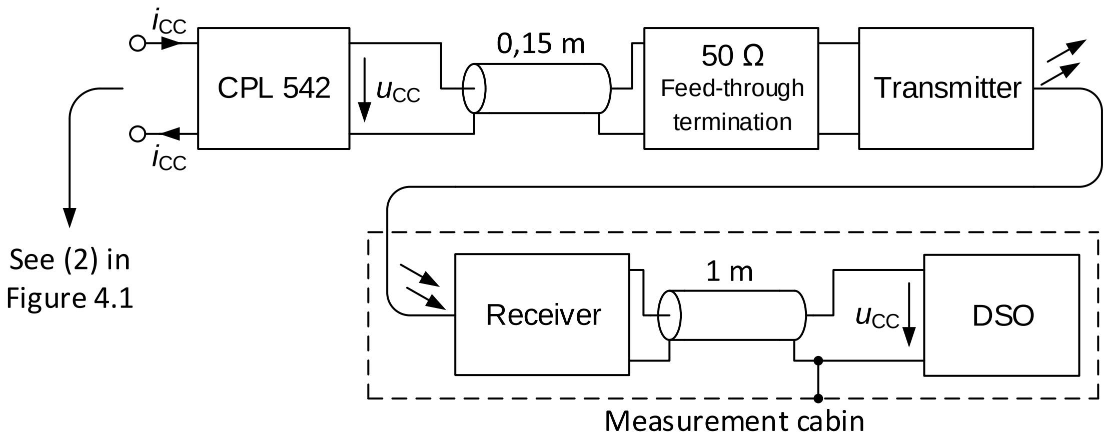

Figure 4.8: Measurement setup for the microparticle detection

5 Experimental methodology

For the investigation of the rarely occurring late breakdown phenomenon, a high number of tests is required in order to derive statistically realiable results. Since only a certain number of tests can be performed with the test circuit in a defined time window, time is the limiting factor. To reduce the time demand of experiments as far as possible and thus increase efficiency, a test procedure shall be developed that increases the probability of late breakdowns within the most realistic possible conditions of the capacitive switching case. Especially in newly developed systems or processes, such as the present newly developed synthetic test circuit, the impact of various factors and their interaction on the response are often unknown. Therefore, experiments to identify and analyse their influence are essential. The Design of Experiments (DOE) is an efficient statistical method for the planning, implementation, data analysis and interpretation of such experiments. Within this work concepts provided by DOE are adopted to efficiently analyse the effect of different factors that can be varied realiably with the test circuit on the late breakdown behaviour of 72.5 kV VI.

Various experiment designs are provided by DOE. In this research factorial designs are applied. Therefore, this chapter introduces the basics of factorial designs and describes their respective strengths and drawbacks. Statistical aspects with regard to the analysis of the breakdown behaviour, which is characterised by the breakdown rate, are discussed afterwards.

5.1 Factorial designs

In a full factorial design all possible combinations between factor settings are examined. Even though several factors are varied simultaneously, their respective effect on the response can be clearly attributed. Furthermore, this type of design allows for the estimation of interaction effects. An interaction is present, when the effect of one factor depends on the setting of another factor. This cannot be accomplished in experiments with only one factor varied at a time. Apart from that, the successive variation of only one factor at a time with the other factors held constant refers to just a single reference point. However, this does not allow for statements how a system or a process behaves at other reference points. Therefore, this approach is less efficient compared to factorial designs. The levels l_i of a factorial design with k factors denote the number of settings for each factor i. They can either contain quantitative or qualitative characteristics. The resulting factor combinations are also referred to as treatments. The total number of treatments equal to the total number of experimental runs N is derived by the multiplication of the levels:

$$N = \prod_{i=1}^{k} l_i. \tag{5.1}$$

If the number of levels is chosen to be equivalent for each factor, Equation 5.1 can be simplified to

$$N = l^k. \tag{5.2}$$

It follows that with an increasing number of factors or levels the factorial design increases rapidly. In a first step, the minimum number of levels, which is two, is typically specified for each factor. This results in a 2^k full factorial design that is especially useful in the early stages of an empirical investigation to determine which factors affect the response. Since just two settings exist for each factor, only linear relationships for the response can be determined. However, more in-depth testing with the remaining, significant factors can be conducted afterwards [Mon12, SvBH17].

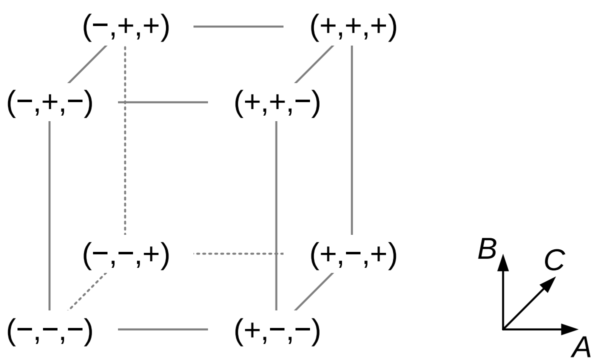

Figure 5.1: Visual representation of a 2^3 full factorial design

Hereinafter, the construction of this type of design shall be explained by a 2^3 full factorial design. Hereby, the influence of three factors A, B and C shall be investigated. This results in a total of eight different treatments or runs. The design can be represented geometrically as a cube, see Figure 5.1. Each axis represents one factor, and each corner denotes one treatment. For reasons of clarity, the low and high level for each factor is coded as "−"

Table 5.1: Design matrix of a full factorial 2^3 design

Run	Treatment	$\boldsymbol{A}$	$\boldsymbol{B}$	AB	$\boldsymbol{C}$	AC	BC	ABC	Response
1	(1)	$-$	$-$	$+$	$-$	$+$	$+$	$-$	y_1
2	a	$+$	$-$	$-$	$-$	$-$	$+$	$+$	y_2
3	b	$-$	$+$	$-$	$-$	$+$	$-$	$+$	y_3
4	ab	$+$	$+$	$+$	$-$	$-$	$-$	$-$	y_4
5	c	$-$	$-$	$+$	$+$	$-$	$-$	$+$	y_5
6	ac	$+$	$-$	$-$	$+$	$+$	$-$	$-$	y_6
7	bc	$-$	$+$	$-$	$+$	$-$	$+$	$-$	y_7
8	abc	$+$	$+$	$+$	$+$	$+$	$+$	$+$	y_8

and "+", respectively.[32] The corresponding design matrix is shown in Table 5.1. Hereby, the run number represents the standard order of all treatments for this design. However, the run order may also be randomised to minimise the influence of systematic errors. A specific treatment can also be described by small letters. The presence of a letter refers to the high level of the corresponding factor, whereas the absence refers to the low level of the corresponding factor. If all factors are set to their low level, this is typically represented by "(1)". Besides the three factors four different interactions for a 2^3 full factorial design exist: three two-way interactions (AB, AC and BC) and one three-way interaction (ABC). Their associated columns can be derived by multiplication of the corresponding factor signs. For example, the two-way interaction column AB is generated by the multiplication of the signs in column A and B. All column vectors are orthogonal, which allows for the independent estimation of effects. An effect characterises the change in response caused by the change in the level of factors or interactions. Main effects are allocated to just one factor, whereas effects resulting from interactions are termed interaction effects. Any of these effects are calculated by the averaged responses containing a plus sign subtracted by the averaged responses containing a minus sign in their respective columns:

$$\text{Effect}(x) = \overline{y}_{x+} - \overline{y}_{x-} \tag{5.3}$$

For example, the effect of factor A is derived as follows:

$$\text{Effect}(A) = \overline{y}_{A+} - \overline{y}_{A-} = \frac{1}{4}(y_2 + y_4 + y_6 + y_8) - \frac{1}{4}(y_1 + y_3 + y_5 + y_7). \tag{5.4}$$

Thus, for every factor and interaction four responses at the low or the high level are available for the estimation of the corresponding effect, even though only eight experimental runs have to be conducted [Mon12, SvBH17].

[32]Alternatively, the levels can also be coded as "−1" and "+1" or as "0" and "1".

If more than three factors shall be investigated, the required number of runs can be reduced by the application of fractional factorial designs. These designs only use a subset of the full factorial design at the expense of confounding. Confounding means that factors and interactions share the same column vectors. Thus, their corresponding effects cannot be estimated independently from each other anymore. Instead, the calculated effect is made up of the sum of their respective effects. However, most systems or processes are primarily determined by main effects and low-order interactions, whereas effects of higher-order interactions are typically insignificant.[33] This circumstance can be used to apply this type of design efficiently with only a minimum loss of information. The design of a fractional factorial experiment is represented by 2^{k-p} with 2^{-p} signifying the fraction of the full factorial [Mon12, SvBH17].

In the following, the construction of a fractional factorial design shall be explained with the example of a $2^{4\text{-}1}$ design. Four factors with two levels will result in 16 treatments if the full factorial design is applied. This can be illustrated geometrically by two cubes with each corner matching one treatment, see Figure 5.2. Hereby, the low and high level of the newly added fourth factor D are represented by each cube, respectively. Besides the four factors eleven potential interactions exist: Six two-way interactions (AB, AC, AD, BC, BD, CD), four three-way interactions (ABC, ABD, ACD, BCD) and one four-way interaction ($ABCD$). This amounts to 15 possible effects. For a one-half fraction of the full design, the number of runs is reduced by half to eight runs, which is equivalent to the previously presented 2^3 full factorial design. Hence, the previously described design can be utilised to construct the new fractional factorial design [Mon12, SvBH17].

With the first three factors A, B and C already included in the 2^3 design, only the new factor D has to be incorporated into the $2^{4\text{-}1}$ design. Since all orthogonal column vectors are already occupied, this factor has to be confounded with one of the effect columns. The best result is attained by confounding the factor D with the highest order interaction, which in this case is ABC.[34] The corresponding design matrix is shown in Table 5.2.[35] It can be seen that each main effect is now confounded with one three-way interaction, and each two-way interactions is confounded with another two-way interaction. Since the three-way interactions are unlikely to affect the response, the estimation of the main effects can be considered to be unimpaired by the present confounding. However, a clear distinction between the two-way interactions is not possible anymore. Even though information about interactions is lost, it is still an efficient approach to determine the most important

[33]This is referred to as the sparsity-of-effects principle.
[34]The added factor may be confounded with any interaction or factor. However, this would always result in a less efficient fractional factorial design because of the confounding with lower-order interactions.
[35]In Figure 5.2 the omitted treatments in the reduced design are labelled in grey for reference.

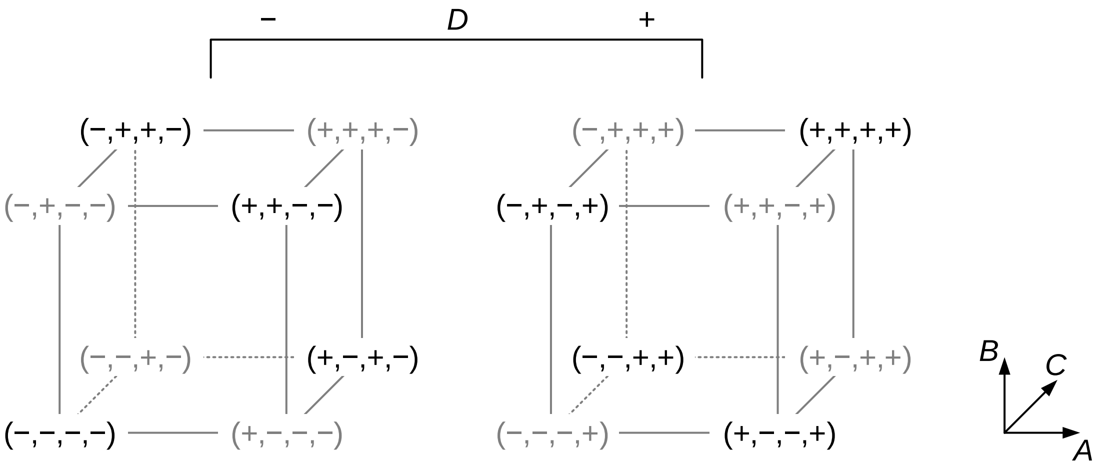

Figure 5.2: Visual representation of a full factorial design with four factors - Treatments labelled in grey font depict the omitted experimental runs in a $2^{4\text{-}1}$ fractional factorial design

Table 5.2: Design matrix of a fractional factorial 2^{4-1} design

Run	Treatment	$\boldsymbol{A}$ BCD	$\boldsymbol{B}$ ACD	AB CD	$\boldsymbol{D}$ ABD	AC BD	BC AD	ABC $\boldsymbol{D}$	Response
1	(1)	−	−	+	−	+	+	−	y_1
2	*ad*	+	−	−	−	−	+	+	y_2
3	*bd*	−	+	−	−	+	−	+	y_3
4	*ab*	+	+	+	−	−	−	−	y_4
5	*cd*	−	−	+	+	−	−	+	y_5
6	*ac*	+	−	−	+	+	−	−	y_6
7	*bc*	−	+	−	+	−	+	−	y_7
8	*abcd*	+	+	+	+	+	+	+	y_8

influencing factors in a first step. On that basis, further experiments can be developed and optimised in an iterative process to obtain additional information. For example, the missing treatments may be applied in a second experiment to achieve the full factorial design, which would then allow for the estimation of all interaction effects. Alternatively, adjustments for one or more factors can be made, new factors be added or unimportant factors be removed [Mon12, SvBH17].

Based on the results obtained by factorial designs, linear regression models can be developed to estimate and predict the behaviour of the analysed system or process and statements about the variability of data can be made. However, the relevant statistical methods will not be explained in further detail at this point.

5.2 Statistical analysis on the dielectric performance of a VI

If electrical equipment, in this case a VI, is stressed dielectrically by a high voltage, a breakdown may randomly occur at different time instants. This happens because of the randomness of physical processes that take effect during the evolution of a breakdown. But even without a breakdown the properties of the interrupter unit might be affected by the applied stress. Therefore, the phenomenon of dielectric breakdown has to be treated statistically. In capacitive current switching tests specified by the standards, e.g. IEC 62271-100, a mandatory number of restrikes in a test series of repeated current and voltage stresses must not be exceeded in order to pass the test. Since restrike-free circuit breakers are considered virtually impossible, two classes of capacitive switching performance are defined by the standard. These classes require certain type tests with multiple switching operations that shall prove either low or very low probabilities of restrike [IEC08]. In any single test two possible outcomes may occur: either a breakdown event or the complement, a withstand event. The outcome of a single test is therefore dichotomous and is considered a bernoulli trial in statistical terms. If the constant voltage stress is repeatedly applied for n times, a relative breakdown frequency h_n can be derived by

$$h_n = \frac{k}{n} \tag{5.5}$$

with the number of breakdowns equal to k. With an infinite number of trials this breakdown rate would eventually become the breakdown probability p:

$$\lim_{n \to \infty} h_n = p \tag{5.6}$$

Therefore, with an increasing number of trials the estimation of the true breakdown probability of occurence becomes more exact. A binomial probability distribution for repeated bernoulli trials can be presumed if independence between each trial is given. Two events are considered indepent from each other if the former event does not influence the result of the subsequent one. One way to verify this precondition is to examine the response data for possible trends. If a clear trend is apparent, the condition for independence between trials cannot be satisfied and thus basic statistical analysis is not permitted anymore [HM84, HL14].

6 Investigation of breakdown behaviour

The synthetic test circuit allows for the variation of several parameters related to capacitive switching. In the following sections, a varying set of parameters is selected for each experiment in order to determine their respective effect on the breakdown behaviour, which is quantified by the breakdown rate. These parameters require a reliable adjustment over many switching tests, while simultaneously allowing for their variation in a reasonable period of time. Pre-breakdown effects found in the experiments are not part of this chapter and are treated separatedly in the following chapter.

The conducted experiments can be categorised as follows:

- An initial factorial experiment on one test sample to determine the dielectric performance at a contact stroke of 38 mm.
- Further experiments conducted at a reduced contact stroke of 20 mm. These are subdivided into a preliminary experiment and a main experiment:
  - The preliminary experiment is conducted on a new test sample to gain a first insight into the breakdown behaviour at the reduced contact stroke.
  - The main factorial experiment is an extensive investigation with three test samples to quantify the breakdown rate for the selected influencing factors with a higher statistical accuracy. The final design choice of this experiment is based on the results of the previously conducted experiments.

All tests are performed with identical 72.5 kV VIs. The test samples have been provided by Siemens AG. Each VI has gone through a regular production process during manufacture including a subsequent conditioning process.

A disruptive discharge during testing will be referred to as breakdown, voltage breakdown or dielectric breakdown. Furthermore, if a breakdown occurs after the recovery voltage has reached its first peak, this is considered a late breakdown (LBD). However, because of the synthetic test method a distinction between restrikes and NSDDs cannot be made [Bau17].

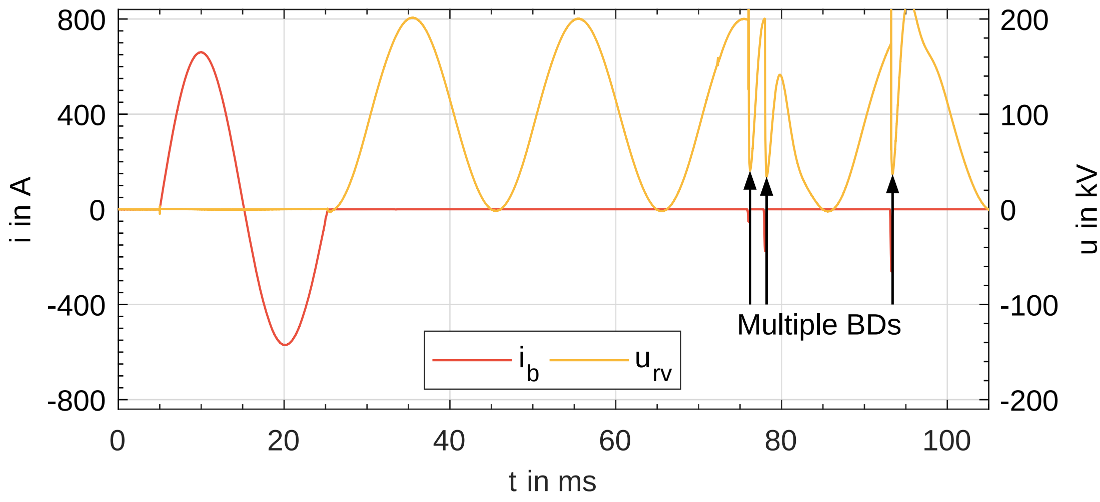

Figure 6.1: Exemplary measurement result with multiple breakdowns

Although the recovery voltage level is known to impact the breakdown behaviour as well, all breaking tests are performed at the highest possible recovery voltage of approximately 201 kV. Lower voltage levels are excluded from testing, because even at the highest voltage level minor breakdown probabilities are expected.

6.1 Factorial experiment at a contact stroke of 38 mm

For the following test runs an untested VI is installed. This test sample is referred to as TS1. The total stroke is set to 38 mm. The hydraulic drive provides an average opening speed of 2.5 m s^{-1} and an average closing speed of 0.2 m s^{-1} during the tests.

Prior to the experiment 192 commissioning tests with varying test parameter settings are performed on TS1. Among them, a long-term test is conducted to verify compliance with legal X-ray emission limits. Simultaneously, the reliability of various parameter settings is improved, and several initial defects are remedied in order to guarantee the execution of subsequent tests as error-free as possible.

Ten of the commissioning tests include breakdown events. The earliest breakdowns occur during the first rise of recovery voltage but later than 5 ms after current interruption. The latest LBD appears during the 15th voltage cycle, 288 ms after current interruption. Repeated breakdowns during one voltage cycle and multiple breakdowns in different voltage cycles are recorded. A measurement example including both occurrences simultaneously is illustrated in Figure 6.1. During the third voltage cycle two successive breakdowns occur that are followed by a third one during the next recovery voltage cycle. Only the first voltage breakdown is considered for further data analysis.

6.1.1 Experiment design

As the previously conducted commissioning test results have shown, only a low breakdown rate can be expected with the VIs. Therefore, the main goal of the experiment is to find a set of test circuit parameter settings within the capacitive switching case that maximises the occurence of LBD. This is to be achieved by determining how different settings of potential influencing factors affect the breakdown rate. For the experiment, the following factors and settings are chosen for a two-level factorial experiment design:

- **Breaking current**: The higher current level is set to a root mean square (RMS) value of 400 A, which corresponds to the rated back-to-back capacitor bank breaking current defined by [IEC08]. For the lower level the RMS value of 45 A is chosen, which is in the range of common unloaded transmission line currents.[36] Zero current stress is excluded in order to guarantee the occurence of arcing, which is deemed necessary for the investigation of the following factor.

  Underlying hypothesis: If a lower breaking current is applied during contact separation, fewer cathode spots should evolve that can smoothen protrusions on the cathode surface. Hence, a less conditioned cathode of the VI should result in a higher breakdown probability.

- **Arcing time**: The arcing time is typically defined as the time interval between arc initiation and arc extinction. Since the arc voltage is not recorded during testing, this information cannot be obtained. Therefore, the interval between the moment of contact separation up to the next current zero crossing is used as an approximate reference. The level settings for the arcing time are only defined for time intervals in the range of milliseconds because of the unavoidable scatter of switching delay with the available operating mechanism. A short arcing time is specified up to 3 ms, whereas a long arcing time has to exhibit a duration of at least 7 ms. This provides a minimum time gap of 4 ms between both settings.

  Underlying hypothesis: If the duration of arcing is shorter, less conditioning should occur. This is directly connected to the previous hypothesis.

[36] This current value also corresponds to the lowest value that can be reliably and accurately set by the test circuit.

- **Inrush current**: The VI is either stressed by an inrush current during closing or it is closed without a current prior to the breaking test.

  Underlying hypothesis: If the VI is pre-stressed by a severe inrush current, the high energy should result in a deconditioning effect by welding of the contact surfaces.

- **Mechanical stop**: The originally mounted mechanical stop made of PTFE with a thickness of 5 mm is replaced by an evenly thick disc made of brass in the mechanical chain of the hydraulic drive.

  Underlying hypothesis: If the dampening with different mechanical stops is decreased during contact separation, the higher induced mechanical shock should increase the probability of microparticle release, which in turn enhances the breakdown probability.

Other factors that may influence the dielectric breakdown behaviour are conceivable as well. One example is the polarity, which is kept constant during all tests. As a result, arcing during current interruption always occurs during the negative current half-wave and the subsequent unipolar recovery voltage always is of positive polarity. This way, the moveable and fixed contact are only ever stressed in the same manner. However, switching the polarity could cause differences in pre-breakdown phenomena like field emission, since the emitting sites always originate on the cathode. Furthermore, the orientation of the VI could also influence pre-breakdown phenomena. Due to gravitational effects, particles may be present in different areas of the VI when the VI is aligned vertically as opposed to horizontally. Moreover, different speeds during contact separation change the mechanical stresses that in turn can affect the extent of microparticle release. However, these potential influencing factors can only be adjusted with considerable time expenditure or are not technically feasible within the scope of the investigation and thus have not been considered any further.

With the four defined factors, a $2^{4\text{-}1}$ fractional factorial design with only eight different treatments is applied to reduce the number of possible treatments while maintaining good information about the main effects. The corresponding factor settings for each run are listed in Table 6.1. Because of the effort to modify the drive system, the run order of treatments is not randomised but sorted in a way that the mechanical stop is replaced only once.

6.1.2 Experiment results

The resulting breakdown rate is shown in the last column of Table 6.1. Each treatment run, except for the last one[37], is repeated 39 times, resulting in a total of 283 breaking tests. Every factor is adjusted to a specific level four times during the experiment, resulting in 127 up to 156 breaking tests for every factor at each individual level.

Table 6.1: Result of the factorial design experiment at full contact stroke

Run order of treatments	Breaking current I_b in A	Arcing time t_arc in ms	Inrush current $\hat{\imath}_\mathrm{m}$ in kA	Mechanical stop	Breakdown rate
1	400	≥ 7	0.0	PTFE	0/39
2	400	≤ 3	16.5	PTFE	3/39
3	45	≤ 3	0.0	PTFE	0/39
4	45	≥ 7	16.5	PTFE	0/39
5	45	≤ 3	16.5	Brass	1/39
6	45	≥ 7	0.0	Brass	0/39
7	400	≥ 7	16.5	Brass	0/39
8	400	≤ 3	0.0	Brass	0/10

According to the previously outlined underlying hypotheses run no. 1 is considered the *best-case* treatment of the VI, for which the lowest breakdown probability is expected. On the contrary, run no. 5 is expected to be the *worst-case* treatment of the VI with the highest number of breakdowns. However, only four voltage breakdowns are recorded in total during this experiment with three breakdowns during treatment no. 2. One breakdown during this run occurs at the peak of the 5th voltage cycle and is therefore considered a LBD. All the other breakdowns happen during the the first rise of recovery voltage, but later than one quarter cycle at mains frequency and voltages above 100 kV. Their contact gap at breakdown amounts to at least 7 mm, which corresponds to approximately 20 % of the total stroke. The averaged breakdown rate is about 3.7 times smaller compared to the previous commissioning tests. At this point, the underlying hypotheses are not confirmed, but they also cannot be rejected due to the small number of events and taking potential statistical dispersion into account. Even though all four tests with breakdowns have a short arcing time and a preceding inrush current in common, their influence on the breakdown behaviour cannot be verified as well.

In order to achieve a sufficient number of breakdowns for statistical analysis, the number

[37] The last treatment had to be aborted due to a larger partial damage to the test circuit. A continuation has been discarded, because a significant change of the outcome is deemed unlikely.

of repeated trials would have to be increased vastly. Since this approach would be too time-consuming, this issue is overcome by reducing the contact stroke to 20 mm for the subsequent investigations.

6.2 Factorial experiments at a contact stroke of 20 mm

6.2.1 Preliminary experiment

A new test sample TS2 is installed with the total stroke set to 20 mm. Furthermore, the making current source is modified in favour of a slightly higher peak value by replacing the air coil. This allows for peak values of approximately 20 kA instead of the previously achievable 16.5 kA, see Section 4.3 for reference. The variation of the mechanical stop is not included any further for two reasons. First, the high frequent vibrations that might be induced by this component cannot be quantified by measurements, whereas the low frequent vibrations are primarily affected by the contact-pressure spring. Second, replacements of the mechanical stop are very time-consuming in the long run, since these also require subsequent fine-tuning of the contact stroke. Therefore, only the originally installed mechanical stop made of PTFE is used hereafter.

Table 6.2: Result overview of the preliminary experiment

Run order of treatments	Breaking current I_b in A	Arcing time t_arc in ms	Inrush current $\hat{\imath}_\mathrm{m}$ in kA	Breakdown rate
1	45	≤ 3	20	2/39
2	400	≥ 7	0	2/39
3	45	≤ 3	20	1/39
4	400	≥ 7	0	1/39

Preceding the experiment, a short commissioning phase is conducted with the reduced contact stroke. During this commissioning five out of nine breaking tests include breakdowns. For the experiment, a significantly reduced experiment design is applied.[38] Only the assumed *worst-case* treatment, which is expected to increase the breakdown probability, is compared with the assumed *best-case* treatment. The factor level settings and the results are listed in Table 6.2. Both treatments, consisting of 39 repeated trials, are run once again. This results in a total of 156 breaking tests in the reduced experiment design.

[38] Simultaneously, a long term test is conducted to verify compliance with legal X-ray emission limits for the reduced contact spacing.

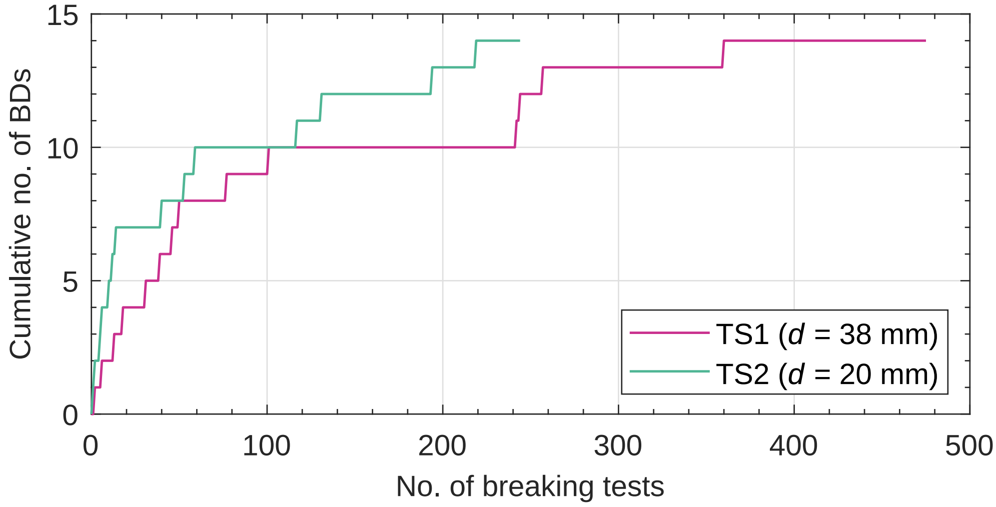

Figure 6.2: Cumulative number of breakdowns for test samples TS1 and TS2

It is apparent that the breakdown rate reveals no difference between the two different treatments, although decreasing to just one breakdown during the second run. Because of the small number of events no sound statement about the influence of the factor settings can be made at this point.

In Figure 6.2 the cumulative number of breakdowns for test samples TS1 and TS2 is shown including the commissioning tests previously carried out. The depiction highlights the difference in number of breakdowns per breaking tests for the different contact spacings. The reduction of contact stroke results in a higher breakdown yield for TS2, even though the difference is comparatively small with regard to TS1. Yet, a further reduction of contact stroke is discarded. Both curve shapes show a steep slope within their first hundred switching operations. From then on, the curves start to flatten. This trend indicates the presence of a conditioning effect, which substantially affects the response with increasing number of breaking tests. Furthermore, this trend seems to be independent of contact spacing and parameter variation.

6.2.2 Experiment design

Up to this point, the hydraulic drive only accomplishes very slow closing speeds of $0.2\,\mathrm{m\,s^{-1}}$. However, this speed is rather unlikely to be used for common operating mechanisms. Therefore, an overhaul of the hydraulic drive is realised prior to the main investigation to allow for the variation of closing speed.[39] This facilitates the integration of a new influencing factor:

- **Closing speed**: The average closing speed levels are set to $0.4\,\mathrm{m\,s^{-1}}$ and $1.2\,\mathrm{m\,s^{-1}}$.[40]

  Underlying hypothesis: The occurence of contact bouncing is intensified with increasing speed. This results in a higher mechanical stress and more rupture of the created weld spots during the repeated lift-off of the contacts, and thus, this should increase the contact wear.

Including this additional factor, the following four factors are selected for the final experiment: *breaking current*, *arcing time*, *inrush current* and *closing speed*. For the experiment, the total number of possible trials is estimated to a total of around 1200 tests due to time constraints. The following methods are applied to allow statements to be made about the variability of effects and the variability of the breakdown rate per treatment. They further shall help to reduce the potential influence of the conditioning effect observable in the previous results.

- **Test samples**: The experiment is conducted on three new test samples TS3, TS4 and TS5 to deduce the variability between identically manufactured VIs.
- **Randomisation and replication**: For each test sample the treatments of the factorial design are replicated four times. Within each replicate the treatments are randomised. Due to the replication each treatment is examinded at four different points of time during the successive switching operations, which increases robustness against the uncontrollable conditioning effect.

By defining the variables mentioned above, only the remaining variables, i.e., the number of treatments and the number of repeated trials per treatment, need to be weighed against each other. For a factorial design experiment with four factors, the number of possible combinations results in 16 treatments for a full factorial design and 8 treatments for the half fractional factorial design. As more trials per treatment allow for a more exact determination of the breakdown rate, this quantity shall be maximised within the given constraints. Consequently, a $2^{4\text{-}1}$ fractional factorial design is chosen in spite of confounding all two-way interactions. This concludes in the final experiment design consisting of:

[39] Within the scope of the overhaul the issue with the deviating delay times for the different speed settings could not be fixed. However, in the case of the inrush current making test this is of no concern, since the current flow is initiated by the pre-strike in the VI and therefore does not depend on a precise switching time unlike for breaking tests.

[40] As a result of the modification the former closing speed of $0.2\,\mathrm{m\,s^{-1}}$ could not be realised anymore. Higher closing speeds have not been applied because of the excessive mechanical stress on the acrylic glass housing.

$$3 \text{ test samples} \times 4 \text{ replicates} \times 8 \text{ treatments} \times 12 \text{ trials} = 1152 \text{ breaking tests}$$

As a result, a total of 48 trials per treatment and test sample is obtained. Each factor at a fixed level setting has a total of 192 breaking tests per test sample. Each replicate contains 96 breaking tests per test sample. The factors, their corresponding level settings and the resulting treatments for the $2^{4\text{-}1}$ design are listed in Table 6.3. The levels are coded in such a way that the "+"-setting represents the setting with the higher expected breakdown yield. The variables A, B, C and D are assigned to the factors *breaking current*, *arcing time*, *inrush current* and *closing speed*, respectively. This allows for the coding of the different treatments. Each treatment is composed of lower case letters. The presence of a lower case letter refers to the high level of the corresponding factor, whereas the absence refers to the low level of the corresponding factor. With all factors set to their low level, this treatment is represented by "(1)".

Table 6.3: Design pattern of the fractional factorial design at a contact stroke of 20 mm

Coded level setting	Breaking current I_b in A	Arcing time t_arc in ms	Inrush current $\hat{\imath}_\mathrm{m}$ in kA	Closing speed v_close in $\mathrm{m\,s^{-1}}$
−	400	≥ 7	0	0.4
+	45	≤ 3	20	1.2
Treatment	A	B	C	D
(1)	−	−	−	−
ad	+	−	−	+
bd	−	+	−	+
ab	+	+	−	−
cd	−	−	+	+
ac	+	−	+	−
bc	−	+	+	−
abcd	+	+	+	+

Table 6.4 shows the randomised run order of the treatments for the experiment. The generation of the randomised run order is achieved by a random permutation without repeating elements.

6.2.3 Experiment results

In the following, the results of the factorial experiments conducted on the test samples TS3, TS4 and TS5 are presented. First, a brief overview of the recorded breakdowns for

Table 6.4: Randomised run order of treatments for each replicate and test sample

Test sample	Replicate	Run order of treatments							
TS3	I	*ac*,	*bd*,	*bc*,	*abcd*,	*cd*,	(1),	*ad*,	*ab*
	II	*cd*,	*ad*,	(1),	*bc*,	*ac*,	*abcd*,	*bd*,	*ab*
	III	*bd*,	*bc*,	*ac*,	(1),	*ad*,	*ab*,	*cd*,	*abcd*
	IV	(1),	*ad*,	*ac*,	*cd*,	*bd*,	*bc*,	*abcd*,	*ab*
TS4	I	*ad*,	*abcd*,	*bd*,	(1),	*ac*,	*cd*,	*ab*,	*bc*
	II	*ac*,	(1),	*ab*,	*bd*,	*abcd*,	*bc*,	*ad*,	*cd*
	III	*bd*,	*ab*,	*bc*,	*ac*,	*abcd*,	*ad*,	(1),	*cd*
	IV	*ad*,	*ac*,	*bc*,	*bd*,	*ab*,	*abcd*,	*cd*,	(1)
TS5	I	*bc*,	*ac*,	*bd*,	*abcd*,	*cd*,	*ab*,	(1),	*ad*
	II	*cd*,	*ad*,	*ac*,	*ab*,	*abcd*,	*bc*,	(1),	*bd*
	III	*abcd*,	(1),	*ad*,	*bd*,	*ac*,	*cd*,	*bc*,	*ab*
	IV	*ab*,	*ac*,	(1),	*ad*,	*bc*,	*abcd*,	*cd*,	*bd*

the different treatments is given before the calculated effects for the individual factors are presented. Subsequently, further characteristic values from the various recorded measurement signals are examined in more detail with regard to the dielectric behaviour of the VIs. A discussion of the results then follows separately at the end of this chapter.

A tabular overview of all breakdowns is given in Table 6.5. The result is sorted by treatment, and the total number of dielectric breakdowns k is listed instead of the breakdown rate h_n. The breakdown rate per treatment, replicate and test sample is obtained by dividing by the number of repeated trials $n = 12$.

The results of the table show that the number of breakdowns varies over a wide range between the different treatments, but also between different replicates of the same treatment. On the one hand, for treatments "(1)" and *ab* by far the lowest number of breakdowns is given. In both cases, two out of three test samples do not exhibit a single breakdown during testing. On the other hand, treatment *ac*, which is the first conducted run of TS3, exhibits the highest breakdown yield of the entire experiment with a total of nine breakdowns. This is very noticeable, as the following replicates of the same treatment show only one to no breakdown. This strong deviation is also apparent in other cases, e.g., in treatment *bd* for TS5 with seven breakdowns during the first replicate and none during the others. Looking at the last column, which contains the sum of all breakdowns for each replicate, it can be seen that each replicate exhibits a highly varying degree of breakdowns. For TS3 and TS4 approximately 50 % and for TS5 60 % of all breakdowns occur during their first replicate. For replicate II and III the total number of breakdowns decreases by more

Table 6.5: Number of breakdowns per treatment and replicate

Test sample	Replicate	No. of breakdowns per treatment (1)	*ad*	*bd*	*ab*	*cd*	*ac*	*bc*	*abcd*	Σ
TS3	I	0	0	0	2	2	9	3	1	17
	II	0	0	1	0	4	0	1	2	8
	III	0	0	0	0	0	1	1	1	3
	IV	0	0	0	1	4	0	0	2	7
	Σ	0	0	1	3	10	10	5	6	35
TS4	I	0	4	0	0	3	0	1	6	14
	II	0	0	0	0	1	1	4	0	6
	III	0	0	0	0	1	1	1	0	3
	IV	0	0	0	0	1	0	2	3	6
	Σ	0	4	0	0	6	2	8	9	29
TS5	I	0	1	7	0	3	2	8	6	27
	II	0	3	0	0	0	1	1	0	5
	III	0	0	0	0	0	0	1	3	4
	IV	2	2	0	0	0	0	2	3	9
	Σ	2	6	7	0	3	3	12	12	45
Σ		2	10	8	3	19	15	25	27	109

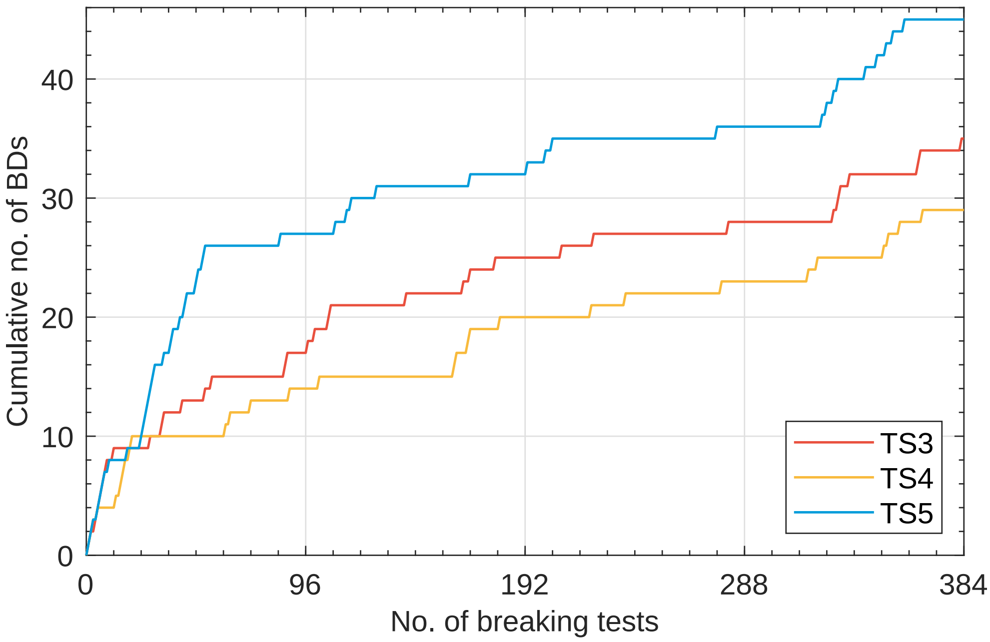

Figure 6.3: Cumulative number of breakdowns for test samples TS3, TS4 and TS5

than a half compared to the first replicate, whereas all test samples show a slightly higher number of breakdowns during their last replicate. Especially the latter features underline the presence of a conditioning effect. This also becomes apparent by the different curve progressions in Figure 6.3, which depicts the cumulative number of breakdowns for TS3, TS4 and TS5. Furthermore, there are significant differences in breakdown rate between the tested VIs, which are most dominant during the first replicate. Here, TS5 has 60 % to 90 % more breakdowns compared to TS3 and TS4, respectively.

Analysis of main effects

Hereinafter, the potential effects of the different factors are analysed to determine the extent to which they affect the breakdown behaviour. Usually, the mean response of all replicates is determined to estimate the effects of a factorial experiment and to gain information about the variability of the response data. However, despite the use of randomisation and replication, the response cannot be considered to have a constant mean and variance. This is because of the superimposed conditioning effect, which cannot be ascribed to independent random behaviour. Therefore, in Figure 6.4 the calculated main effects are represented separately for each replicate. The effects are calculated according to Equation 5.3 using the actual breakdown rate instead of the absolute number given in Table 6.5. A positive effect bar represents a higher breakdown rate at the “+”-level, whereas a negative effect points to the opposite. It can be seen that in most cases the most pronounced effects appear during the first replicate. This is explained by the high number of breakdowns during the first switching operations and the strong decrease towards the end of the first replicate. Hence, these effects are more biased than the others. With the exception of the factor *inrush current* (C) all main effects for the other factors contain both positive and negative effect values that fluctuate between different replicates and test samples. It seems that these effects are rather affected by random behaviour. Therefore, it is concluded that the factors *breaking current* (A), *arcing time* (B) and *closing speed* (D) have no significant influence on the breakdown rate within their investigated range. In contrast, all effects of the factor *inrush current* (C) with one exception exhibit a positive effect. This indicates that inrush currents exert a significant influence on the dielectric behaviour of a VI during capacitive switching.

Analysis of inrush current test data

The pre-strike behaviour of inrush current making tests can provide additional information about the dielectric condition of a VI, since a breakdown occurs every time in contrast to

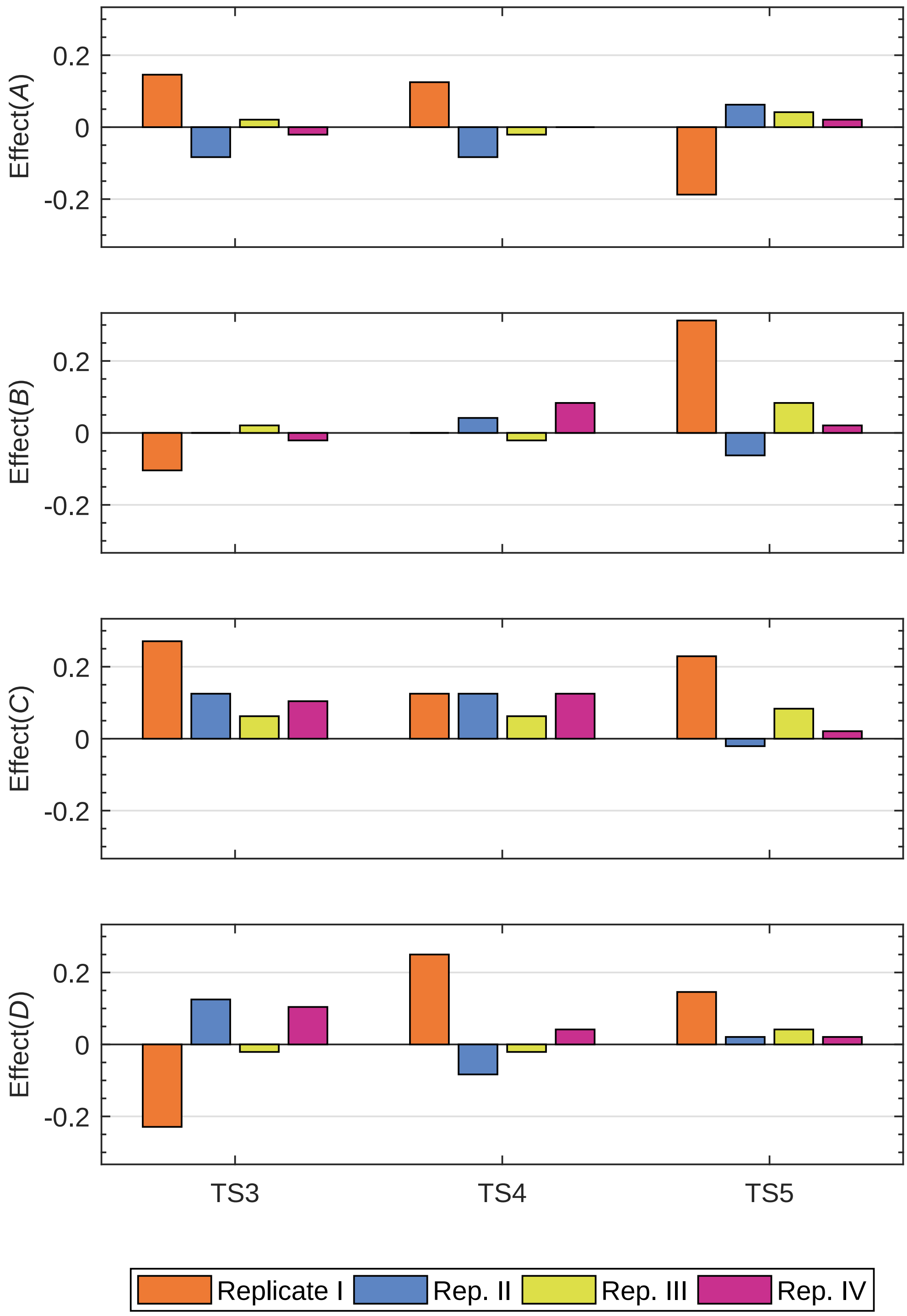

Figure 6.4: Main effects per test sample and replicate with $A \rightarrow$ *breaking current*, $B \rightarrow$ *arcing time*, $C \rightarrow$ *inrush current* and $D \rightarrow$ *closing speed*

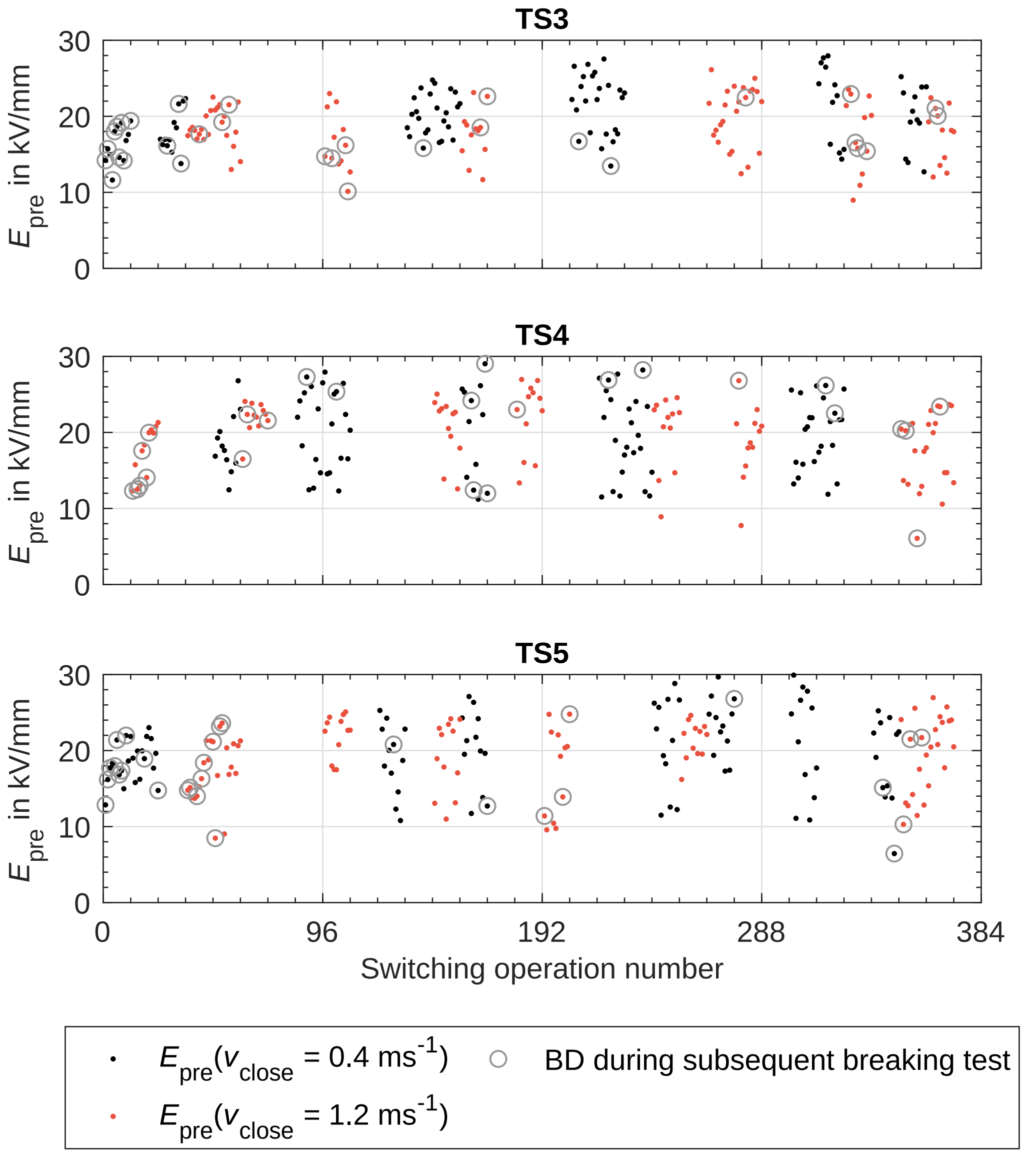

Figure 6.5: Uniform electric field strength at the first pre-strike for each conducted inrush current test

breaking tests. Therefore, in Figure 6.5 the uniform pre-strike field strength

$$E_{\mathrm{pre}} = \frac{U_{\mathrm{pre}}}{d_{\mathrm{pre}}} \tag{6.1}$$

is depicted for each inrush current test. The pre-strike voltage U_{pre} is equal to the charging voltage of the making current source $U_{\mathrm{m},0}$, see Section 4.3, and amounts to (59.1 ± 0.2) kV for all tests. Since deviations from the mean are negligibly small, the voltage can be considered constant. Thus, the contact spacing during the first pre-strike d_{pre} is inversely proportional to E_{pre}. It can be seen that the data points are distributed over a wide range from 6.1 kV mm^{-1} to 29.9 kV mm^{-1}. This corresponds to a pre-strike contact spacing d_{pre} from 9.8 mm to 2.0 mm, respectively. For every treatment a large scatter of the pre-strike field strength is apparent. These abrupt changes between tests indicate significant changes on the contact surfaces. A high pre-strike field strength may be attained with a smooth contact surface, whereas a low pre-strike field strength indicates the presence of irregularities on the surface that favour the occurrence of early pre-strikes. With increasing number of testing the maximum field strength exhibits a slight tendency towards higher values for all test samples during the first two to three replicates, which may be related to the observed conditioning effect. However, there seems to be no correlation between E_{pre} and subsequent breakdowns, as the corresponding data points are distributed over the whole range. This is also true for pre-strike field strengths subsequent to breaking tests, which include a breakdown. Furthermore, no correlation between the factor *closing speed* and pre-strike field strength can be identified. This also applies to the factors *breaking current* and *arcing time*.

Analysis of switching speed during contact opening

Although the opening speed setting is kept constant during testing, the determined values reveal a large variability. These fluctuations arise mainly because of differing operating times, temperature dependent viscosity of the hydraulic oil and deviations in the actual pressure of the hydraulic drive. The speed values range from 2.0 m s^{-1} to 2.8 m s^{-1} resulting in differences up to ±33 % from the mean. Their distribution is visualised in Figure 6.6. To deduce if these variations impact the breakdown rate, the distribution of speed has been further subdivided into measurements with or without breakdown. Overall, no clear trend is observable that would indicate an influence on the breakdown behaviour within this range.

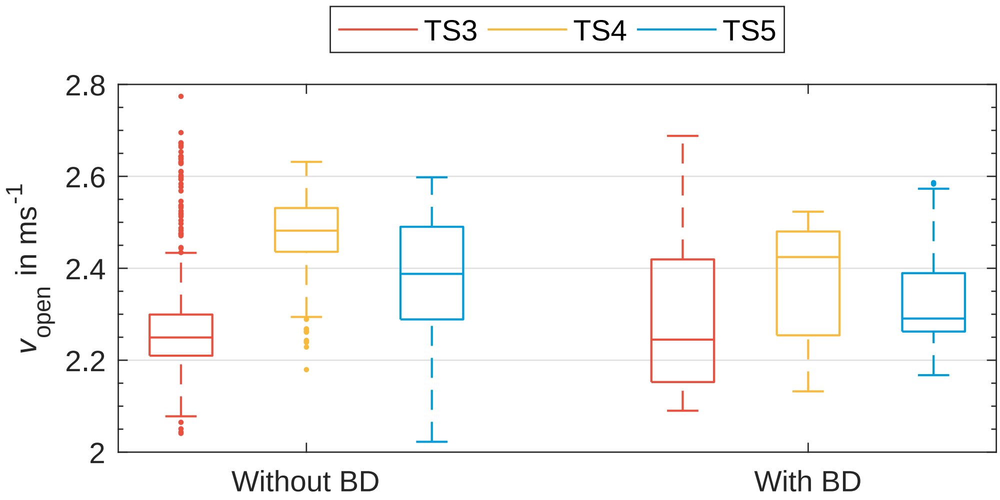

Figure 6.6: Distribution of opening speed distinguished by measurements with and without breakdown

Analysis of breakdown contact gaps

The dynamic change of contact gap at the beginning of the recovery voltage affects the breakdown behaviour. Especially the narrowing of the contact gap during rebound leads to an increased dielectric stress on the VI if the voltage is simultaneously close to its peak. In Figure 6.7 the momentary contact spacings during breakdown d_{BD} are visualised in reference to the total stroke d_{tot}, maximum contact gap during overtravel $d_{\mathrm{tot}} + \Delta d_{\mathrm{ovtr}}$ and minimum contact gap during rebound $d_{\mathrm{tot}} - \Delta d_{\mathrm{rbd}}$.[41]. The breakdown data points are further subdivided into the corresponding setting of arcing time. It can be seen that the maximum overtravel leads to contact gaps in the range of 28.4 mm to 33.7 mm, approximately 50 % larger than the total stroke d_{tot}. Even though the dielectric stress is less pronounced during overtravel, several breakdowns relating thereto have been detected. Breakdown gaps close to or identical to d_{tot} are commonly attributed to LBD. The maximum rebound results in once more narrowing contact gaps down to 12.5 mm.[42] It is apparent that almost all breakdowns during rebound happen in breaking tests with short arcing times. This is especially noticeable for many breakdowns during the first replicate of TS5, which is also responsible for the large resulting effect(B) for the factor *arcing time*, see Figure 6.4. Furthermore, there are only few breakdowns prior to overtravel.

[41] One breakdown event for TS3 during replicate II is missing because of an erroneous measurement of contact spacing d.

[42] The discrepancy of stroke data at the beginning of TS3 is caused by loosening of a screw connection in the kinematic chain of the hydraulic drive that was fixed after the 103rd breaking test.

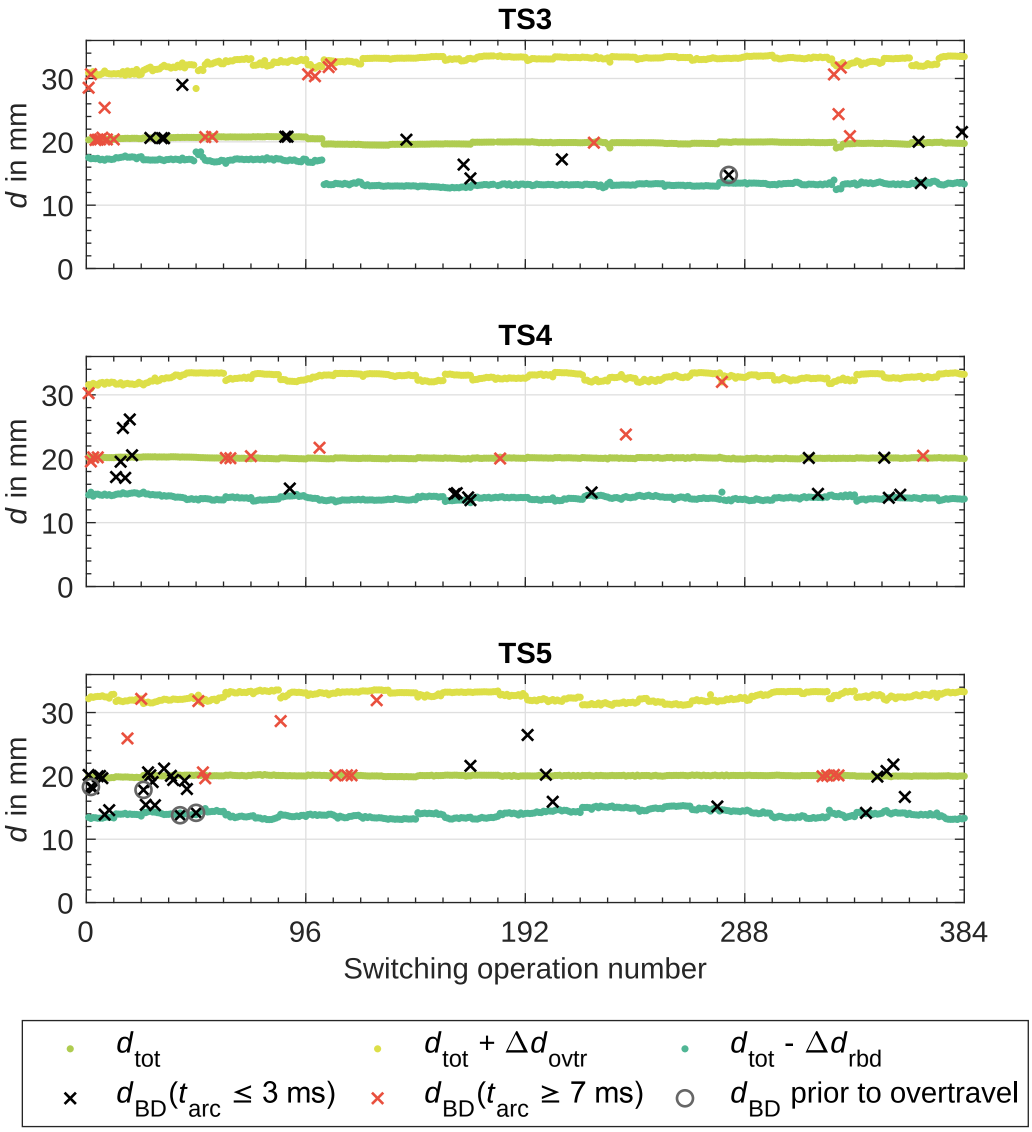

Figure 6.7: Characteristic values of contact gap and breakdown contact gaps

Analysis of uniform field strength at a contact stroke of 20 mm

Especially the latter two findings in the previous paragraph can be explained by two exemplary breaking test measurements that are compared with each other in Figure 6.8. There, the contact gap d, the recovery voltage u_{rv} and the resulting uniform electric field strength

$$E_{\mathrm{rv}} = \frac{u_{\mathrm{rv}}}{d} \tag{6.2}$$

are depicted. In example (a) the arcing time is close to zero, whereas in (b) a long arcing time of $t_{\mathrm{arc}} \geq 9.5\,\mathrm{ms}$ is present. In the first case, even though the contacts start to separate just prior to the first recovery voltage rise, the uniform field strength only slightly exceeds the peak value of $10\,\mathrm{kV\,mm^{-1}}$, which is obtained during the steady state. This is because of the fast opening speed that enables the contact gap to reach at least full contact stroke, once the voltage reaches its first peak. For longer arcing times the first peak of field strength is even reduced, since larger contact gaps are obtained at an earlier time instant, and the moment of maximum overtravel coincides more closely with the moment of the first voltage peak. This may explain the low occurrence of breakdowns prior to overtravel. For long arcing times the voltage only attains values below 100 kV during maximum rebound, which in turn results in a low E_{rv}. Yet, for arcing times close to zero, the moment of maximum rebound coincides with the second voltage peak. This results in an increase of field strength, which in many cases leads to maxima, which are approximately 50 % higher compared to maxima during the steady state. This may explain, why a majority of breakdowns during rebound appears only in breaking tests with short arcing times.

6.3 Data comparison of all test samples

In this section, various data from all tests conducted with the test samples TS1, TS2, TS3, TS4 and TS5 are compared with each other. Since the dynamic change of the uniform field strength during the recovery voltage period is previously analysed for a contact stroke of 20 mm, the field strength at 38 mm is presented first for a direct comparison. Afterwards, the temporal distribution of the breakdown events is examined in more detail. This is followed by a graphical representation of the voltage values and field strength values depending on the contact gap at the moment of breakdown. At the end, a few photos of the inner state of the test samples, which were taken after the experiments, are shown and analysed. Subsequently, the results of this chapter are discussed.

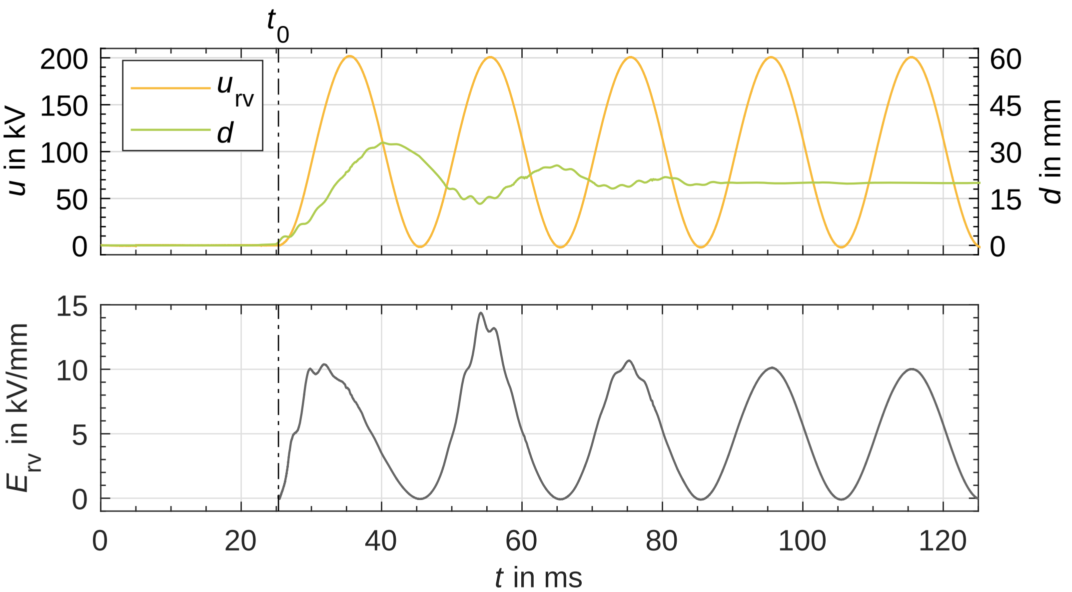

(a) Arcing time $t_{arc} \approx 0\,\mathrm{ms}$

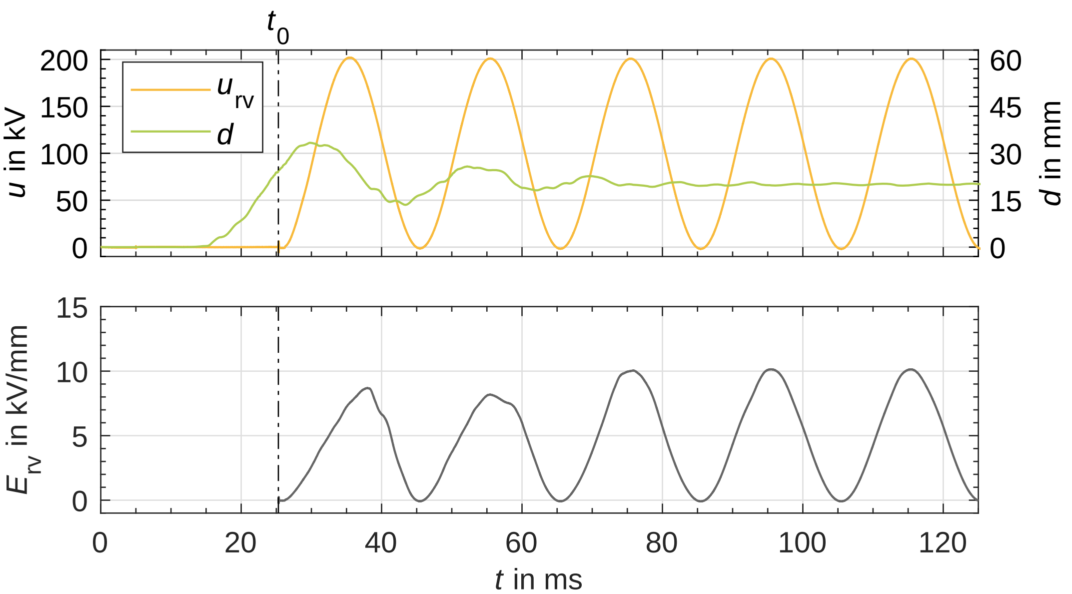

(b) Arcing time $t_{arc} \geq 9.5\,\mathrm{ms}$

Figure 6.8: Uniform electric field strength at a contact stroke $d_{tot} = 20\,\mathrm{mm}$ for different arcing times

Analysis of uniform field strength at a contact stroke of 38 mm

Previously, the influence of the switching characteristic on the time-dependent uniform electric field strength E_{rv} was discussed only for a contact stroke of 20 mm. For a comparison with the time-dependent uniform field strength at 38 mm a graphical representation is given in Figure 6.9. Again, two measurement examples are given at the extreme limits of the different arcing time levels. In example (a) a measurement with an arcing time close to zero and in example (b) a measurement with an arcing time longer than 9.5 ms are presented. It can be seen that for the late contact separation the highest dielectric stress arises during the first rise of recovery voltage. The voltage reaches its first peak even before the total stroke is achieved. In the example, this results in a field strength of $13.7\,\mathrm{kV\,mm^{-1}}$. This is more than twice the maximum field strength of $5.3\,\mathrm{kV\,mm^{-1}}$ during the following steady state.[43] In contrast, for long arcing times the first voltage peak coincides with the maximum overtravel. Thus, this field strength is always lower than during the steady state. In both cases and especially for arcing times in between these extreme limits, the maximum rebound is close to the second voltage peak. Therefore, the maximum field strength is higher during the second voltage cycle compared to the steady state. However, since the relative gap difference between rebound and contact stroke $\Delta d_{\mathrm{rbd}}/d_{\mathrm{tot}}$ or overtravel and contact stroke $\Delta d_{\mathrm{ovtr}}/d_{\mathrm{tot}}$ is smaller for 38 mm compared with the reduced contact stroke, this results in a less pronounced difference in field strength. In conclusion, for both contact strokes the highest uniform field strength arises, when the arcing time is close to zero. For $d_{\mathrm{tot}} = 38$ mm the maximum is obtained during the first recovery voltage cycle, whereas for 20 mm the maximum is obtained during the second voltage cycle, which coincides with the moment of rebound.[44]

Analysis of temporal breakdown distribution

To show the ratio between LBDs and breakdowns that occur before the first recovery voltage peak, the temporal distribution of relative breakdown frequencies is represented for all five test samples in Figure 6.10. The corresponding total number of breakdowns is shown on top of each bar. The diagram is split into four time segments. The first segment includes breakdowns, which occur during the first, but later than one quarter

[43] The difference of field strength maxima during the first rise of recovery voltage between the full and the reduced contact stroke setting are caused by different acceleration characteristics of the operating mechanism.

[44] Note: The short arcing time setting has been defined for a range up to 3 ms because of scatter. Measurements with arcing times closer to the upper limit only exhibit a smaller increase or even a small decrease of field strength.

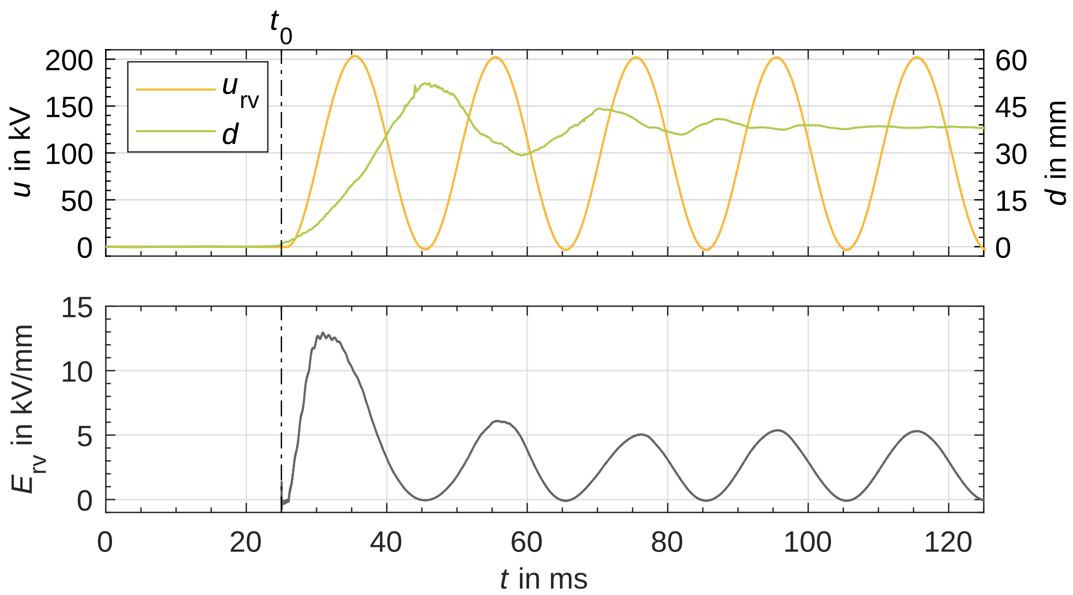

(a) Arcing time $t_{arc} \approx 0\,\mathrm{ms}$

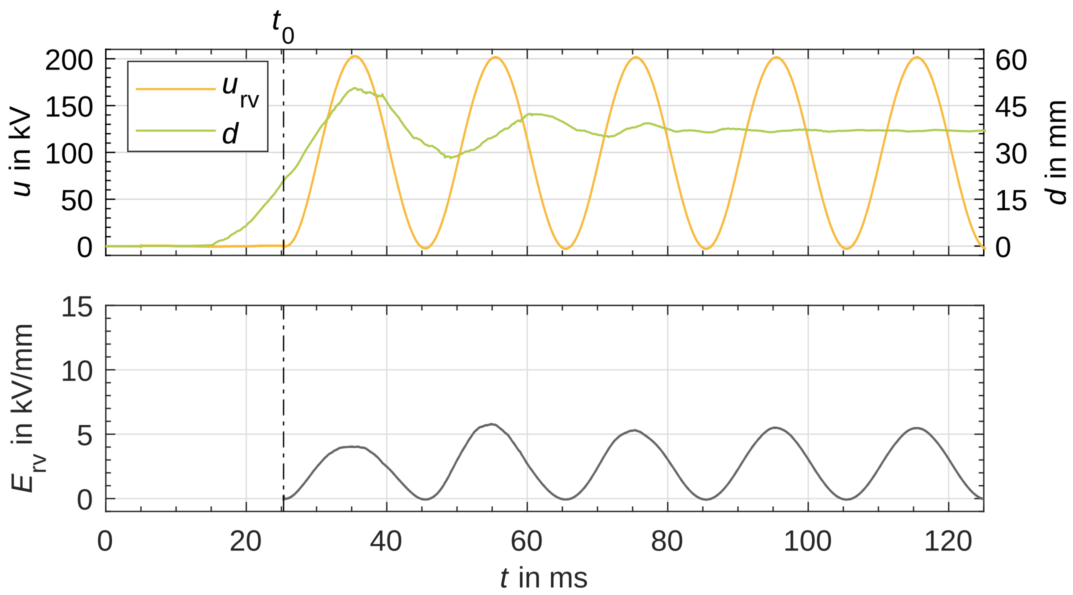

(b) Arcing time $t_{arc} \geq 9.5\,\mathrm{ms}$

Figure 6.9: Uniform electric field strength at a contact stroke $d_{tot} = 38\,\mathrm{mm}$ for different arcing times

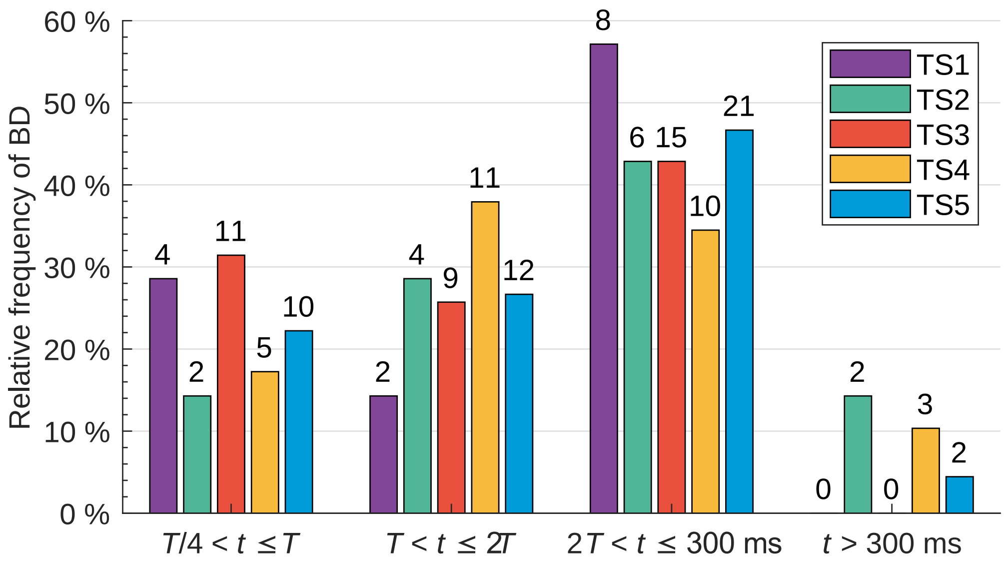

Figure 6.10: Relative frequency of breakdowns for different time segments with the absolute number of breakdowns represented on top of each bar

cycle of recovery voltage.[45] With only one exception, these breakdowns occur during the rising edge or close to the first peak of the voltage. Every breakdown after this peak is considered a LBD. The second segment consists of breakdowns within the second voltage cycle. This time segment is listed separatedly, since it is often affected by the rebound during contact opening. Approximately 75 % of all detected breakdowns during this cycle can be assigned to breakdowns during rebound. All test samples examined with a reduced contact stroke exhibit a similar or even a higher relative frequency of breakdown during the second voltage cycle compared to the first one. Even though the absolute numbers are small for TS1, the higher relative frequency during the first voltage cycle compared to the second one is attributed to the higher dielectric stress, see the preceding paragraph. Since the excursion of rebound is strongly affected by the mechanical chain, the relative breakdown frequency during the first two voltage cycles can be completely different for other operating mechanisms. The third segment covers all breakdowns up to 300 ms[46], and the last one includes all remaining breakdowns that happen thereafter. For each test sample, it can be seen that about 50 % of breakdowns occur subsequently to the second

[45] Breakdowns prior to one quarter cycle are re-ignitions that appeared only three times during all evaluated tests and have therefore been excluded from the analysis.

[46] The standard requires that the recovery voltage must not decay by more than 10 % within 300 ms [IEC08]. Hence, this can be considered as the minimum duration to verify the absence of LBD.

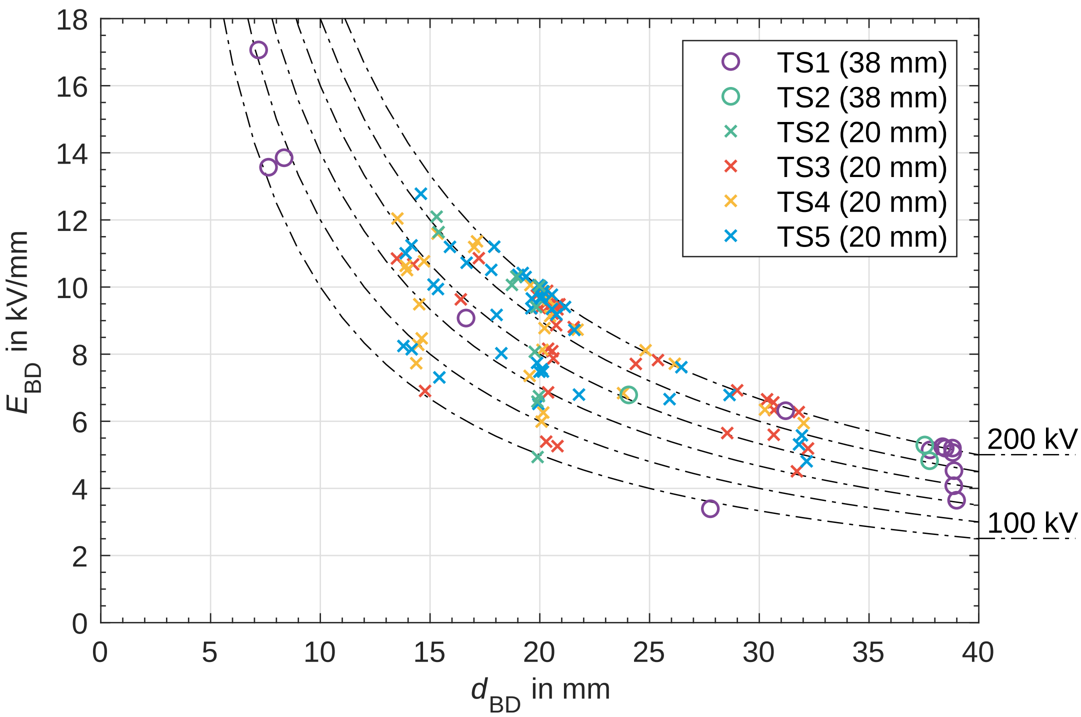

Figure 6.11: Distribution of the uniform breakdown field strength depending on contact spacing

voltage cycle. Yet breakdown events later than 300 ms are rather sparse.[47] The high emergence of LBD signifies the importance of analysing this phenomenon, which is typically attributed only to vacuum circuit breakers.

Analysis of uniform breakdown field strength and breakdown voltages

Dielectric breakdowns do not neccessarily occur near recovery voltage peaks, but can also appear far before or after it. This and the dynamic change in field strength over a wide range during which a breakdown can occur are to be evaluated graphically in the following. In Figure 6.11 the uniform breakdown field strengths

$$E_{\mathrm{BD}} = \frac{u_{\mathrm{BD}}}{d_{\mathrm{BD}}} \tag{6.3}$$

are represented in relation to their momentary contact spacing d_{BD} for all test samples. The dash-dotted lines represent equipotential lines for voltage values between 100 kV and

[47] The recovery voltage was applied to TS1 for 1000 ms and to all other test samples for 600 ms. Theoretically, LBD could occur even later, but it was presumed that the probability of occurence is negligibly small.

200 kV with a step width of 20 kV. It can be seen that breakdowns not only occur close to the peak of the recovery voltage, but also at lower values during either the rising or the falling edge of the voltage even when full contact stroke is achieved. The lowest breakdown voltage u_{BD} at a contact gap of 20 mm is 95 kV. Even for the contact stroke setting of 38 mm the breakdown voltage u_{BD} could become as low as 140 kV. The lowest recorded breakdown gaps d_{BD} for TS1 occur during the first rise of recovery voltage. These also exhibit the highest E_{BD} with more than $13\,\mathrm{kV\,mm^{-1}}$. The lowest E_{BD} of $3.4\,\mathrm{kV\,mm^{-1}}$ is present during a breaking test with TS1 as well. In this case, a voltage of just 94 kV is sufficient to trigger the breakdown during rebound. As has been stated before, many of the lower breakdown gaps for TS2, TS3, TS4 and TS5 refer to the moment of rebound. However, there are also a few events with larger d_{BD}, which occur during overtravel. The widespread distribution of data shows the large scatter and stochastic behaviour of the dielectric withstand capability in vacuum. Furthermore, the presence of lower breakdown voltages highlights that breakdowns can even occur at lower voltage stresses than were present before the event.

Visual inspection of VIs after testing

As a consequence of the conducted switching tests, which are more severe than required by the standards, the test samples show visible signs of wear. In Figure 6.12 six photos of different locations inside the VI are depicted.[48] An exemplary side view of the moveable contact (1) reveals multiple traces of overlapping craters that have been left behind by cathode spots moving down the side of the contact. Some traces even expand to the back of the contacts. The tree-like patterns are created by the splitting of cathode spots. Because of the stronger erosion, the deeper and wider tracks are considered to stem from slow moving cathode spots with a current close to the maximum current carrying capacity of approximately 100 A. The photos (2) and (3) show the top view of the moveable and fixed contact, respectively. Both contact surfaces exhibit severe alterations due to melting of the contact material. A consequence of this is the welding of slots especially towards the contact edge. This deformation is assumed to adversely affect the AMF principle, thereby impeding the arc control especially during inrush current tests. This may explain the renewed increase in breakdowns during the last replicate observed for TS3, TS4 and TS5. Furthermore, coarse elevations, fissures and craters are present. Since both contacts are eroded to a similar degree, the wear is mainly attributed to the impact of inrush current. The diffuse arc due to the breaking current would more likely result in a dissimilar

[48] Even though the photos are not taken from a single test sample, the phenomena described below are similar for all inspected test samples.

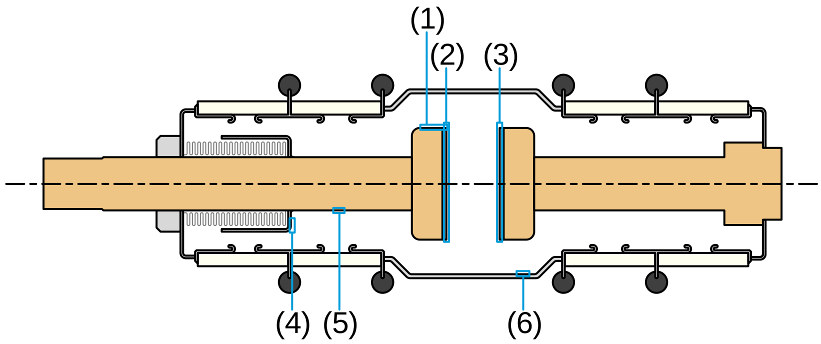

(1)

(2)

(3)

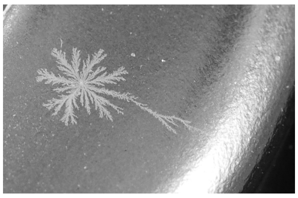

(4)

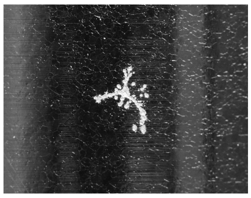

(5)

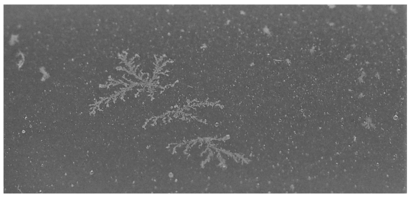

(6)

Figure 6.12: Visible signs of wear after the conducted experiments with their respective location indicated by the schematic sectional drawing of the VI

alteration, because of its greater impact on the cathode and since arcing occurs at only one polarity during testing. In the photos (4) to (6) three cathode spots found on the bellow protection shield, the contact stem and the centre shield respectively are illustrated. These cannot be associated to switching arcs because of their exceptional location inside the VI. They are rather assumed to be the result of dielectric breakdowns. This indicates that breakdowns occur not only between the contacts, but via the vapour shields as well due to the most likely path of the discharge. However, as their visible presence is low in number, such an event is deemed rare.

6.4 Discussion of results

In this chapter, the conducted factorial experiments to determine the impact of various test circuit parameters on the breakdown rate of identically designed 72.5 kV VIs are presented. The examined factor levels are chosen to the greatest possible extent within realistic conditions of the capacitive switching operation. During all tests the recovery voltage peak is kept fixed at the highest possible level specified by the standard for single-phase testing with a capacitive voltage factor of 1.7. On that basis, the goal is to find a set of factor settings that is most likely to trigger late breakdowns. Thus, future investigations of this phenomenon can be optimised by reducing the number of necessary test runs. In the first factorial experiment only four breakdowns in 283 breaking tests with the contact stroke set to 38 mm are recorded. However, the small sample size does not allow to draw firm conclusions about the potential influence of the tested factors. To overcome this issue, a smaller contact spacing is chosen for further experiments. It has to be noted though that the change of interelectrode spacing may affect the involved pre-breakdown processes responsible for a disruptive discharge.

The final factorial experiment conducted on TS3, TS4 and TS5 reveals a large variation in breakdown rate between the test samples, although all of them are subjected to the same stresses except for a randomised run order. A similar behaviour was also found in [DSG+06]. In their experiments, capacitive switching tests with a synthetic test circuit were conducted on 24 kV VIs with the contact stroke set to either 8 mm, 12 mm or 14 mm, respectively. For each contact stroke a large scatter of the cumulated breakdown rate is visible. This circumstance highlights the need to use multiple samples during experiments to reduce the chance for erroneous conclusions. Furthermore, all experiments show a pronounced reduction of the breakdown rate over consecutive switching operations independent from any factor setting. For all tested VIs around half of all detected breakdowns appear during the first one hundred breaking tests. A similar observation was made in [Kör08]. It is reported that more than 50 % of all breakdowns appear within the first quarter in several test series conducted on a model vacuum chamber with different interchangeable contacts. The capacitive switching tests, including preceding inrush current tests, were carried out with a recovery voltage of 50 kV for 500 ms with a contact stroke of 12 mm. In [YMA+95] it was decided to exclude the data of the first half of 2000 tests conducted on two 24 kV model VIs with different contact materials due to the higher number of breakdowns during the beginning. This effect was also attributed to conditioning. This conditioning effect is more pronounced than any influence of the varied factors in the factorial experiments. Therefore, stochastic independence between consecutive switching tests cannot be assumed. Moreover, it is questionable if a particular moment is reached during testing, when the test results can be considered virtually unaffected, especially with the once more increasing breakdown rate seen for TS3, TS4 and TS5 during their last replicate. Since independence is a prerequisite for the application of basic stochastic models, further analysis in this regard is not permitted. Thus, all results on factorial effects cannot be quantified statistically and have to be carefully interpreted.

The change of the breakdown rate and the variation between samples can be attributed to the impact of electrical, thermal and mechanical stresses exerted during testing. Since these stresses are an inherent part of switching operations, they cannot be avoided, and their actual effect on the contact surface condition, which is decisive for the dielectric withstand capability of vacuum gaps, is unknown. To counteract the adverse effect of conditioning and variability to a certain extent, the process of randomisation, replication and repeated trials on three identical test samples have been applied within this work. Despite these measures more testing may be necessary to confirm or refute the following conclusions drawn from the factor main effect analysis.

According to the effect results, no influence of the factor *breaking current* on the breakdown behaviour within the range of 45 A to 400 A can be determined. A similar finding for the range of 25 A to 400 A is reported in [GRR+12], in which the restrike probability of 72.5 kV VIs in a direct test was investigated. At this point, it cannot be excluded that higher breaking currents can have an influence on the breakdown behaviour. However, a survey result in [Cig20] shows that capacitive load currents of capacitor banks are typically only around 400 A regardless of the voltage level. This also corresponds to the value specified for type tests by the standard [IEC08]. Towards the lower end zero current is the final limit. In [DSG+06] it is argued that the absence of breaking current increases the breakdown probability, which is explained by absent conditioning of the contact surface during contact separation. However, no scientific contribution with experimental proof of this hypothesis could be found. Despite this potential effect, zero capacitive current stress is deemed unnatural for power grid applications and thus poses an unrealistic switching condition.

Higher breaking currents and longer arc durations are considered to reduce irregularities on the contact surface [SWB+12]. However, it is also stated that the arc energy and the spatial extent of the arc on the contact surfaces during capacitive current interruption is not sufficient to eliminate protrusions [Cig14] or broken welding spots [GM10], which were previously created by inrush current arcing. Both statements are not mutually exclusive and are further discussed in the next chapter about pre-breakdown phenomena. Yet the latter offers an explanation, why neither the factor *breaking current* nor the factor *arcing time* seem to have an effect on the breakdown rate. Still, the *arcing time* is found to affect the moment of breakdown during a breaking test especially at the beginning of recovery voltage by the related moments of overtravel and rebound. Their characteristic depends significantly on the design of the operating mechanism. Within the scope of this work the pronounced mechanical balancing process led to many breakdowns during rebound when a late contact separation is present. This is mainly due to the temporal overlap with the second recovery voltage peak resulting in a higher electric field stress. However, many breakdown events have also been observed during overtravel, which results in an even reduced electric field stress. These breakdowns are deemed to be caused by microparticles, which are detached from the contact surface by arcing or by mechanical shocks during impact with the mechanical stop, since microparticle impacts depend on voltage rather than electric field strength.

Pre-stressing the test samples with inrush current results almost exclusively in an increased breakdown rate. Thus a direct influence seems to be unambiguous. This result is further supported by the findings in [SEG+10] that show a higher breakdown probability for 20 kA back-to-back capacitor bank switching compared to 6 kA single bank switching. Moreover, it was observed in [DSG+06] by optical measurements that the created weld spots coincide with subsequent restrike locations. These results further prove the negative impact of back-to-back capacitor bank energisation on the breakdown behaviour of VIs. Thus, for power grid applications the use of precautionary current-limiting measures is advised, even more since a high number of switching operations is required for this type of loads. However, for investigations of the late breakdown phenomenon, the inrush current making test is a suitable way to increase the probability of occurence.

In contrast to breaking tests, every inrush current making test results in a dielectric breakdown during pre-strike. Thus, it seems reasonable to evaluate the dielectric state of the VI on the basis of its pre-strike behaviour and possibly draw conclusions towards the likeliness of dielectric breakdown during capacitive current interruption. When investigating the uniform pre-strike field strength, a large scattering is apparent between consecutive tests.

This kind of behaviour was also observed in [Kör08] for inrush currents with a frequency of 250 Hz and a first current peak of 4.3 kA. The abrupt changes of the field strength indicate severe alterations of the contact surface, which do not only have to result in a weakened dielectric strength of the vacuum gap. Rather, existing protrusions and other irregularities could be eliminated by melting due to the high energy input of the arc. Therefore, it is concluded that these abrupt changes are mainly caused by the inrush current itself and that the subsequent breaking test is of low impact due to the comparatively lower energies provided during arcing or a dielectric breakdown. This assumption is further supported by the lack of influence of the different arc durations and breaking current magnitudes on the pre-strike field strength. Moreover, no direct correlation between the pre-strike field strength and a breakdown during the previous, but also the following breaking test can be identified. This is also consistent with the observations made in [Kör08]. However, if the highest pre-strike field strengths for TS3, TS4 and TS5 are considered, a slight positive trend towards higher values over the course of testing can be seen with a minor decrease towards the end. As the pre-strike field strength increases a higher dielectric strength of the vacuum gap is attained. Therefore, this behaviour may be correlated to the continuously decreasing breakdown rate during testing with the once more increasing occurence towards the end.

As depicted in Figure 4.4, after the first pre-strike the inrush current arc extinguishes at each current zero. If the dielectric strength can be regained by the vacuum gap at that moment, the current flow is interrupted until the contact distance has sufficiently decreased for another pre-strike. This inrush current interruption phenomenon was also observed in [WGL+17, SKC+12, DRG10]. Within this work, arc interruptions up to several milliseconds are found at slow closing speeds of $0.4\,\mathrm{m\,s^{-1}}$. These long periods of time without current conduction occur especially during very early pre-strikes and may influence the degree of melting. In contrast, the higher speed of $1.2\,\mathrm{m\,s^{-1}}$ results in an increased contact bouncing after the initial contact touch. This evokes continued arcing during bouncing, which in turn may also affect the degree of welding as well as the breaking of welds. However, the calculated effects in Figure 6.4 do not indicate a definite impact of the factor *closing speed* on the breakdown rate, although it can be safely assumed to affect the inrush current and closing behaviour in several ways. In [DRG10] it was found that for 24 kV VI a slower closing speed of $0.6\,\mathrm{m\,s^{-1}}$ resulted in more breakdowns compared to the faster closing speed of $1.8\,\mathrm{m\,s^{-1}}$. However, the higher number of breakdowns only became visible after approximately 230 breaking tests. For each setting of closing speed two test samples were used. It has to be noted though that for these experiments an inrush current of 5.6 kA with a frequency of 270 Hz was applied. Due to the comparatively lower frequency, this also increases the duration of arcing until the next current zero crossing and can therefore have a different effect on the phenomenon of current interruption, which makes a direct comparison difficult. In contrast, the results for 72.5 kVVI in [GRR+12] indicate a higher breakdown probability for faster closing speeds. However, only relative reference values for the applied speeds are stated. Because of these contradictory results, no generally valid conclusion can be drawn with regard to this factor. In this case, a variety of variables seem to affect the resulting behaviour, e.g. the inrush current frequency, the number of repeated tests, bouncing behaviour and the range of applied closing speeds.

7 Investigation of pre-breakdown phenomena

In this chapter, recorded pre-breakdown phenomena commonly attributed to the development of dielectric breakdown in vacuum are examined in detail. The corresponding measuring systems are designed primarily for the measurement of field emission currents and the detection of charged microparticle impacts, but other phenomena like microdischarges have also been captured. In the following, these phenomena are analysed separatedly. At the end of this chapter, their potential effect on dielectric breakdown and especially on LBD is assessed and discussed.

7.1 Field emission related phenomena

In VIs the occurence of field emission strongly depends on local field enhancements on a microscopic scale, because common geometric designs do not give rise to electric field strengths high enough for this phenomenon to occur. These enhancements are primarily caused by microscopic irregularities and impurities on the electrode surfaces. During the experiments varying behavioural patterns were observed. Since the resulting electric field strength also depends on the contact spacing of the electrodes, the analysis is further subdivided into the two applied contact stroke settings.

Field emission at a contact stroke of 38 mm

For breaking tests with the contact stroke set to 38 mm the presence of field emission in the range accessible to measurement is rare. In only 22 out of 475 breaking tests field emission currents above 100 µA are detected. Furthermore, this current appears only during the first recovery voltage cycle and only rarely during the second cycle at far lower amplitudes. All of the breaking tests with field emission current have a very late contact separation in common. In this case, the contact system has not yet attained full contact stroke, when

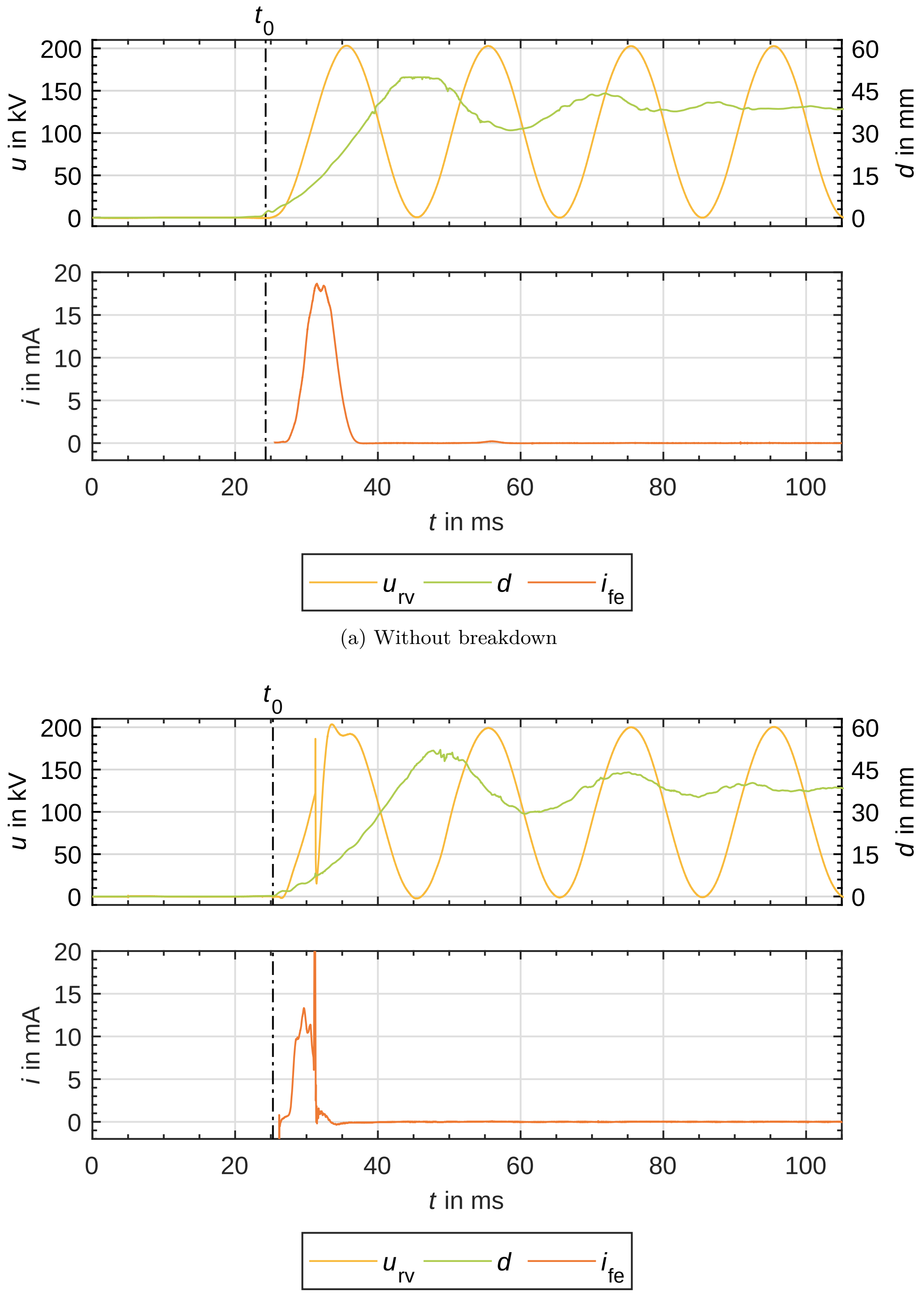

(a) Without breakdown

(b) With breakdown

Figure 7.1: Two exemplary field emission current measurements at $d_{\mathrm{tot}} = 38\,\mathrm{mm}$

the recovery voltage reaches its first peak. This in turn results in a higher uniform field strength compared to the subsequent steady state.[49]

In Figure 7.1 two exemplary measurement results with field emission current i_{fe} are presented. In example (a), a measurement with one of the highest detected field emission current peaks for that contact stroke is shown.[50] The peak value of $\hat{\imath}_{\mathrm{fe}} = 18.6\,\mathrm{mA}$ appears at a time instant, when the voltage is $u_{\mathrm{rv}} = 126\,\mathrm{kV}$ and the contact spacing is $d = 12.9\,\mathrm{mm}$. The current then starts to decrease even before the voltage reaches its peak, which is attributed to the still slightly accelerating contact opening. During the second voltage cycle coinciding with the time span of rebound the current amounts to just 220 µA and is barely visible in the graphic representation. Afterwards, no field emission is detectable anymore. Field emission current peaks above 10 mA are captured eight times. In three of those cases, a voltage breakdown occurs during the first recovery voltage cycle as well. However, the moment of breakdown does not necessarily happen close to the current peak. Example (b) shows such a case. The current reaches a maximum value of 13.3 mA, before it starts to decrease again. The breakdown occurs at a voltage of 122 kV and a contact spacing of 7.3 mm. At this moment, the field emission current has already decreased to 7.5 mA. Only one further breakdown is detected during the first recovery voltage cycle. However, in this case, no field emission current is present before. This is also true for all other breakdowns that are recorded at subsequent voltage cycles during breaking tests performed on TS1.

Field emission at a contact stroke of 20 mm

For breaking tests with the contact stroke set to 20 mm the occurence of field emission is more frequent with varying characteristics. In the following, some particular examples are presented.

In Figure 7.2 two breaking test examples are shown, which contain one of the highest field emission currents that were recorded during the experiments. In both cases, the maximum value is close to 60 mA and appears during the second voltage cycle. The considerably larger peak values during this voltage cycle are explained by the rebound of the movable contact, which coincides with the recovery voltage peak due to the late contact separation.

[49] See example (a) in Figure 6.9 for reference.

[50] The distortion of the field emission current near its peak is caused by minor transient processes on the voltage at the beginning of the recovery voltage period as well as on the contact gap during contact opening. These result in a distorted field strength curve, see for example in Figure 6.9, example (a) during the first peak of the field strength. Because of the non-linear relationship of the field emission current with the field strength, this distortion is to some extent even intensified.

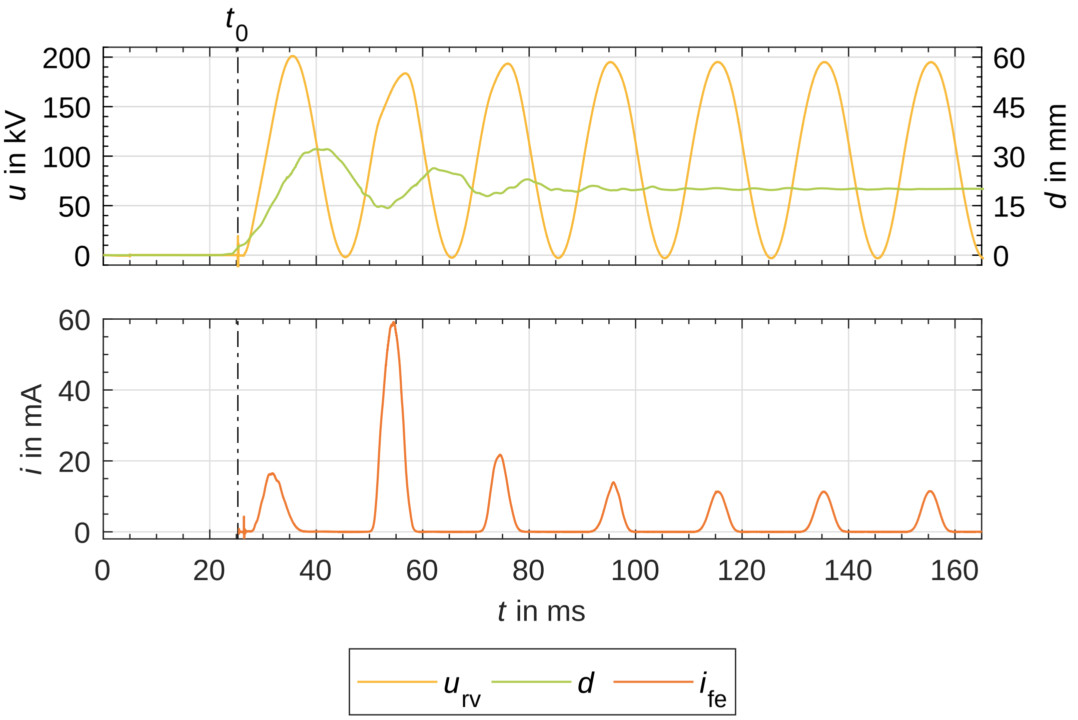

(a) Without breakdown

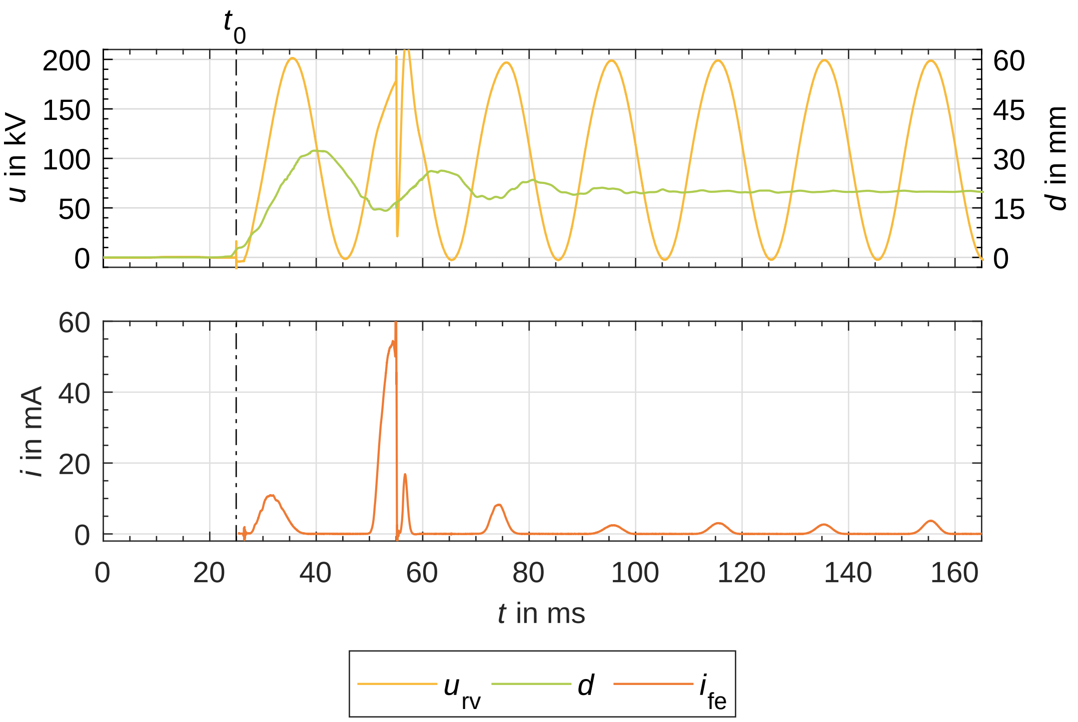

(b) With breakdown

Figure 7.2: Two exemplary field emission current measurements with a maximum field emission current close to 60 mA

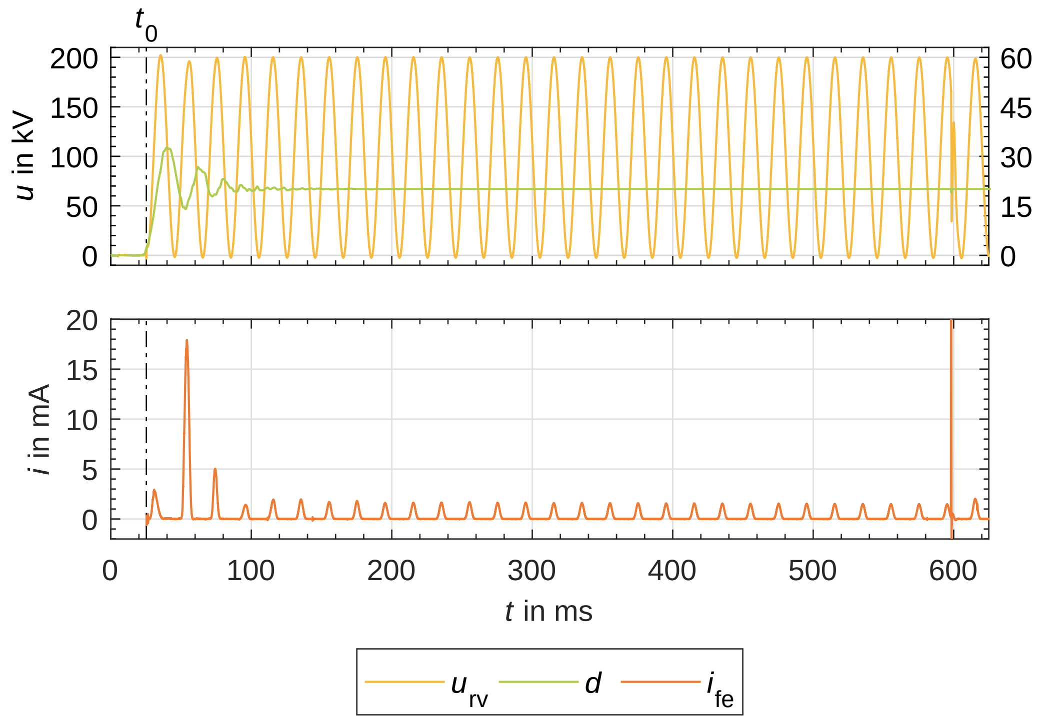

Figure 7.3: Exemplary field emission current measurement with a LBD in the 29th recovery voltage cycle

For the smaller contact stroke setting the momentary contact spacing can become as low as 13 mm during rebound. Thus, a much higher electrical field strength is temporarily obtained.[51] In contrast to the first example, example (b) contains a breakdown shortly after reaching a current peak of $\hat{\imath}_{fe} = 54\,\mathrm{mA}$. Field emission currents in the range of tens of milliamperes result in a high load on the recovery voltage source, which leads to a distortion of the voltage waveform. On the one hand, this results in a minor, yet permanent reduction of the direct voltage and on the other hand in a strong, yet temporary voltage drop of the alternating voltage. It is assumed that the field emission current could have become even higher with a stronger power supply. Nevertheless, it can be seen that even though this leads to a reduction of the recovery voltage amplitude, a breakdown can still happen.

Figure 7.3 depicts an example with a very late breakdown. The second field emission current peak reaches 17.9 mA and decreases to a range of 1.4 mA to 2.0 mA subsequent to the fourth voltage cycle. This peak range is maintained for the remaining breaking test. The higher peak values during the second and third voltage cycle are again attributed to the contact rebound. During the 29th voltage cycle the LBD occurs. However, no increase of field emission can be seen prior to the breakdown. It rather happens during the falling

[51] See example (a) in Figure 6.8 for reference.

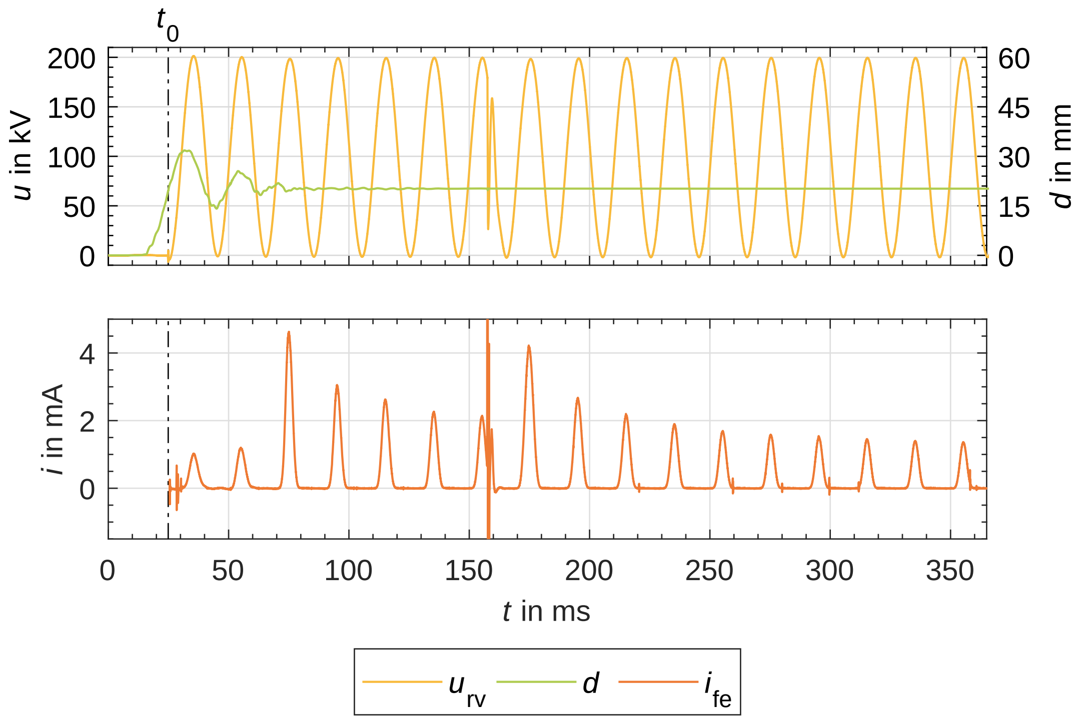

Figure 7.4: Exemplary field emission current measurement with changing current peak after the LBD

edge of the voltage, when i_{fe} has decreased to just 0.2 mA.

The last example in Figure 7.4 shows a field emission current with peak values in the range of 1 mA to 5 mA. Since the overtravel coincides with the first and second recovery voltage peak due to the long arcing time setting, the first two current peaks are comparatively small with maxima close to 1 mA. Thereafter, the peak value increases to 4.6 mA before it gradually decreases during the following voltage cycles. In the seventh cycle a LBD occurs at a moment, when i_{fe} has already declined to less than one third of its former maximum. During the next voltage cycle after the breakdown, the field emission current exhibits a peak higher than before. This indicates that the discharge has increased the roughness of the contact surface.

The previous examples show that the magnitude of field emission current can vary over a wide range from a few microamperes up to tens of milliamperes. To see how these magnitudes change during consecutive breaking tests a representative graphical overview for all breaking tests conducted on TS4 is illustrated in Figure 7.5 and Figure 7.6.[52] In these figures the 384 breaking tests are split into the first and second half, respectively;

[52] An identical overview for TS3 and TS5 can be found in Appendix A.

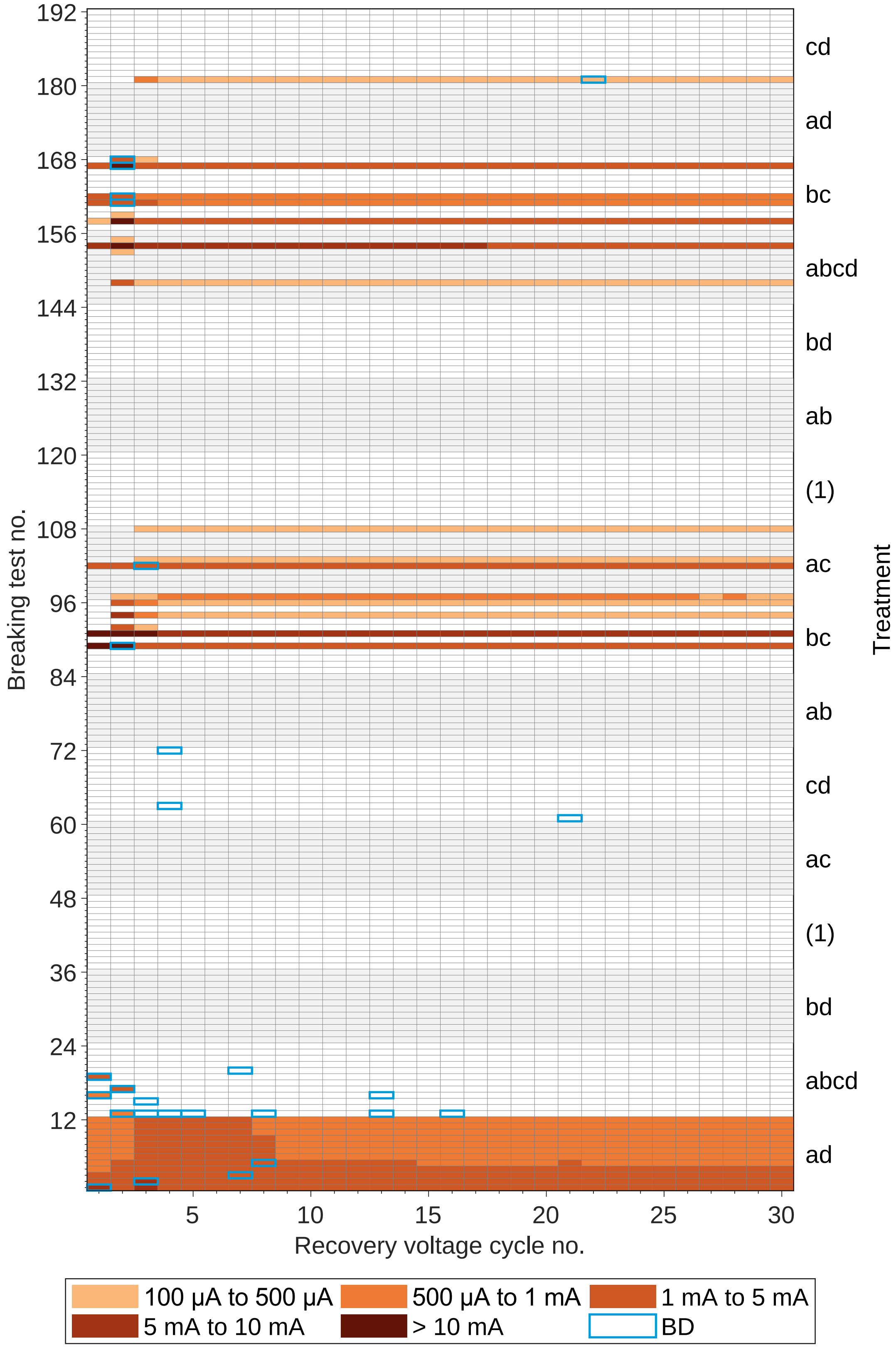

Figure 7.5: Field emission current peaks $\hat{\imath}_{\text{fe}}$ for TS4 during breaking tests no. 1 to 192

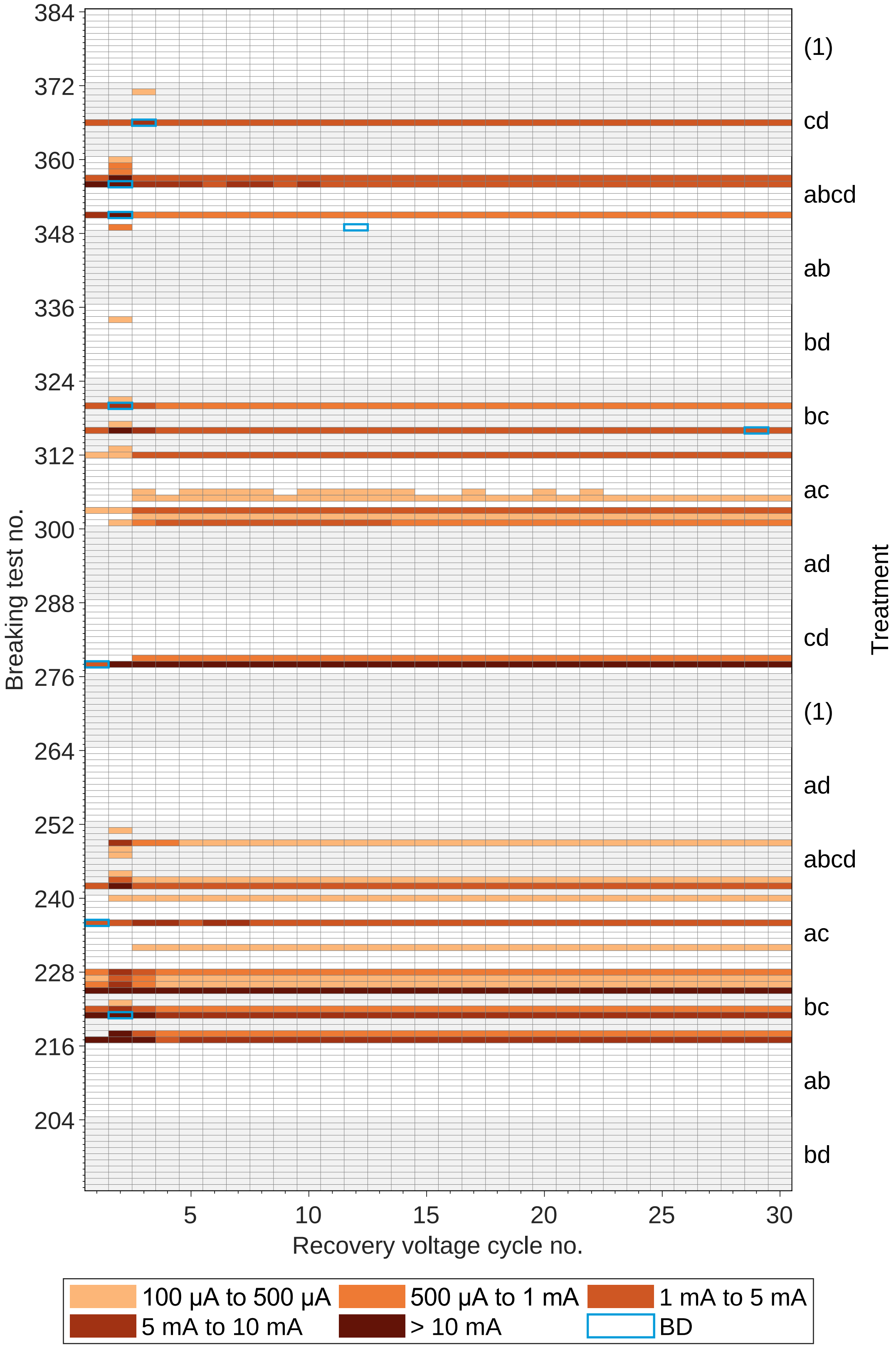

Figure 7.6: Field emission current peaks $\hat{\imath}_{\mathrm{fe}}$ for TS4 during breaking tests no. 193 to 384

i.e. breaking tests no. 1 to 192 and breaking tests no. 193 to 384. For each recovery voltage cycle the corresponding peak value $\hat{\imath}_{\mathrm{fe}}$ is represented.[53] Voltage cycles including a breakdown are additionally marked by a blue frame. On the right axis the factor settings are represented by their corresponding coded treatments.[54]

The illustrations show that the peak value of field emission currents can change significantly between successive breaking operations. However, throughout a single breaking test the relative proportion of current peaks rarely changes during the steady state. In contrast, deviating values can occur especially at the beginning, which is usually related to the increased field stress during mechanical rebound. These results suggest that the irregularties on the contact surfaces responsible for the field emission are changing substantially between switching operations, but remain nearly identical during the recovery phase. In some cases, the peak values are slowly decreasing over time, which can be attributed to a smoothening of the emitting sites, but this effect is only weak.

Many breakdowns do not exhibit any significant field emission current prior to the event. This is especially true for LBD during the steady state. Furthermore, in some instances with preceding field emission, the current peak is already declining to a lower value before the disruptive discharge occurs. Still, there are also cases, especially during the second voltage cycle, when the current is higher than 10 mA just prior to the breakdown. Yet, a definite correlation between the amount of field emission current and breakdown behaviour cannot be identified.

TS4 is a special case, since all trials during the first treatment exhibit a high level of field emission current. This indicates a less conditioned original state of this test sample. However, the field emission current is abruptly reduced in the 13th breaking test. This is also the first time that this VI has been stressed before by an inrush current. Furthermore, sudden changes of field emission, sometimes with very high peak values, appear most often during treatments with prior inrush current stress, see treatments including the letter *c*. This points towards a strong impact of inrush current on the conditioned state of the contact surface. Since a reduction of field emission current has also been observed, it is assumed that this impact does not necessarily result in a constantly worse condition than before.

[53] Not all field emission current peaks could be accurately extracted, since some breaking tests gave rise to unexpectedly high currents that exceed the measurement range. The sense resistance was adapted twice over the course of the investigation to allow for higher measurement ranges with a first range of ± 20 mA and a final range of ± 60 mA. Additionally, the retroactive influence of the accompanying voltage drop at higher load is unknown. In consequence, no further distinction is made for $i_{\mathrm{fe}} > 10$ mA.

[54] See Table 6.3 for the respective coding of treatments.

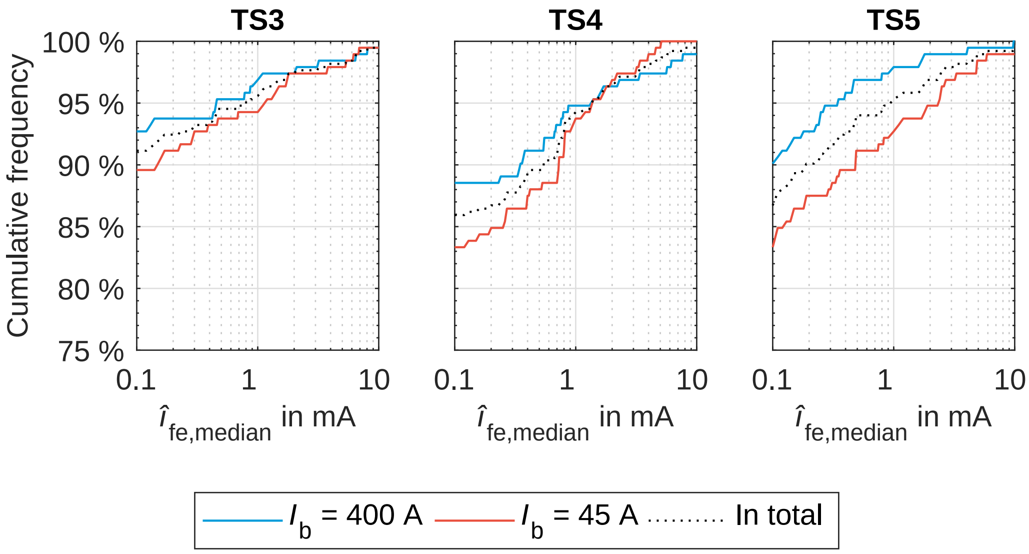

(a) Breaking current

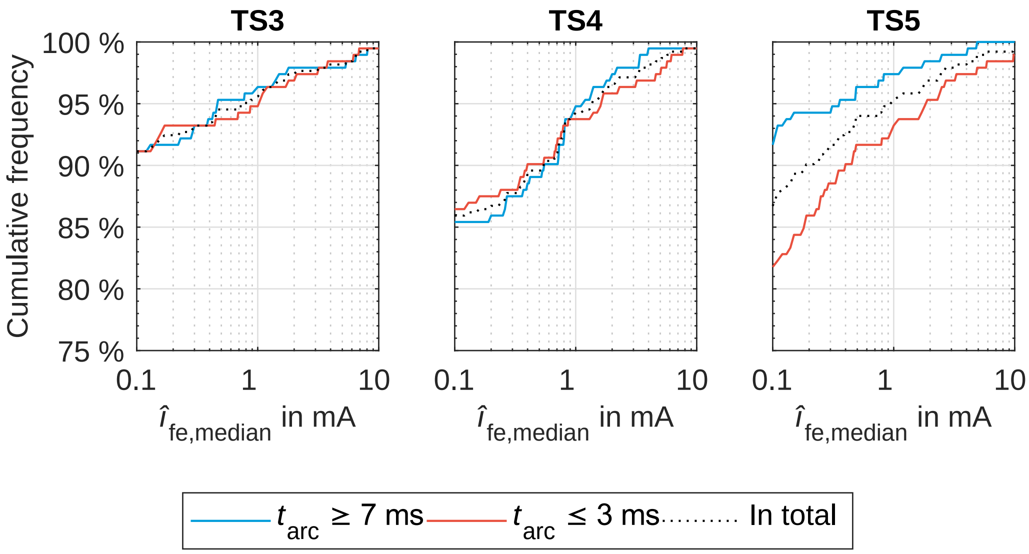

(b) Arcing time

Figure 7.7: Cumulative frequency distribution of field emission current depending on (a) breaking current or (b) arcing time

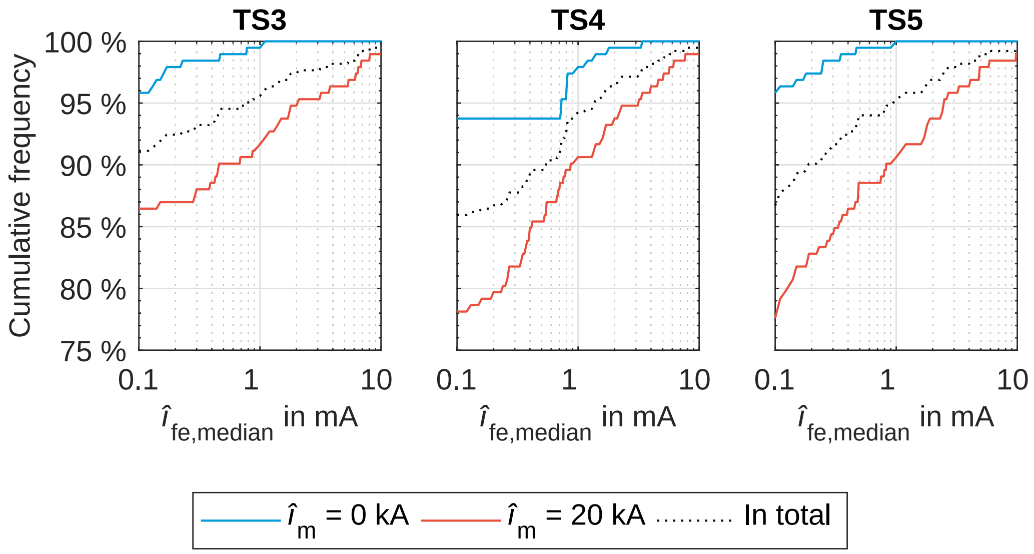

(a) Inrush current

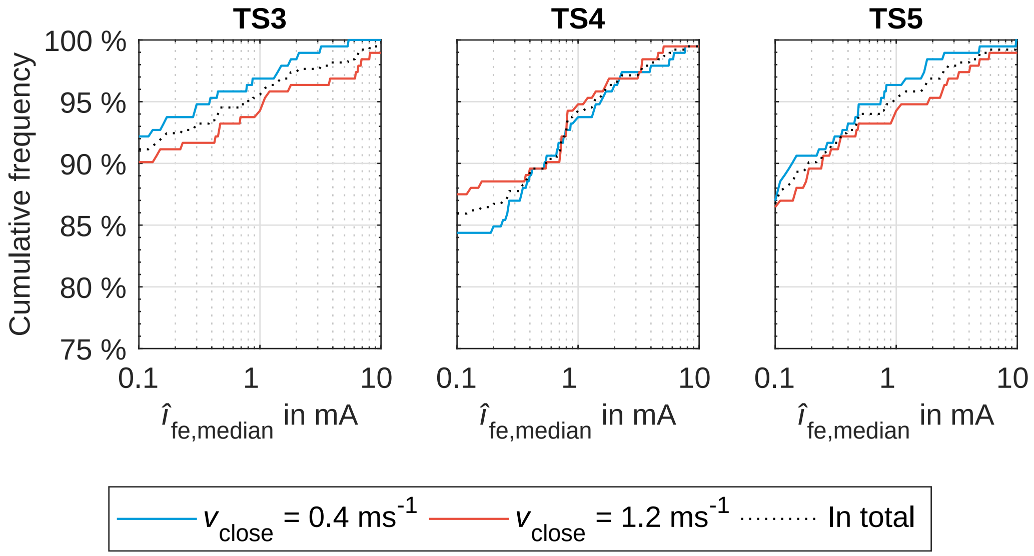

(b) Closing speed

Figure 7.8: Cumulative frequency distribution of field emission current depending on (a) inrush current or (b) closing speed

It is apparent that certain treatments affect the emergence of field emission currents differently. Figure 7.7 and Figure 7.6 present the cumulative frequency distribution of field emission current for each level setting of the varied factors *breaking current*, *arcing time*, *inrush current* and *closing speed*, respectively. To eliminate the influence of outliers, such as particularly high values caused by field increase during contact rebound, the median for all peak values of field emission current within a breaking test is used for reference. The dotted line represents the distribution for all breaking tests irrespective of any factor setting. Except for TS5, the variation of breaking current seems to have only a minor influence on the level of field emission current, whereas for the variation of arcing time no effect becomes visible. However, the results for TS5 suggest that low breaking currents and short arcing times may favour the occurrence of higher field emission currents. In contrast, a distinct difference is evident for the factor *inrush current*. Without prestressing the VIs with the high frequent current, the magnitude of field emission is typically smaller. This emphasises the large impact of inrush current on field emission phenomena. Even though, there is a minor tendency towards more field emission activity at faster closing speeds for TS3 and TS5, this is not the case for TS4. At this point, no definite conclusion can be drawn, wether the closing speed may affect the occurrence of field emission as well.

7.2 Microdischarge related phenomena

In addition to field emission currents, several self-limiting, unipolar current pulses are also observed in the computed current signal i_{comp}. Since their waveform behaviour cannot be described by the FN equation, these pulses are not attributed to field emission and are therefore treated separately in this section. Instead, these pulses are classified as microdischarges. In the following, their general characteristics are described in more detail and some examples are presented.[55]

Typically, these pulses exhibit a fast rise time with peak values up to the milliampere range. Their decay time is almost as fast as their rise time. Yet sometimes the current remains on a fraction of the former peak for a few milliseconds with varying pulse peaks before it ultimately deceases. Furthermore, these microdischarges always do appear close to the recovery voltage peaks.

Figure 7.9 includes two examples of microdischarges for the contact stroke setting of 38 mm. Example (a) shows one microdischarge in i_{comp} during each of the first two recovery voltage

[55] For the following measurement examples, the label i_{comp} is used instead of i_{fe} to emphasise the difference between microdischarge phenomena and field emission currents.

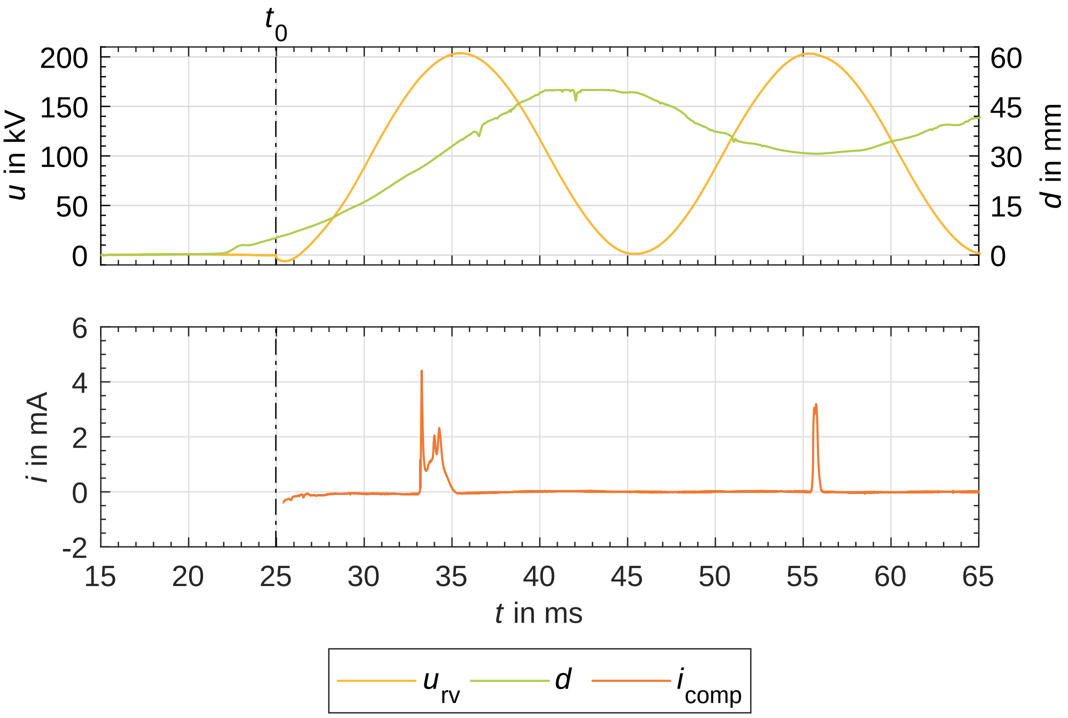

(a) Microdischarges during the first and second recovery voltage cycle

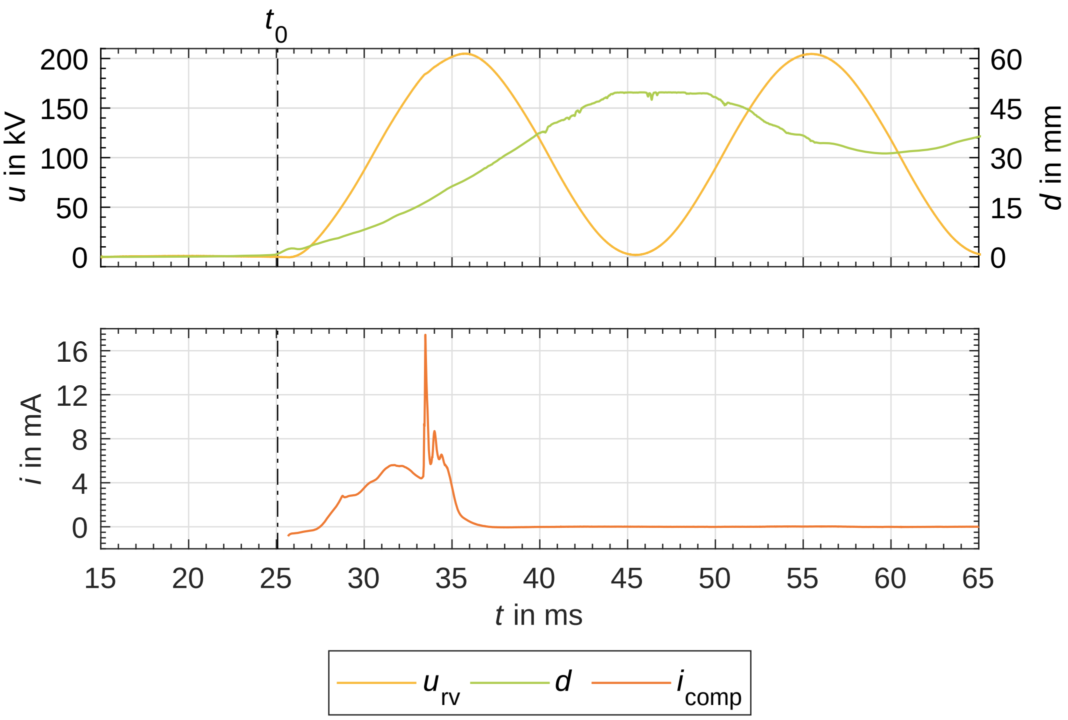

(b) Field emission superimposed by a microdischarge

Figure 7.9: Examples of microdischarges occuring at a contact stroke of 38 mm

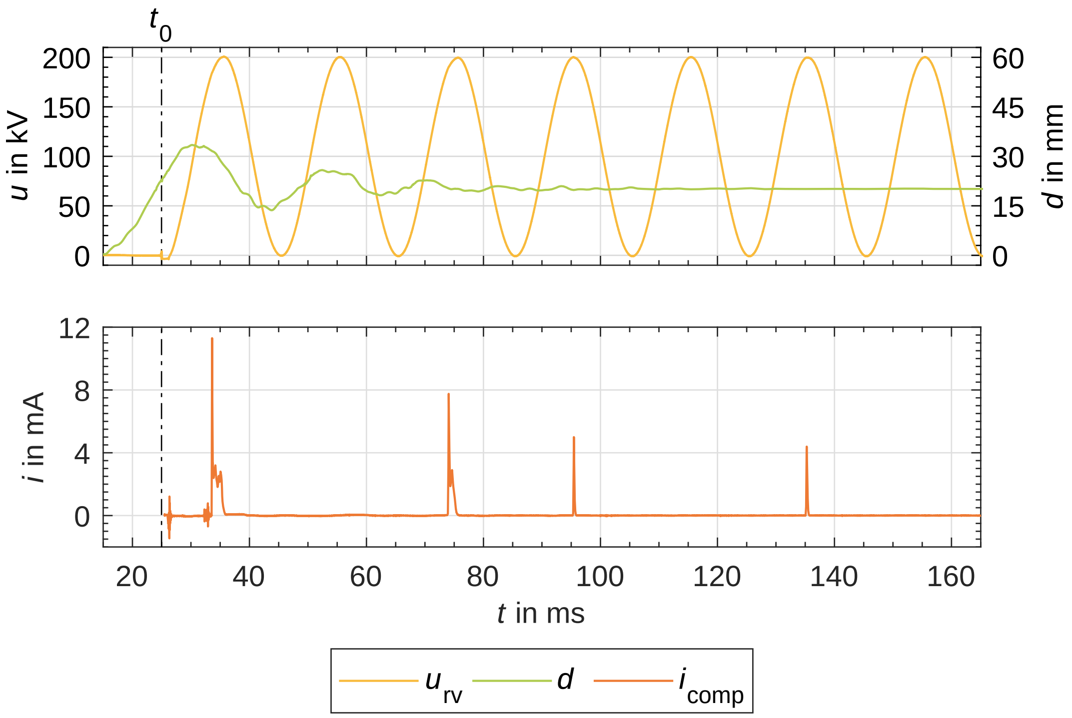

Figure 7.10: Example of microdischarges occuring at a contact stroke of 20 mm

cycles without any field emission current during that time. The first pulse has a total duration close to 2.0 ms consisting of multiple peaks. In contrast, the second pulse lasts for only 0.5 ms. Example (b) shows a field emission current with a peak value close to 6 mA at the beginning of the recovery voltage. During its decline a microdischarge current is superimposed, which reaches a value of 17.4 mA at the first peak. It is unclear wether the latter is evoked by the former or just coincidental. However, in most identified cases, microdischarges occur without a field emission current being present at all. This applies to both contact stroke settings. With current peaks up to the milliampere range, they also give rise to small temporary voltage drops, similar to high field emission currents, due to the higher load on the recovery voltage source. Such voltage drop can also be seen in example (b) between 33.5 ms to approximately 35.0 ms, coinciding with the appearance of the microdischarge.

Figure 7.10 shows a measurement example for a contact stroke setting of 20 mm containing multiple microdischarges. Four different microdischarges occur during the first, third, fourth and sixth recovery voltage cycle. Most breaking tests at the smaller contact stroke that exhibit these current pulses include multiple events during different voltage cycles. In case of TS3 and TS4 no microdischarge appears later than the seventh voltage cycle. However, for TS2 they may be present up to the 30th cycle. No current pulses have been identified for TS5. For TS1 with the contact stroke set to 38 mm only three out of 34 breaking tests that contain microdischarges emerge during multiple voltage cycles with the latest being the fourth one. The remaining ones include microdischarges only during the first cycle except for one. All test samples have in common that approximately 95 % of all measurements including microdischarges appear after the VIs were stressed by an inrush current prior to the breaking test. For the factors *breaking current*, *arcing time* and *closing speed* no clear tendency towards one or the other level setting can be identified.

7.3 Microparticle related phenomena

In this section, two different types of pulses, which are repeatedly recorded with the measuring system intended for the detection of microparticles, are presented. All measurements with this measuring system were conducted exclusively on test samples with a contact stroke set to 20 mm. The behavioural pattern of the recorded pulses cannot be assigned to either field emission or microdischarges. In the following, the common characteristics of each of the two types are described, and their characteristics are assigned to a specific phenomenon.

The first type of pulses is characterised by its frequent but irregular occurrence during breaking tests. Since these pulses appear predominantly in groups, they are referred to as *multiple pulses*. Figure 7.11 shows a measurement example of multiple pulses with the upper subplot illustrating the entire measurement time range and the two bottom subplots representing zoomed-in sections of that measurement. All multiple pulses have in common that they occur only during the rising and the falling edge of the recovery voltage. Pulses during the rising edge of the recovery voltage exhibit a positive polarity, while pulses during the falling edge exhibit a negative polarity. They may appear and also disappear suddenly on several occasions. At times, they do not emerge for several power cycles or are absent during the entire breaking test. Their peak value may steadily increase, remain almost constant or steadily decrease over the course of several power cycles, but sudden changes of their maxima were also observed.[56]

This type of behaviour is attributed to internal partial discharges. These discharges may occur in defects, voids or cavities within solid or liquid dielectrics. The corresponding locations consist of media that exhibit a lower dielectric strength compared to the desired insulating material. Furthermore, the relative permittivity is usually lower, which leads to an

[56] Additional examples of these pulses can be found in Appendix B. The presence of multiple pulses also results in an increased noise level in i_{sense} and hence in i_{fe}, see Figure B.3.

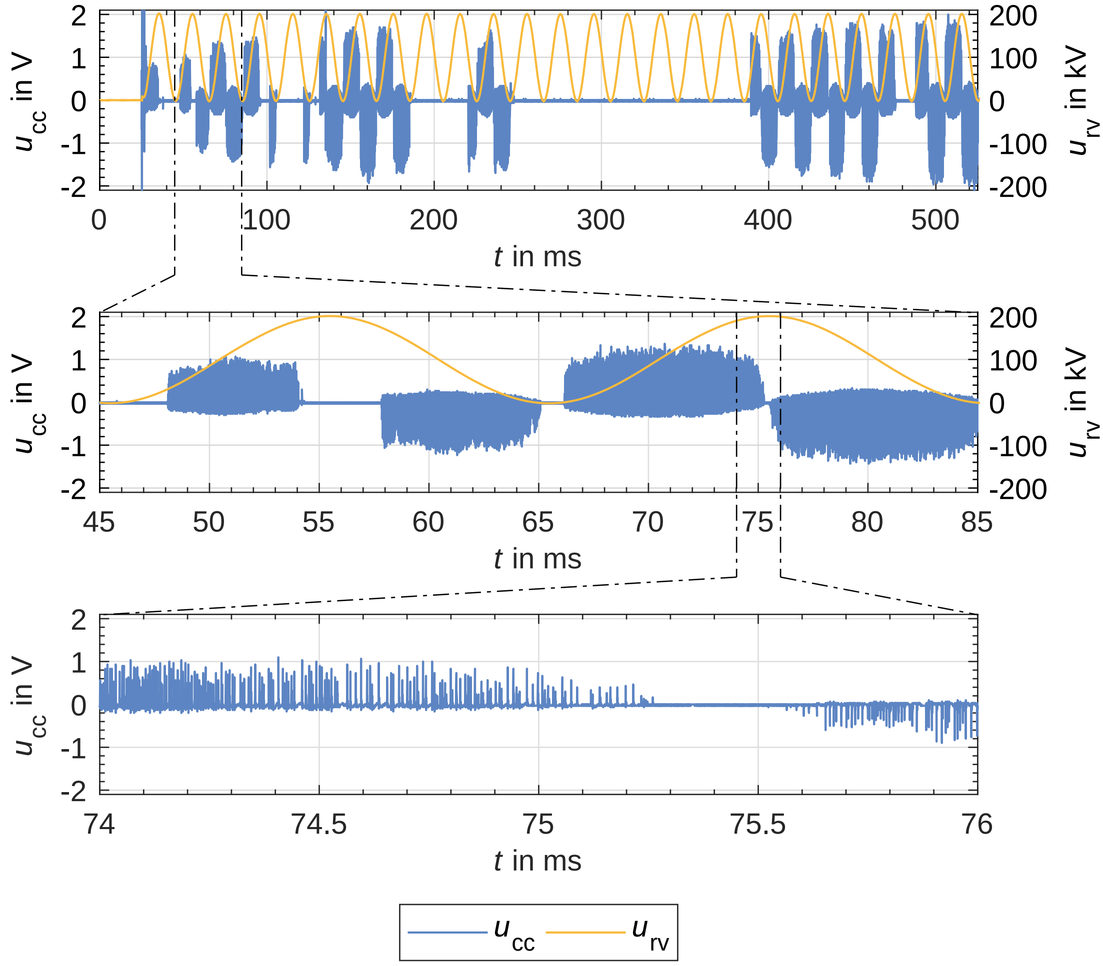

Figure 7.11: Example of multiple pulses likely caused by internal partial discharges

enhanced field stress at these irregularities. When the insulation is subjected to a sufficiently high alternating voltage, positive and negative current pulses appear simultaneously to the rising and falling edges of the voltage, respectively [KZK00, Küc18].

In the given test setup, a potential source for internal partial discharges is the insulating liquid FC-40 around the VI. Since FC-40 is chemically inert, cavities of water or air may form, which then constitute dielectric weak points due to their lower dielectric strength. In [Bau17] a low partial discharge level was demonstrated. It is therefore suspected that during the process of replacing the test samples, foreign substances were added unintentionally, which would then allow for the occurrence of partial discharges. The fluctuating occurrence of the pulses can be explained by the movement of cavities or particles during and subsequent to the switching operations. Since internal partial discharges are deemed the most likely cause for the appearence of multiple pulses, they will not be considered further.

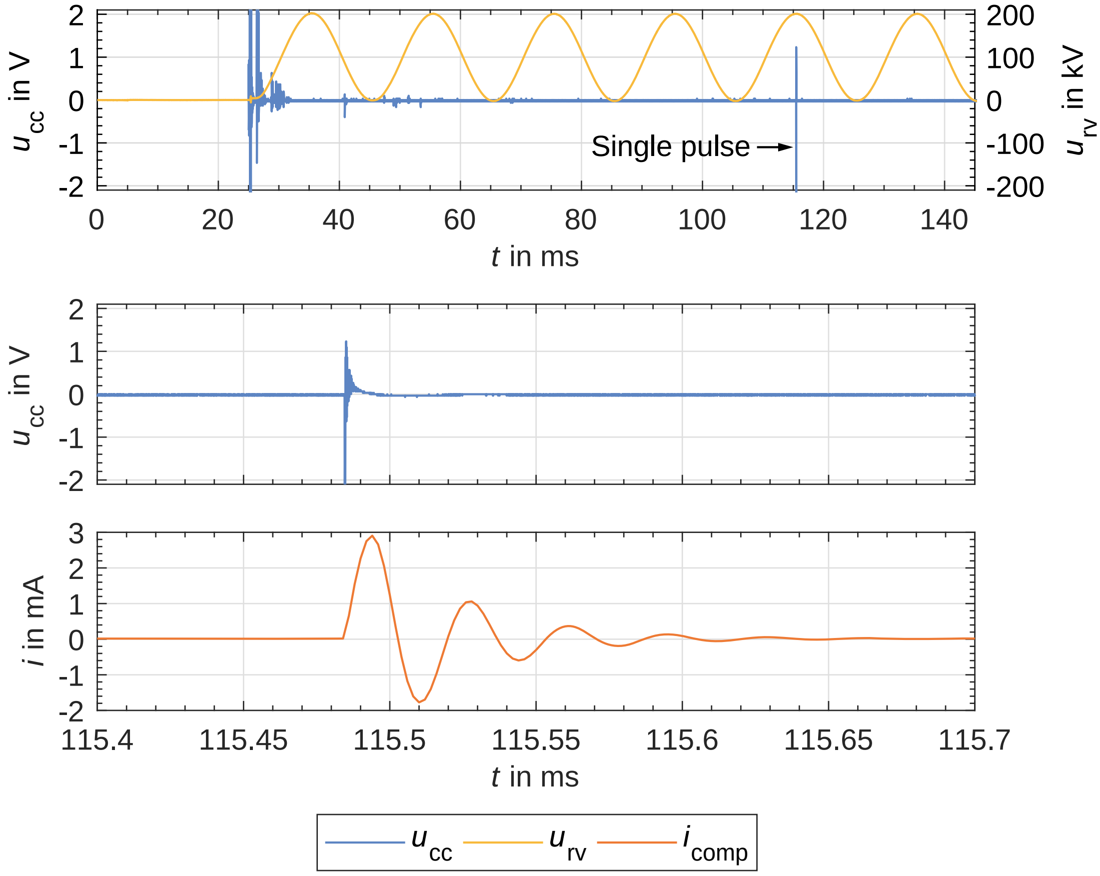

Figure 7.12: Example of a single pulse at the fifth recovery voltage peak

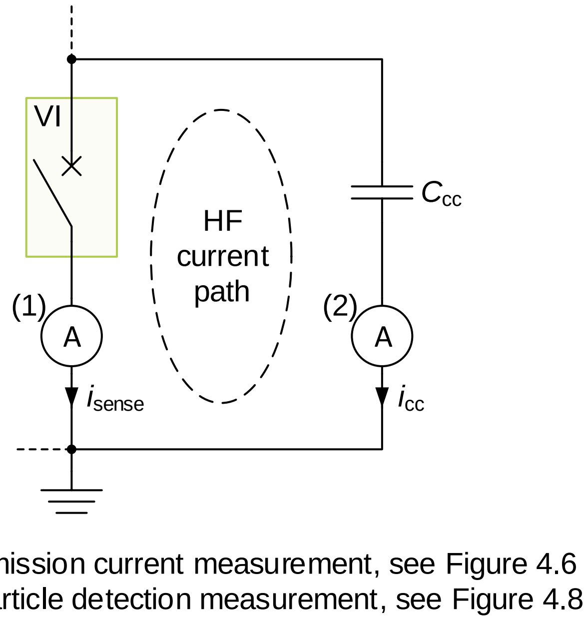

Figure 7.13: High frequency current path during a microparticle impact

The second type of pulses appears only occasionally and then usually close to the recovery voltage peaks. Since these pulses are singular events, they will also be referred to as *single pulses*. Figure 7.12 shows an example of such a single pulse event. The pulse appears when the recovery voltage reaches its fifth peak. Its characteristic behaviour cannot be attributed to either partial discharges or electromagnetic interferences and is therefore likely to be caused by a charged microparticle that impacts with one of the contact surfaces. In that case, a high frequent current will flow that is partially provided by the coupling capacitor C_{cc}. Due to the configuration of the measurement setup, this current also flows through the field emission current measurement system, which is illustrated by Figure 7.13, and is therefore also visible in the current signal i_{comp} computed from i_{sense}. Because of the different impulse responses of the individual measurement systems, this results in dissimilar signal shapes in u_{cc} and i_{comp}.

Single pulses are observed up to the end of the recovery voltage period of 600 ms. In some instances, they appear several times in different recovery voltage cycles. In most cases just one pulse appears during one cycle of recovery voltage, but in rare instances up to five pulses during a single cycle are observed. However, no correlation between more frequent occurences of particle impacts and a higher breakdown rate can be identified. Figure 7.14 shows an example with three pulses occuring after a LBD. No pulses can be seen prior to the breakdown. The large time gap between the LBD and the first pulse also does not allow

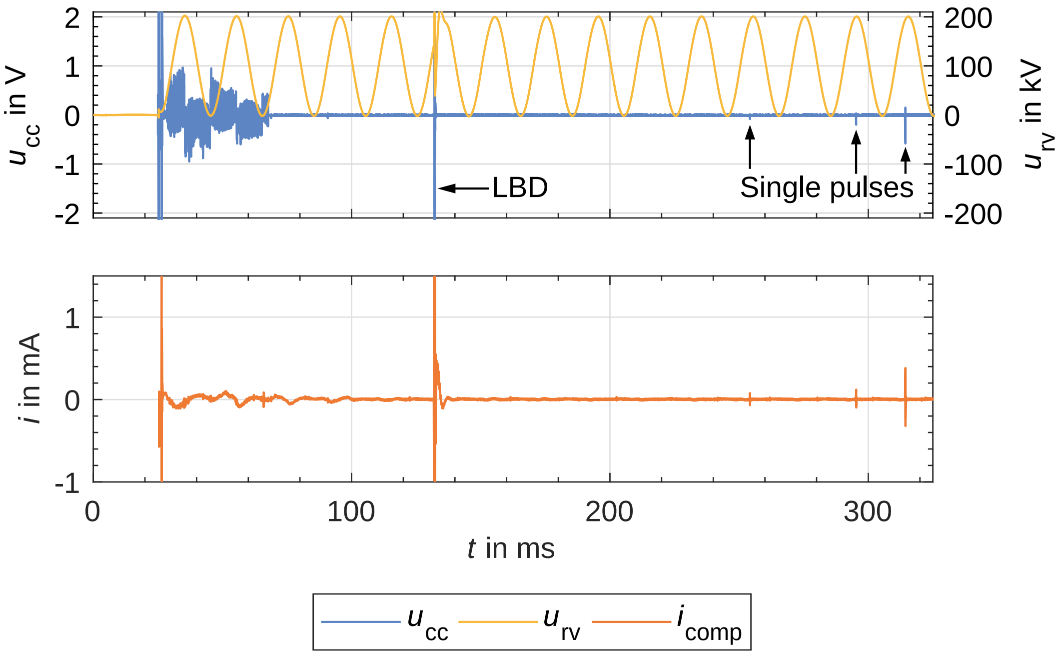

Figure 7.14: Presence of several single pulses after LBD

the conclusion that microparticles are triggered as a result of the disruptive discharge.

7.4 Discussion of results

At a contact stroke of 38 mm significant field emission currents rarely appear and then only during the beginning of recovery voltage application with the contact system still separating. A prerequisite for this is a late contact separation very close to the next current zero crossing. Since field emission is dependent on the interelectrode spacing, see Equation 2.6, larger contact gaps would result in decreasing current peaks if all other dependencies are assumed to be constant. Therefore, the contact stroke of 38 mm seems to be sufficient to restrict this effect only to the duration of initial contact opening. Since the highest capacitive voltage factor for the capacitive switching case is applied during testing, field emission currents are expected to be even lower in grid applications for the tested type of VI. At a contact stroke of 20 mm field emission currents up to 60 mA are observed. However, such high peak values only appear during the pronounced mechanical contact rebound. Thus, with a more dampened mechanical balancing process, these high currents are less likely to occur. Even though breakdowns happened at both contact strokes with preceding field emission currents in the milliampere range, the majority of breakdowns does not exhibit any significant field emission prior to the event. Furthermore, the highest field emission currents do not necessarily result in a disruptive discharge. Similar to [SWB+12] and [KHS+11] it is therefore concluded that field emission is unlikely to be the prime cause to trigger the breakdown process. However, it is assumed that the simultaneous presence of field emission may attribute further electrons for the final discharge development and thus result in a lower energy threshold for the actual trigger event.

In [SKC+12] the arc duration during current interruption and in [KHS+11] also the arc current magnitude were shown to affect the field emission current behaviour. With higher breaking currents and longer arcing times field emission currents were significantly reduced. Within this work, a similar effect can only be detected for TS5, whereas the influence for TS3 and TS4 is rather small if not absent. This deviation is assumed to be related to statistical scatter. Since only a low number of cathode spots and low energy input during the capacitive current interruption is present, only a small part of the existing protrusions are expected to be smoothened by this arc. This in turn would increase the probability for the continued existence of further imperfections on the surface and thus only occasionally result in a minor impact. However, if an influence is assumed, the unchanged breakdown rate in relation to these factors shows a further aspect, namely that a direct correlation between field emission and dielectric breakdowns is unlikely.

The fluctuating behaviour of field emission currents between consecutive tests is an indication of continuous changes of the contact surface structure during switching operations. This behaviour is mainly caused by the inrush current because of the high energy input, which causes local meltings and weldings on the surface that are broken during the next contact separation. The large scatter between consecutive tests shows that these changes do not necessarily result in a rougher surface structure, which would favour the occurrence of field emission. Yet overall, the application of inrush current results in higher field emission currents. This is consistent with the findings in [KHS+11] and [YWY+14]. There, an increase of field emission for increasing inrush current magnitudes was observed. Furthermore, the results in regard to microdischarges show that their emergence is strongly affected by preceding inrush current stress. It is assumed that the alteration of the contact surface increases the probability for volatile gas layers or the release of gas atoms that have been bound to the subsurface before, which are a potential source for these incomplete discharges.

The detected single pulses are considered to be the result of microparticles accelerating between the contacts and impacting on the opposite side. As these events are rarely observed, it is assumed that microparticle movements in the contact gap occur only rarely. This could be due to the horizontal orientation of the VI, since loosened particles tend to fall towards the central vapour shield because of the gravitational force. However, once a charged particle is accelerated in the presence of the high electric field between the contacts, it is assumed that it gains enough energy either to be evaporated during impact or to stick tightly to the surface resulting in just a single transition within the gap. The hypothesis of sole single-transits is supported by the fact that most detected single pulses during a recovery voltage cycle are non-repetitive events. Since the impact energy also depends on the applied voltage, it is more likely that multiple transitions of a single particle are rather a phenomenon at the lower voltage levels, as reported in [YWC+20, EKH+19, KMK+14]. Ultimately, an immediate voltage breakdown is only triggered if the energy during the impact is high enough to release enough vapour for the following ionisation process. Otherwise this process dies off again, resulting in the measured single pulse. Furthermore, since no single pulses are observed prior to a breakdown, the voltage breakdown triggered by a single microparticle seems to be the most likely case.

8 Conclusions and recommendations

One major challenge to adapt the vacuum switching technology to the transmission voltage levels is the switching of capacitive loads, because of the long-lasting high dielectric stress imposed on the interrupter units. This favours the occurrence of harmful dielectric breakdowns up to several hundred milliseconds after current interruption. Therefore, investigations into the cause of this late breakdown phenomenon are essential for future developments and represent the aim of this work. Two objectives are pursued: The investigation of different factors that may influence the breakdown rate and the investigation of pre-breakdown phenomena commonly attributed to the initiation of the dielectric breakdown process in vacuum. Commercially available 72.5 kV vacuum interrupters serve as the objects of investigation in this work. A synthetic test circuit is used to simulate the capacitive switching operation. In total, 1871 breaking tests with a recovery voltage of 201 kV are carried out. 475 of those tests are conducted at a contact stroke set to 38 mm. However, due to the small number of only 14 dielectric breakdowns the majority of breaking tests is performed at a reduced contact stroke of 20 mm. In the latter case, this results in 123 breakdowns. A total of 76.6 % of all breakdowns occur later than the first rise of the recovery voltage and can thus are classified as late breakdown (LBD).

Within this work factorial designs are applied in order to efficiently conduct and analyse the influence of several factors related to capacitive switching. The experiment results show that the identically designed test samples exhibit a high variability. Furthermore, a conditioning effect over the course of switching operations is prevalent to all test samples. These inevitable circumstances highlight that great care has to be taken when analysing effects on the breakdown behaviour. Since there is no statistical independence, basic statistical methods cannot be applied. For example, with a breakdown rate resulting from repeated capacitive switching tests, a binomial distribution cannot be assumed. However, a careful analysis of the results suggest that back-to-back capacitor bank inrush currents have a significant impact on the breakdown rate. In contrast, it was found that the degree of arcing during current interruption, caused by breaking current and the arcing time, and the variation of the closing speed have no significant impact. Since inrush currents are found to be the most detrimental factor, it is therefore essential to establish measures in the power grid, wich help to avoid or reduce these currents. As an alternative to the application of current limiting devices or synchronous switching, two VIs could also be used in series that switch on with a small time delay as suggested in [ZHL+15]. In this case, the contact pair of the current-carrying VI would have to be made with a contact material with better anti-welding properties. The use of multiple interrupters in series is also accompanied by an overall improved dielectric strength, which at this stage is a potential step for vacuum switching technology towards the highest voltage levels.

Simultaneously to the experiments two different measurement systems are used for the detection of pre-breakdown phenomena. Different phenomena are observed with these systems that can be attributed to field emission, microdischarges and microparticles. During contact rebound field emission current peaks can take values of up to 60 mA without resulting in a voltage breakdown. Even though in some cases the field emission effect may have attributed to the development of breakdown, the majority of breakdowns is not correlated to a significant field emission current. Therefore, field emission is not considered to be the decisive cause for a breakdown in a high-voltage VI, especially for contact gaps in the centimetre range. In the case of microparticles, several pulse events are detected that are likely to be the result of particles impacting with the contact surface. Since no breakdown is directly preceded by any of these pulses, it is assumed that a single impact will trigger the fast evolving breakdown process. It should be noted though that due to the lack of proof of a correlation between the detected pulses and microparticle impact, further investigations are still needed to validate the applied measurement principle.

Even though the breakdown rate may be increased by a careful selection of test circuit parameters, the nevertheless low probability of late breakdowns will neccessitate a high number of switching operations resulting in a high expenditure of time and costs. Moreover, the high variability between identical VIs also requires a large number of test samples in order to make reliable statements. Both issues make it all the more important to use efficient experiment designs, such as those provided by DOE, which allows for the analysis of multiple influencing variables simultaneously.

With an increasing voltage level the requirements for synthetic capacitive switching test circuits and thus their complexity increases as well.[57] This results in an increased maintenance effort, which is critical with regard to the high number of switching operations. Therefore, simplifications in test circuit design by omission of test circuit variables that have little to no influence may be a way to reduce such negative effects. Since the arcing during current interruption is found to be of minor or even no importance with regard to the breakdown behaviour, one possibility may be the omission of the breaking current

[57] A comprehensive discussion on this topic can be found in [Bau17].

source. This would reduce the number of necessary test components and the complexity in design significantly. Such a design approach has been applied for example in [DSG+06] and [YMA+95] for synthetic capacitive switching tests in the medium voltage range. A test cycle would then only consist of an inrush current making test that pre-stresses the contact surfaces during closing and a recovery voltage stress during opening. However, further testing is advised prior to this approach, e.g. a direct comparison of breaking tests with and without breaking current.

During the experiments the VI is always in its horizontal position. Even though this is a common orientation in dead tank circuit breakers, in the alternative live tank application the VI is typically in a vertical position. Changing the alignment could lead to a different type of microparticle deposition in different areas of the VI because of a different gravitational direction of force and thus may impact microparticle initiated breakdowns. Furthermore, the polarity is always kept constant during the tests. Whereas arcing occurs during the negative current half-wave the subsequent recovery voltage is of positive polarity. Therefore, the contact pair is always stressed the same way. By changing the polarity the contacts are stressed the opposite direction. Field emission would then occur on the opposite electrode, since its origin is always on the cathode. Both approaches may result in a different dielectric breakdown behaviour of the VI.

In conclusion, it is still unclear which processes trigger late breakdowns. However, the results of this work shall provide a further basis for future research in this field.

Appendix

A Additional figures for the temporal distribution of field emission currents

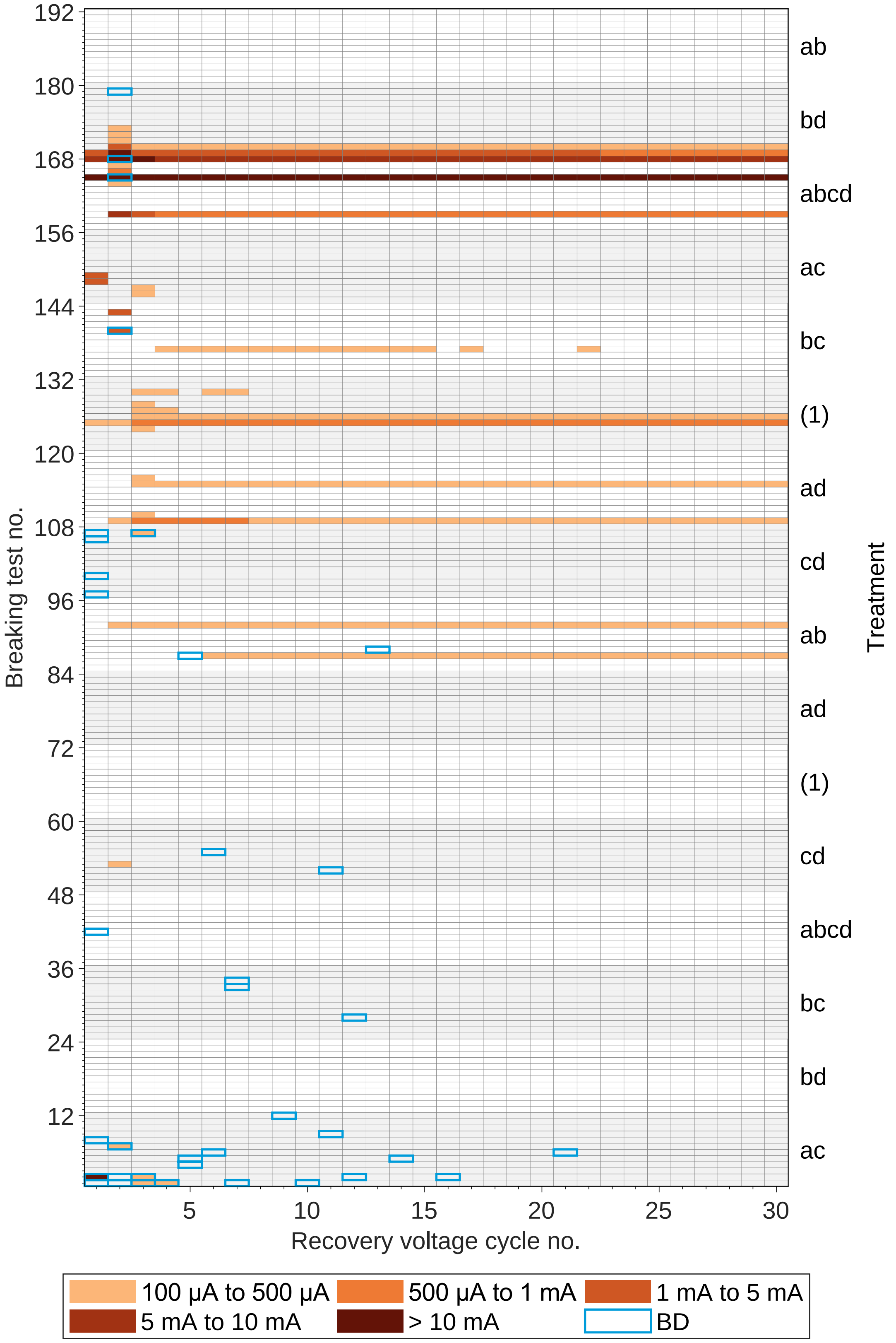

Figure A.1: Field emission current peaks $\hat{\imath}_{fe}$ for TS3 during breaking tests no. 1 to 192

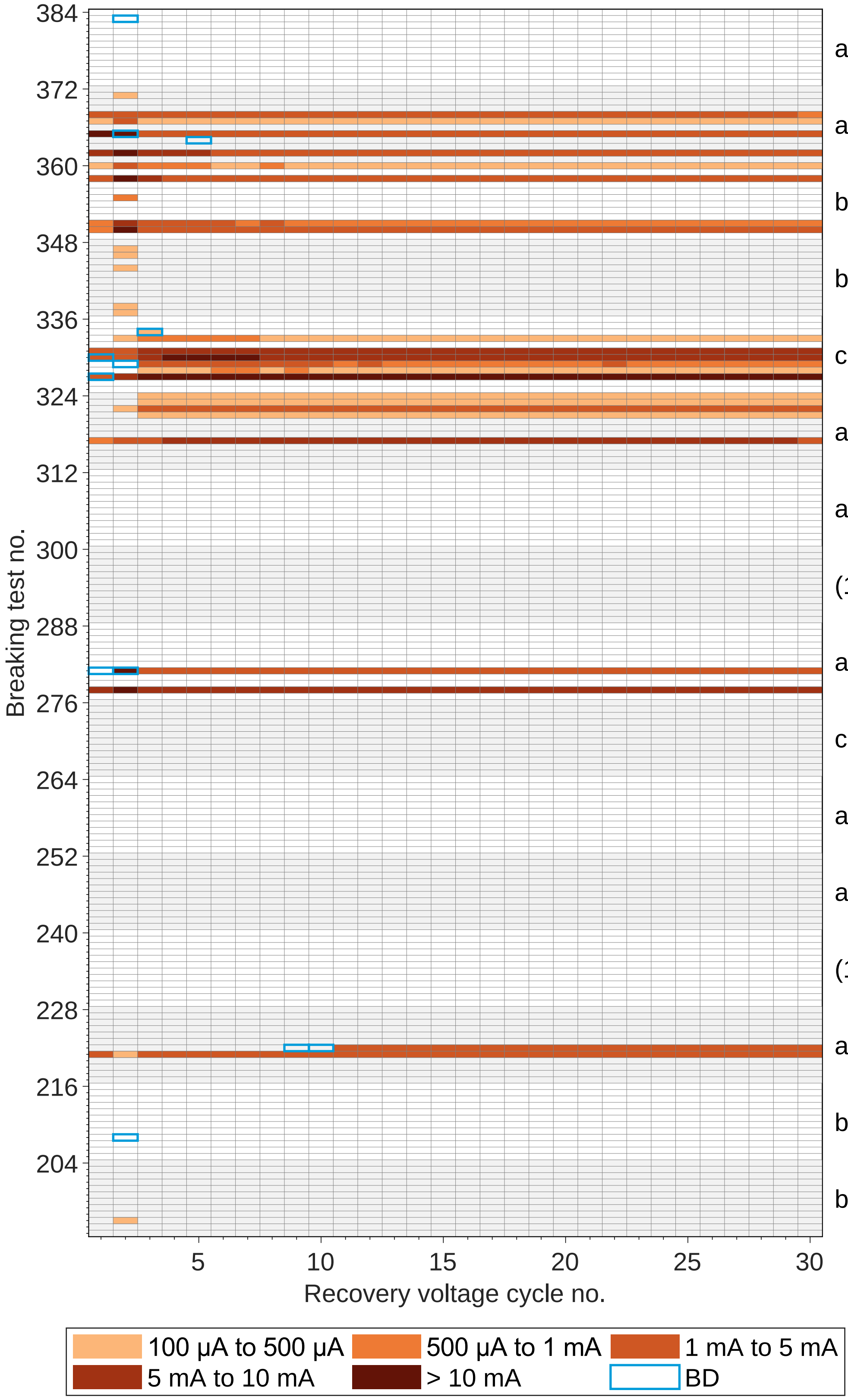

Figure A.2: Field emission current peaks $\hat{\imath}_{\mathrm{fe}}$ for TS3 during breaking tests no. 193 to 384

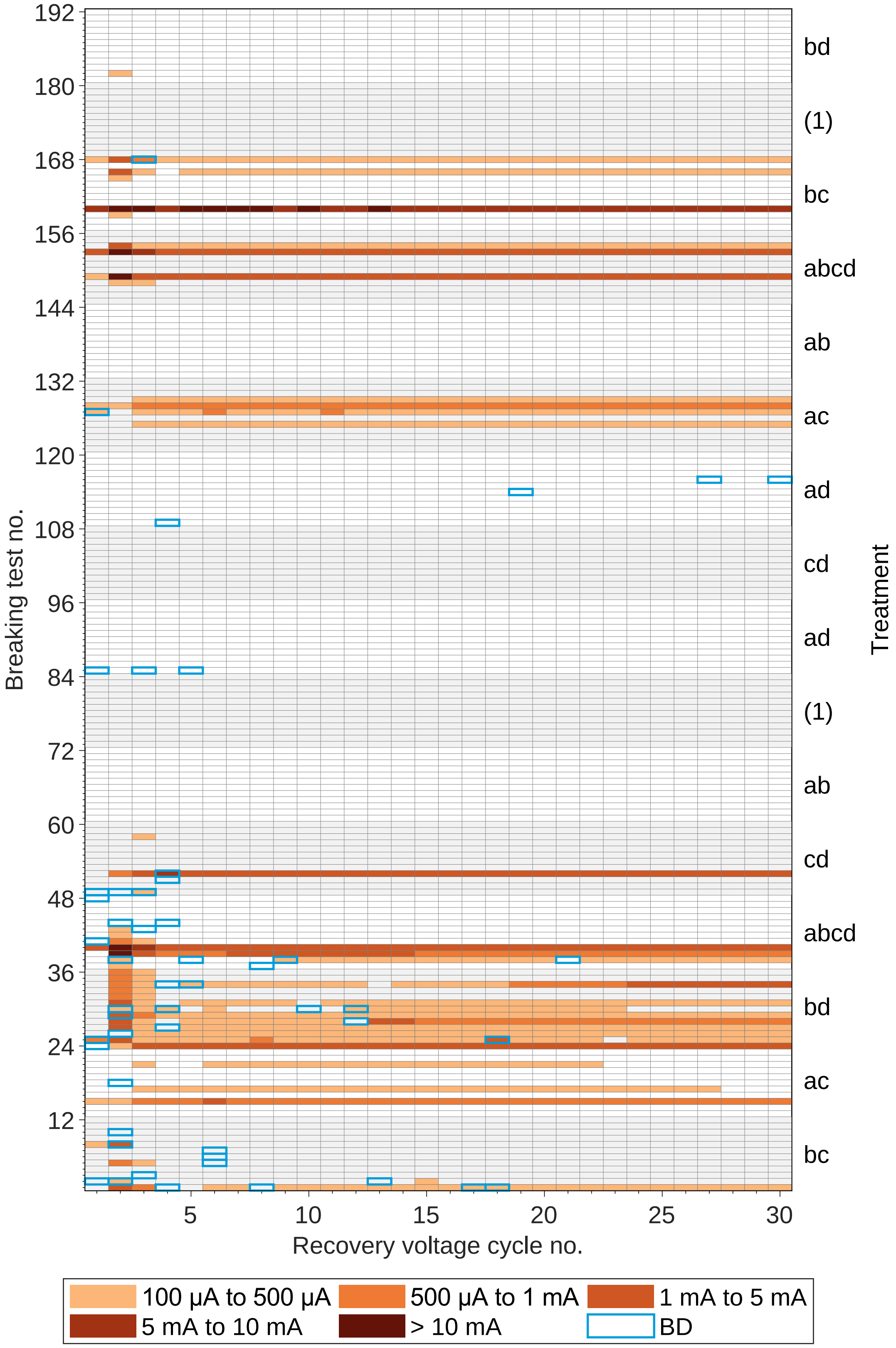

Figure A.3: Field emission current peaks $\hat{\imath}_{\mathrm{fe}}$ for TS5 during breaking tests no. 1 to 192

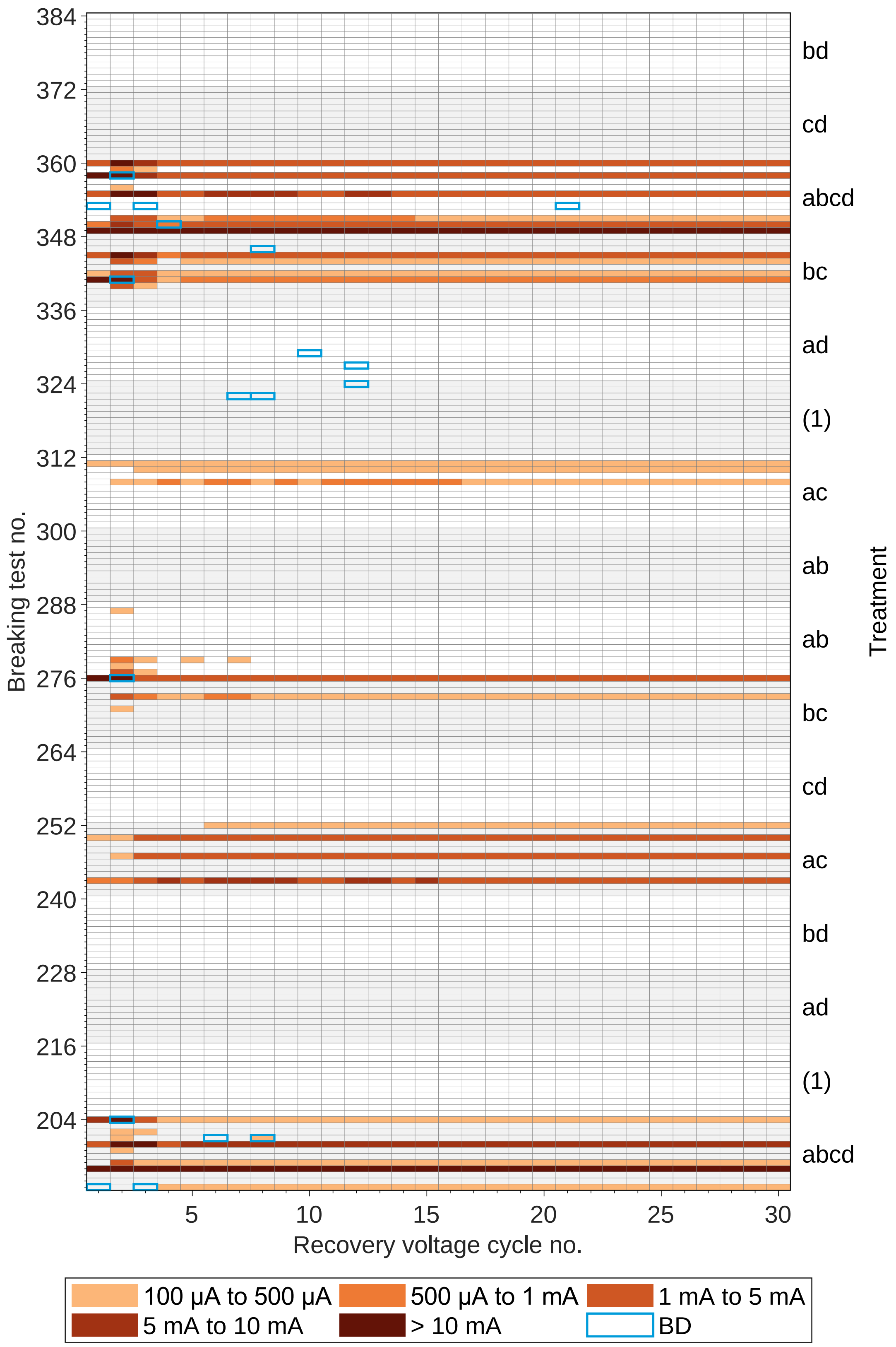

Figure A.4: Field emission current peaks $\hat{\imath}_{\mathrm{fe}}$ for TS5 during breaking tests no. 193 to 384

B Additional figures for different pulse patterns

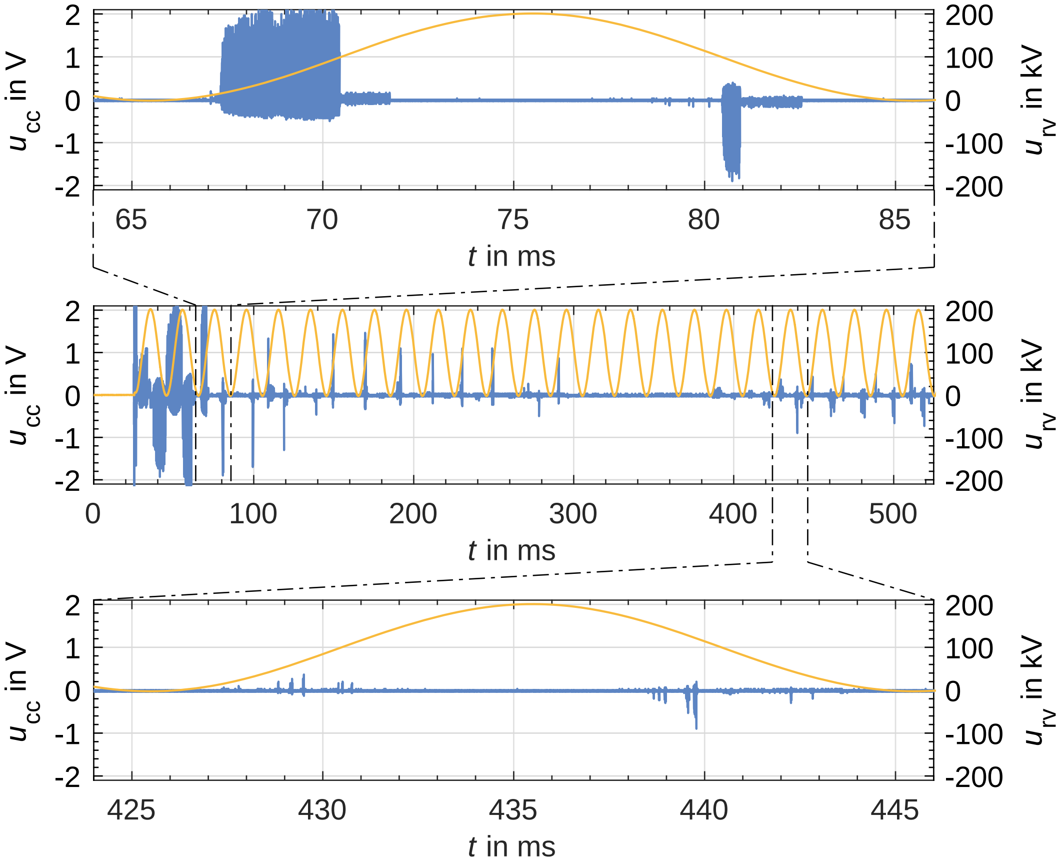

Figure B.1: Multiple pulses - Sudden changes of peak value and frequent emergence and disappearance during several recovery voltage cycles

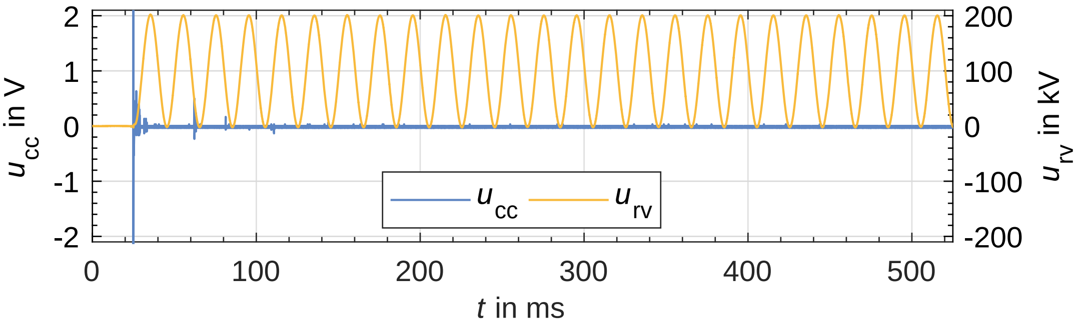

Figure B.2: Pulses almost completely absent during the breaking test

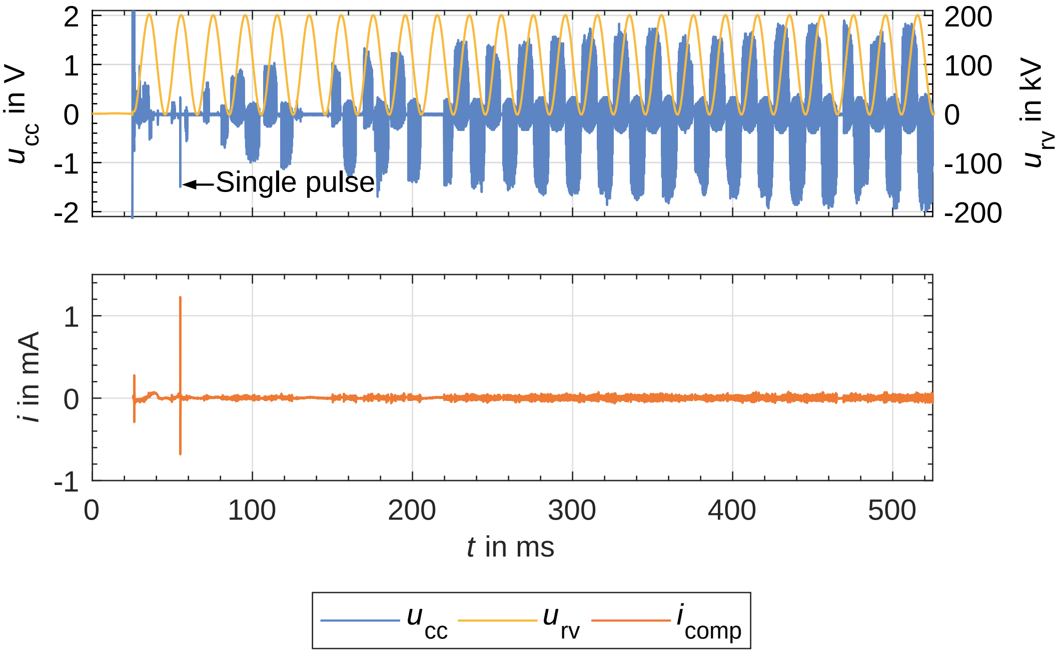

Figure B.3: Single pulse in the second recovery voltage cycle and increased noise level caused by multiple pulses

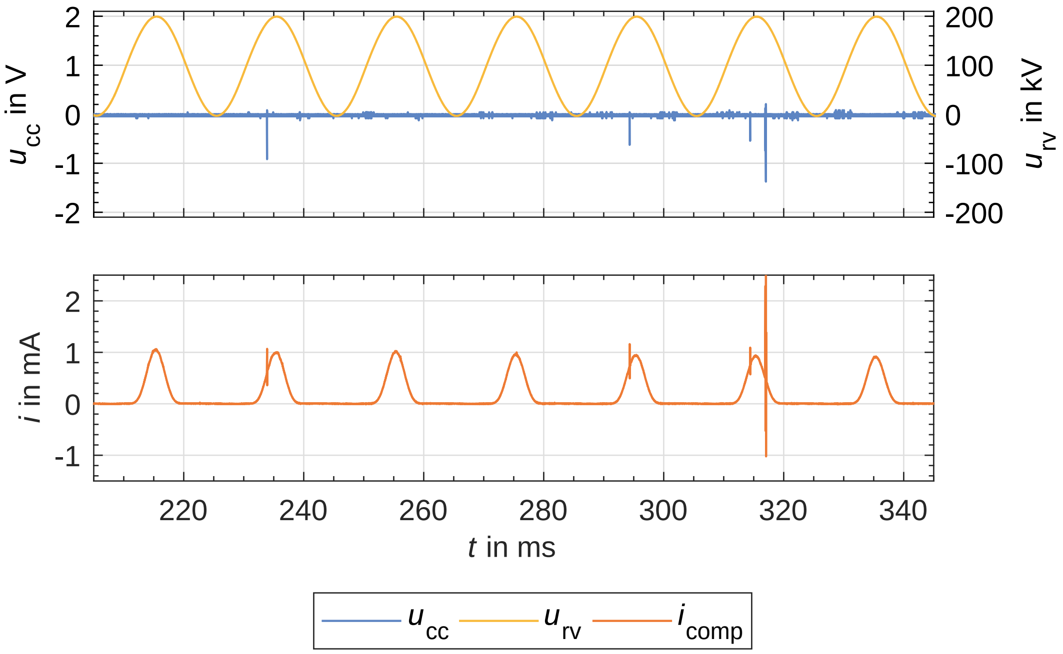

Figure B.4: Occurence of single pulses and field emission at the same time

C Photos of the test circuit

Figure C.1: Recovery voltage source

Figure C.2: Making current source in the foreground and breaking current source in the background

Figure C.3: Auxiliary switch in the foreground and current sources in the background

References

[3M10] 3M: *3M Fluorinert - Electronic Liquid - FC-40*, Product Information Brochure, 2010

[ABB14] ABB: *Live Tank Circuit Breakers - Buyer's Guide - Section Explanations*, Product Information Brochure, 2014

[And08] André Anders: *Cathodic Arcs - From Fractal Spots to Energetic Condensation*, Springer-Verlag New York, 2008

[And35] H. W. Anderson: "Effect of total voltage on breakdown in vacuum," in *Electrical Engineering*, vol. 54, no. 12, pp. 1315-1320, 1935

[Bau17] Benjamin Baum: *Design and implementation of a test environment to study late-breakdowns in high voltage vacuum circuit breakers*, Dissertation, Technische Universität Darmstadt, 2017

[BMS96] Raymon L. Boxman, Philip J. Martin, David M. Sanders: *Handbook of Vacuum Arc Science and Technology - Fundamentals and Applications*, Noyes Publications, New Jersey, 1995

[BN16] Gerd Balzer, Claus Neumann: *Schalt- und Ausgleichsvorgänge in elektrischen Netzen*, Springer Vieweg, Berlin Heidelberg, 2016

[BSH15] B. Baum, B. Surges, V. Hinrichsen: "Dielectric Testing of HV Vacuum Interrupters during Capacitive Current Switching," in *19th International Symposium on High Voltage Engineering* (ISH), Pilsen, Czech Republic, 2015

[Cig06] *Guide for application of IEC 62271-100 and IEC 62271-1 - Part 1 - General subjects*, Cigre, Technical Brochure 304, Working Group A3.11, 2006

[Cig14] *The Impact of the Application of Vacuum Switchgear at Transmission Voltages*, Cigre, Technical Brochure 589, Working Group A3.27, 2014

[Cig15] *Influence of Shunt Capacitor Banks on Circuit Breaker Fault Interruption Duties*, Cigre, Technical Brochure 624, Working Group A3.26, 2015

[Cig20] *Shunt capacitor switching in distribution and transmission systems*, Cigre, Technical Brochure 817, Working Group A3.38, 2020

[DRG10] T. Delachaux, F. Rager, D. Gentsch: "Study of vacuum circuit breaker performance and weld formation for different drive closing speeds for switching capacitive current," in *24th International Symposium on Discharges and Electrical Insulation in Vacuum* (ISDEIV), pp. 241-244, Braunschweig, Germany, 2010

[DSG+06] E. Dullni, W. Shang, D. Gentsch, I. Kleberg and K. Niayesh: "Switching of capacitive currents and the correlation of restrike and pre-ignition behavior," in *IEEE Transactions on Dielectrics and Electrical Insulation*, vol. 13, no. 1, pp. 65-71, 2006

[EKH+19] H. Ejiri, A. Kumada, K. Hidaka, T. Donen, K. Kokura: "Motion and Breakdown Related to Microparticles in Vacuum Gap," in *IEEE Transactions on Plasma Science*, vol. 47, no. 8, pp. 3384-3391, 2019

[Far93] G. A. Farrall: "Electrical breakdown in vacuum interrupters," in *IEEE Transactions on Electrical Insulation*, vol. 28, no. 4, pp. 580-591, 1993

[FK03] T. Fugel, D. Koenig: "Influence of Grading Capacitors on the Breaking Performance of a 24-kV Vacuum Breaker Series Design," in *IEEE Transactions on Dielectrics and Electrical Insulation*, vol. 10, no. 4, pp. 569-575, 2003

[Flu82] Charles H. Flurscheim: *Power Circuit Breaker Theory and Design*, Rev. ed. Stevenage: Peregrinus on behalf of the Institution of Electrical Engineers, Institution of Electrical Engineers. I.E.E. Power Engineering Ser. 1, 1982

[Flü56] S. Flügge: *Electron-Emission Gas Discharges I / Elektronen-Emission Gasentladungen I*, Springer-Verlag Berlin Heidelberg, pp. 176-231, 1956

[FN28] R. H. Fowler, L. Nordheim: "Electron Emission in Intense Electric Fields," in *Proceedings of the Royal Society of London. Series A, Containing Papers of a Mathematical and Physical Character*, Volume 119, Issue 781, pp. 173-181, 1928

[For08] Richard G. Forbes: "Physics of generalized Fowler-Nordheim-type equations," in *Journal of Vacuum Science & Technology B: Microelectronics and Nanometer Structures Processing, Measurement and Phenomena*, vol. 26, pp. 788-793, 2008

[GCG+14] Xavier Godechot, Subir Chakraborty, A. Girodet, Paul Vinson: "Design and Tests of Vacuum Interrupters for High Voltage Circuit Breakers," in *26th International Symposium on Discharges and Electrical Insulation in Vacuum* (ISDEIV), Mumbai, India, 2014, pp. 417-420

[GH93] R. Gebel, W. Hartmann: "Mechanical shocks as cause of late discharges in vacuum circuit breakers," in *IEEE Transactions on Electrical Insulation*, vol. 28, no. 4, pp. 468-472, 1993

[GKK01] S. Giere, H. C. Kärner, H. Knobloch: "Dielectric Strength of Double and Single-Break Vacuum Interrupters: Experiments with Real HV Demonstration Bottles," in *IEEE Transactions on Dielectrics and Electrical Insulation*, vol. 8, no. 1, pp. 43-47, 2001

[GKS02] S. Giere, H. Knobloch, J. Sedlacek: *Double and Single-Break Vacuum Interrupters for High Voltage Application - Experiences on Real High-Voltage Demonstration-Tubes*, 39th CIGRE Session, Paris, France, 2002

[GM10] S. Griot, A. Moreau: "Vacuum Circuit Breaker's Electrical Life for Shunt Capacitor Switching," in *24th International Symposium on Discharges and Electrical Insulation in Vacuum* (ISDEIV), pp. 194-197, Braunschweig, Germany, 2010

[GRR+12] S. Giere, R. Renz, F. Richter, N. Trapp: "Capacitive current switching capability of 72.5 kV high-voltage vacuum interrupters," in *25th International Symposium on Discharges and Electrical Insulation in Vacuum* (ISDEIV), pp. 217-220, Tomsk, Russia, 2012

[GSE+08] Xavier Godechot, Martin Schlaug, Uwe Ernst, Mounir Hairour, John Jenkins: "Vacuum Interrupters in High Voltage Applications," in *23rd International Symposium on Discharges and Electrical Insulation in Vacuum* (ISDEIV), pp. 103-106, Bucharest, Romania, 2008

[HGW+18] T. Heinz, S. Giere, S. Wethekam, M. Koletzko, N. Wenzel: "Control of Vacuum Arcs in High-Voltage Vacuum Interrupters by Suitable Stroke Trajectories of Opening AMF Contacts," in *28th International Symposium* *on Discharges and Electrical Insulation in Vacuum* (ISDEIV), pp. 535-538, Greifswald, Germany, 2018

[HL14] Wolfgang Hauschild, Eberhard Lemke: *High-Voltage Test and Measuring Techniques*, Springer-Verlag Berlin Heidelberg, 2014

[HM84] Wolfgang Hauschild, Wolfgang Mosch: *Statistik für Elektrotechniker*, VEB Verlag Technik Berlin, Ed. 1, 1984

[IEEE14] *IEEE Guide for the Application of Capacitance Current Switching for AC High-Voltage Circuit Breakers Above 1000 V*, IEEE Std C37.012-2014, 2014

[IPCC13] *Climate Change 2013: The Physical Science Basis. Contribution of Working Group I to the Fifth Assessment Report of the Intergovernmental Panel on Climate Change* [T.F. Stocker, D. Qin, G.-K. Plattner, M. Tignor, S.K. Allen, J. Boschung, A. Nauels, Y. Xia, V. Bex, P.M. Midgley (eds.)], Cambridge University Press, Cambridge, United Kingdom and New York, NY, USA, Intergovernmental Panel on Climate Change 2013

[Ito18] Hiroki Ito et al.: *Switching Equipment*, CIGRE Green Book, Springer Cham, CIGRE Study Committee A3 Activity, 2018

[Jen18] Kevin Jensen: *Introduction to the Physics of Electron Emission*, John Wiley & Sons Ltd, pp. 121-206, 2018

[Jüt69] B. Jüttner: "Über die Gültigkeit der Fowler-Nordheim-Gleichung bei der Feldemission von Mikrospitzen auf ausgedehnten Metalloberflächen," in *Contributions to Plasma Physics*, vol. 9, issue 2, pp. 179-188, 1969

[KHS+11] M. Koochack Zadeh, V. Hinrichsen, R. Smeets, A. Lawall: "Field Emission Currents in Vacuum Breakers after Capacitive Switching," in *IEEE Transactions on Dielectrics and Electrical Insulation*, vol. 18, no. 3, pp. 910-917, 2011

[KKG+18] Benjamin Kühn, Michael Kurrat, Dietmar Gentsch, Fabian Hain: "Breaking Operations of a Double Break Vacuum Interrupter Test Setup Using a Belt Drive," in *28th International Symposium on Discharges and Electrical Insulation in Vacuum* (ISDEIV), pp. 631-634, Greifswald, Germany, 2018

[KMK+14] Y. Kikuchi, S. Matsuoka, A. Kumada, K. Hidaka, T. Donen, M. Tsukima: "Motion observation of particles between electrodes and subsequent breakdown phenomena in vacuum," in *26th International Symposium on Discharges and Electrical Insulation in Vacuum* (ISDEIV), pp. 133-136, Mumbai, India, 2014

[Koo11] M. Koochack Zadeh: *Field Emission Current Analysis for the Assessment of Dielectric and Switching Performance of Vacuum Interrupters*, Dissertation, Technische Universität Darmstadt, 2011

[Kör08] F. Körner: *Kontaktverhalten von Vakuumschaltern beim kapazitiven Schalten*, Dissertation, Technische Universität Carolo-Wilhelmina zu Braunschweig, 2008

[Küc18] Andreas Küchler: *High Voltage Engineering: Fundamentals - Technology - Applications*, Springer Vieweg, VDI-Buch, 1st edition, 2018

[KZK00] E. Kuffel, W. S. Zaengl, J. Kuffel: *High Voltage Engineering: Fundamentals*, Newnes (imprint of Butterworth-Heinemann Ltd), 2nd edition, 2000

[Lat95] Rod V. Latham: *High Voltage Vacuum Insulation: Basic Concepts and Technological Practice*, Academic Press Ltd., London and San Diego, 1995

[Lip03] Hans J. Lippmann: *Schalten im Vakuum: Physik und Technik der Vakuumschalter*, VDE Verlag GmbH Berlin und Offenbach, 2003

[Mei16] Meidensha Corporation: *Vacuum Interrupters*, Product Brochure, 2016

[Mon12] Douglas C. Montgomery: *Design and Analysis of Experiments*, John Wiley & Sons, 8th Edition, 2012

[Nat05] National Instruments: *NI 6122/6123 Specifications*, Technical Brochure, 2005

[Nor13] North Star: *Voltage Probe Manual and Data - North Star High Voltage, Inc. - Rev Feb 1, 2013*, Manual, 2013

[Omi17] Omicron: *MPD 600 - High-end partial discharge measurement and analysis system*, Technical Brochure, 2017

[Ren00] R. Renz: "On criteria of optimized application of AMF- and RMF-contact systems in vacuum interrupters," in *19th International Symposium on Discharges and Electrical Insulation in Vacuum* (ISDEIV), pp. 176-197, Xi'an, China, 2000

[RKT+10] J. S. Ryu, Y. K. Kim, S. J. Tak, S. W. Park, J. B. Kim, C. W. Park, M. S. Kim, W. P. Song: *The Challenge of SF_6 Gasless Type Switchgear for Distribution and Transmission Voltage Class in Korea*, Cigré A3 308, 2010

[SC76] B. P. Singh, P. A. Chatterton: "A new model of microdischarge current growth in vacuum," in *Journal of Physics D: Applied Physics*, vol. 9, no. 12, pp. 1797-1808, 1976

[SEG+10] G. Sandolache, U. Ernst, X. Godechot, S. Kantas, M. Hairour, L. Dalmazio: "Switching of capacitive current with vacuum interrupters," in *24th International Symposium on Discharges and Electrical Insulation in Vacuum* (ISDEIV), pp. 129-132, Braunschweig, Germany, 2010

[Sho38] W. Shockley: "Currents to Conductors Induced by a Moving Point Charge," in *Journal of Applied Physics*, vol. 9, pp. 635-636, 1938

[Sie18] Siemens AG: *3AV1 blue circuit-breakers - Your solution for a CO_2-neutral footprint*, flyer, 2018

[SK11] Adolf J. Schwab, Wolfgang Kürner: *Elektromagnetische Verträglichkeit*, VDI-Buch, Springer-Verlag Berlin Heidelberg, 2011

[SKF00] S. Sato, K. Koyama, H. Fujii: "Behavior of conductive microparticles under electric field in vacuum and their influence on breakdown characteristics," in *19th International Symposium on Discharges and Electrical Insulation in Vacuum* (ISDEIV), pp. 25-28, Xi'an, China, 2000

[SHT16] B. Surges, V. Hinrichsen and E. D. Taylor: "Simultaneous measurement of high and low frequency pre-breakdown currents on HV vacuum interrupters," in *27th International Symposium on Discharges and Electrical Insulation in Vacuum* (ISDEIV), pp. 1-4, Suzhou, China, 2016

[Sla94] P. G. Slade: "Advances in Material Development for High Power, Vacuum Interrupter Contacts," in *IEEE Transactions on Components, Packaging, and Manufacturing Technology - Part A*, vol. 17, no. 1, March 1994

[Sla08] P. G. Slade: *The Vacuum Interrupter: Theory, Design, and Application*, CRC Press, Boca Raton, London, New York, 2008

[SKC+12] R. P. P. Smeets, S. Kuivenhoven, S. Chakraborty, G. Sandolache: "Field Electron Emission Current in Vacuum Interrupters after Large Inrush Current," in *25th International Symposium on Discharges and Electrical Insulation in Vacuum* (ISDEIV), pp. 157-160, Tomsk, Russia, 2012

[SvBH17] Karl Siebertz, David van Bebber, Thomas Hochkirchen: *Statistische Versuchsplanung - Design of Experiments (DoE)*, VDI-Buch, Springer Vieweg, Berlin, Heidelberg, Ed. 2, 2017

[SvK+15] René P. P. Smeets, Lou van der Sluis, Mirsad Kapetanović, David F. Peelo, Anton Janssen: *Switching in Electrical Transmission and Distribution Systems*, Chichester, West Sussex, United Kingdom, Wiley, 2015

[SWB+12] R.P.P. Smeets, R. Wiggers, H. Bannink, S. Kuivenhoven, S. Chakraborty, G. Sandolache: *The impact of switching capacitor banks with very high inrush current on switchgear*, Proceedings of the 44th CIGRE conference, pp. 1-12, Paris, France, 2012

[Tel15] *WaveSurfer 3000 Oscilloscopes: 200 MHz - 750 MHz*, Teledyne Lecroy, 2015

[WGL+17] H. Wang, Y. Geng, Z. Liu, J. Lin, X. Li, Y. Li: "Prestrike characteristics of arc-melted CuCr40 and infiltration CuCr50 contact materials in 40.5 kV vacuum interrupters under capacitive making operations," in *IEEE Transactions on Dielectrics and Electrical Insulation*, vol. 24, no. 6, pp. 3357-3366, 2017

[YMA+95] K. Yokokura, M. Matsuda, K. Atsumi, T. Miyazawa, S. Sohma, E. Kaneko, I. Ohshima: "Capacitor switching capability of vacuum interrupter with CuW contact material," in *IEEE Transactions on Power Delivery*, vol. 10, no. 2, April 1995

[YWC+20] Wenlong Yan, Zhenxing Wang, Boyang Chen, Liqiong Sun, Yingsan Geng, Zhiyuan Liu, Jianhua Wang: "The Impact of Particles on Post-arc breakdowns in Capacitive Interruptions," in *29th International Symposium on Discharges and Electrical Insulation in Vacuum* (ISDEIV), pp. 359-362, Padova, Italy, 2021

[YWY+14] Y. Yu, J. Wang, H. Yang, Y. Geng and Z. Liu: "The impact of inrush current on field emission current of vacuum interrupters during capacitive current switching," in *26th International Symposium on Discharges and Electrical Insulation in Vacuum* (ISDEIV), pp. 145-148, Mumbai, India, 2014

[ZHL+15] Feng Zhao, Biao Hu, Zhiyuan Liu, He Yang, Yongxiang Yu, Yingsan Geng, Jianhua Wang: "Back-to-back capacitor bank switching performance of vacuum circuit breaker by series technology," in *3rd International Conference on Electric Power Equipment – Switching Technology* (ICEPE-ST), pp. 528-531, Busan, Korea, 2015

[ZM93] W. Ziomek, H. Moscicka-Grzesiak: "Relation of Breakdown Voltage and Prebreakdown Microdischarge Parameters in Vacuum," in *IEEE Transactions on Electrical Insulation*, vol. 28, no. 4, 1993

Standards

[DIN90] DIN 28400-1, *Vakuumtechnik; Benennung und Definitionen; Allgemeine Benennungen / Vacuum technology; terms and definitions; general terms*, 1990

[IEC08] IEC 62271-100, *High-voltage switchgear and controlgear - Part 100: Alternating-current circuit breakers*, 2008

Own publications

1. B. Baum, B. Surges, V. Hinrichsen: “Dielectric testing of HV vacuum interrupters during capacitive current switching,” in *19th International Symposium on High Voltage Engineering* (ISH), Pilsen, Czech Republic, 2015

2. B. Surges, V. Hinrichsen, E. D. Taylor: “Simultaneous Measurement of High and Low Frequency Pre-Breakdown Currents on HV Vacuum Interrupters,” in *27th International Symposium on Discharges and Electrical Insulation in Vacuum* (ISDEIV), pp. 72-75, Suzhou, China, 2016

3. Y. Nakano, B. Surges, V. Hinrichsen: “Internal Breakdown Voltage of Vacuum Interrupters with Shield Potential Control,” in *20th International Symposium on High Voltage Engineering* (ISH), Buenos Aires, Argentina, 2017

4. Y. Nakano, B. Surges, V. Hinrichsen: “Field Emission Inception Voltage of a 72.5 kV VI with Controlled Vapor Shield Potential,” in *28th International Symposium on Discharges and Electrical Insulation in Vacuum* (ISDEIV), pp. 675-678, Greifswald, Germany, 2018

5. Y. Nakano, B. Surges, V. Hinrichsen: “Increasing the Internal Field Strength of Vacuum Interrupters With Vapor Shield Potential Control,” in *IEEE Transactions on Power Delivery*, vol. 33, no. 6, pp. 3155-3161, Dec. 2018

Supervised student research projects

1. Franz Pellmann: *Alternative Isoliermedien für Schaltanlagen der Bahnenergieversorgung*, Master Thesis, No. 1959, Darmstadt, 2015
2. Christoph Bardel: *Aufbau und Erprobung eines Messsystems zur Erfassung der Lichtbogenspannung beim kapazitiven Schalten von Hochspannungsvakuumschaltröhren*, Bachelor Thesis, No. 2017, Darmstadt, 2019

Curriculum Vitae

since 06/2021	Test engineer at VDE Prüf- und Zertifizierungsinstitut GmbH (VDE Testing and Certification Institute), Offenbach, Germany
01/2015 - 12/2020	Scientific Assistant at Fachgebiet Hochspannungstechnik (High-Voltage Laboratories), Technische Universität Darmstadt, Germany
11/2013 - 02/2014	Industry Internship, FGH e.V., Mannheim, Germany
04/2012 - 10/2014	Student at the Technische Universität Darmstadt, Germany Master's degree program "Electrical Engineering and Information Technology" with a specialisation in "Electrical Power Engineering"
10/2007 - 03/2012	Student at the Technische Universität Darmstadt, Germany Bachelor's degree program "Electrical Engineering and Information Technology" with a specialisation in "Electrical Power Engineering"

Benjamin Surges
Darmstadt, den 22.03.2022

Erklärung laut Promotionsordnung

§ 8 Abs. 1 lit. c PromO

Ich versichere hiermit, dass die elektronische Version meiner Dissertation mit der schriftlichen Version übereinstimmt.

§ 8 Abs. 1 lit. d PromO

Ich versichere hiermit, dass zu einem vorherigen Zeitpunkt noch keine Promotion versucht wurde.

§ 9 Abs. 1 PromO

Ich versichere hiermit, dass die vorliegende Dissertation selbstständig und nur unter Verwendung der angegebenen Quellen verfasst wurde.

§ 9 Abs. 2 PromO

Die Arbeit hat bisher noch nicht zu Prüfungszwecken gedient.

Benjamin Surges
Darmstadt, den 22.03.2022